POLITECNICO DI TORINO

Master degree course in Aerospace engineering
Master degree thesis

Sub-Transonic and Supersonic STRATOFLY MR3 Aerodatabase develompment by means of CFD Simulations

Supervisors
Prof. Nicole Viola
Eng. Pietro Roncioni
Eng. Roberta Fusaro

Candidate
Dario De Luca

December 2020

Acknowledgements

My thesis work gave me the opportunity to deepen topics related to ever-changing world of hypersonic transport. I hope that this little contribute will be useful to achieve final purposes.
Firstly, i would like to thank Prof. Nicole Viola and Roberta Fusaro, which have proven to be professional and courteous. In addiction, they gave me the possibility to be part of interesting project.
I would like to express my gratitude to Pietro Roncioni, researcher at the CIRA, with which i had the pleasure to work together. I couldn't have found a better supervisor; he was always open to discussion and very willing to help me.
My family is my safe haven; thank to them i overcame difficulties and shared special moments. I'm proud to you mum, dad and Anto.
Last but not least, i would like to mention my relatives and friends: thanks to all of you.

Abstract

Interest in hypersonic airplane is constantly growing, both in civil applications and in military one. In this scenario, commercial air transport is very attracted by this emerging technology, since time to destination needs to be reduced with a number of passengers predicted to be higher than at present. In this context, the STRATOFLY project arose in a European landscape with the aim to study the feasibility of high-speed passenger stratospheric flight by means of futuristic airplane concept that shall be able to perform cruise at 30 km of altitude at Mach 8 flight speed and a reference Brussels-Sidney flight executed in less than 3 hours. The ambition is to reach a TRL6 by 2035. This thesis work focuses on aerodynamic characterization of the MR3 airplane concept by means of numerical approach (CFD). Aerodynamic coefficients are obtained by adding to the baseline clean configuration the effect of control surfaces deflections. This latter obtained through linear build-up approach of different portions of the aircraft, simulated independently from take-off stage (Mach 0.3) to cruise condition (Mach 8 at an altitude of about 30 Km). Due to wide flow regimes experimented during simulated flight path and massive geometry of aircraft, simplified flow field equations are employed (Euler equations). Firstly, wing, flap and aileron are considered together. Than standalone canard and finally body-flap and rudder. The purpose of this work is to obtain in a rapid way (project phase A like in preliminary analysis) the aerodynamic database of the Stratofly concept in the whole flow regimes in witch airplane operates, in order to give input to flight mechanics analysis for trajectory simulations, and in general to have a better comprehension of the stability characteristics.

Contents

List of Figures

List of acronyms

AoA Angle of attack

ATLLAS Aero-Thermodynamic Loads on Lightweight Advanced Structures II

ATR Air Turbo Rocket

AUSM Advection Upstream Splitting Method

CFD Computation Fluid Dynamic

DMR Dual Mode Ramjet

EFTV Experimental Flight Test Vehicle

ESM External Support Module

FADS Flush Air Data System

HEXAFLY-INT High-Speed Experimental Fly Vehicles – International

LAPCAT Long-Term Advanced Propulsion Concepts and Technologies

LE Leading edge

M Mach

SA Spalart-Allmaras

STRATOFLY Stratospheric Flying Opportunities for High-Speed Propulsion Concepts

TE Trailing edge

Chapter 1

Introduction

The charm of high-speed, joined with desire to fly, have always electrified human being, which has tried to expand its own limits of the knowledge in every way. When curiosity blends with perseverance progress becomes unavoidable and, as Benjamin Franklin said:
Without continual growth and progress, such word as improvement, achievement, and success have no meaning
. According to this statement, during the last century remarkable achievements in aviation have been achieved. Nowadays, interest on hypersonic technology is corroborated by multiple applications that are supported by rising projects all over the world. In particular, Europe is increasingly opening to find alternative approach in support of the growing air traffic, guaranteeing the required safety levels. STRATOFLY project arises in a European research landscape, with the aim to design a hyper-fast passenger transport aircraft. It will perform antipodal flight path in the lower stratosphere (approx. 30 km), at a cruising speed of around 9000 km/h (about Mach 8). By 2035, vehicle concept (MR3) will have to reach the ambitious goal of Technology Readiness Level of six; in other worlds to demonstrate technology in an industrially relevant environment. The purpose of this thesis is to expand aerodynamic database of hypersonic airplane concept MR3, through aerodynamic characterization of all control surfaces. Since we are interested to collect a large amount of data and in a wide range of speed, a simplified method, based on "compartmental approach" was used. Inviscid flow analysis were performed by means of CFD, by using Ansys Fluent; this approach is intended to be a higher order simulation than even before. This work represents a solid starting point because it provides useful data for future evaluation about flight mechanics and trajectory optimization, inasmuch an extensive study like that was never conducted, so far. The structure of this work is arranged in a logical way. In the first chapter an historical perspective is given, so as to understand great difficult and milestone attained over time. Than a description of what STRATOFLY project is and a close-up overview of the concept airplane, in order to know how it works. In the third chapter a brief

illustration of what numerical methods are and how they work. "CFD analysis" chapter represents the core of this work; it was discussed on models chosen and the following analysis that was conducted. Thesis work was conducted in close contact with Centro Italiano Ricerche Aerospaziali (CIRA), which has a significant role in STRATOFLY project, as well as Polytechnic of Turin.

Chapter 2

Historical perspective of hypersonic flight

First airplane in the world was Wright Brothers' Flyer I, that flown for 3 seconds only and at speed of 11 km/h. Since that point, many designers were interested about flight machine, so an exponential development in that field occurs. In addition, to improve the aerodynamics, they focused on the optimization of internal combustion engine till than; this led to develop particular shape like radial engine. Hence, maximum speed in flight significantly improved and thus for aeronautics meant new opportunities. Julian Allen made an important observation in the 1958, 25th Wright Brothers Lecture: "Progress in aeronautics has been brought about more by revolutionary than evolutionary changes in methods of propulsion" [12]. In fact, with the advent of jet engine, long duration flights became feasible, so airline industry arose. The Second World War was an important incubator of aerospace concepts. Designers "were pushed" by governments to design terrible flight machine able to end the conflict. In the following years the interest shifted on conquest space, in order to impose its own supremacy all over the world. This challenge led to rely on rocket engine: it was the only one who could supply sufficient thrust, although was unreliable and tended to burst. In post-war period, two approach were undertaken: first was to use rocket engine for a vertical ballistic launch or to fit it on an airplane. From the latter, X-series research program arose, with the aim to investigate on technical limit of speed and altitude for airplane. After multiple attempts, in 1947 Bell X-1 was able to overcome "sound barrier". It looked like Browning .50-caliber machine gun bullet, known to be stable at supersonic speed. Through B-29 Superfortress mothership was drop launched and equipped by XLR-11 rocket engine, powered by liquid hydrogen and ethyl alcohol, attained Mach 1.06. Thereinafter many technical improvements were done on following airplane. Thanks to many test it was noted that when airplane reached high speed, stability was impaired severely, control surfaces were ineffective at sub-orbital altitude as well as aerodynamics was unappropriated. In order to stabilize high-speed flight several

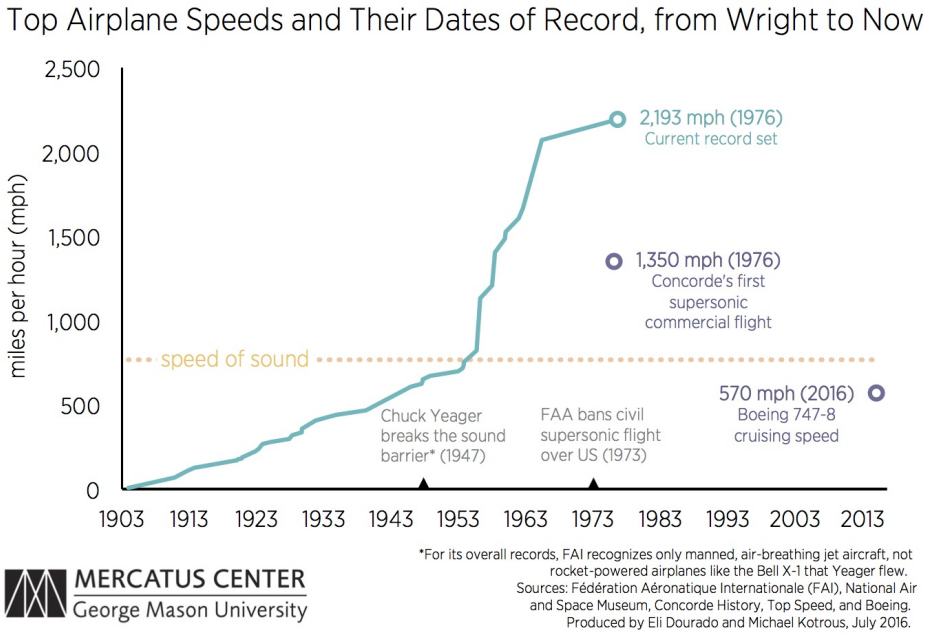

Figure 2.1: Airplane speed during the years.

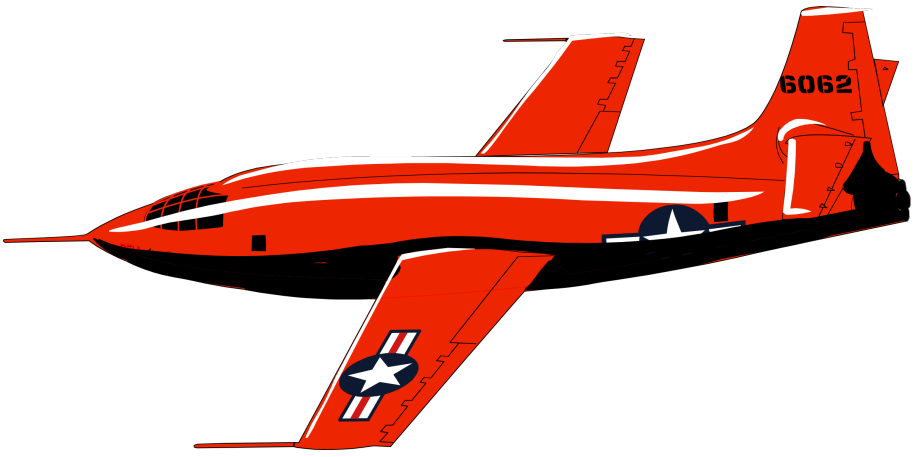

Figure 2.2: Bell X-1 was the first manned aircraft to exceed speed of sound.

changes were done. North American X-15 was equipped by a stability augmentation system, reaction control system (RCS), that used rocket thrusters at high

altitude, and wedge-fin (dorsal and ventral). New high-resistant material, Inconel, was employed for most exposed area thermically. Equipped with more powerful rocket engine (than X-1), the X-15 achieved records as the first "airplane" to reach hypersonic speed and higher flight altitude, Mach 6.7 and 107.8 Km respectively.

In 1955 the US Air Force involved aircraft industry to develop manned, hypersonic, rocket-powered, bombardment and reconnaissance weapon system. Above all, long-range spaceplane turned out to be interesting. The design requirements were to circumnavigate the globe and attain minimum altitude of about 30 Km (100000 ft). After different proposals, boost-glide concept was chosen, even though details of configuration were unknown. At that time status of research on material technologies was lacking and rocket engines weren't reliable enough to allow a safety factor for manned vehicle. There were different set of problem as well. Navigate systems required gravitational and geodetical information to reach the imposed target. The effect of Earth's rotation could not be neglected at hypersonic speed and high altitude. Thermodynamic properties of the atmosphere were studied in order to develop a right heat resistant framework Thus arose Dyna-Soar X-20 (dynamic soaring) program, with the aim to develop a hypersonic manned test vehicle, that was designed to obtain data beyond X-15 flight envelope and to evaluate military subsystems. A typical mission profile for X-20 included to be boosted from Cape Canaveral by means of Titan launcher until 320000 ft and velocity of 24.470 ft/s. After separation stage, glide stage took place for 107 minutes and landed at Edwards Air Force Base. Dyna-soar shape was chosen by two different approach: a ballistic shape configuration, with low lift to drag (up to 0.5), that found affinity with Mercury program[1], or lifting body, that concerned a glide path with a high lift to drag ratio (about 3.0). This meant a big quantity of data collected and a widest selection of landing sites available. However the latter case presented design problems. Hence, it was decided a middle way in order to have a feasible approach: a medium lift-to-drag glider in the range of 1.5 to 2.5. The glider was conceived as low wing delta shape vehicle. The framework was to build of René 41, just like panels on top surface, which would withstand a temperature of around $1000°C$. Because of intense heat flux generated on bottom surface, molybdenum sheets were to chosen, designed for a maximum temperature of about $1500°C$. Nose cup was the most thermically stressed component of whole vehicle. It was to be manufactured of graphite with zirconia rods. At the time there were different aims to be achieved: exploration of the maximum heating areas, knowledge of manoeuvrability during glide phase, demonstration of conventional landing and evaluation of the ability of human being to fly at hypersonic speed. In addiction testing military subsystems as high-resolution radar, infrared sensor and air to fly missiles. After further postponement due to limited budget and limited technological maturity, the project was

[1]It meant much money to invest

Figure 2.3: Boeing X-20 Dyna-Soar:one of the first spaceplane programs.

cancelled in 1963. This pioneering program was unable to fly and very expansive.

Actually, in the late 30s, German Eugen Sänger and his wife Irene Bredt had already conceived a sub-orbital bomber, with the goal to cross the Atlantic sea; it was called Silbervogel. This concept took advantage of futuristic aspect: arising rocket engine technology blended with lifting body principle. The first was useful to reach high altitude in short time, the second one was to increase range of operation. In addiction, re-entry from space was to take place through skip re-entry technique, for which it was to execute a series of skips, allowing the range to be further extended. In order to optimize early flight phase, spaceplane would had to take off horizontally by means of rail track, powered by rocked sled. Be able to provide a certain initial velocity to cratf was an advantage because of heavy weight of airframe. Due to lacking of heat-resistant material and rough methodologies for re-entry parameters, the design never went beyond mock-up test.

Although Dyna-Soar program was set aside because of tremendous cost and other, rocket airplanes (X-15 for example) weren't able to reach considerable range. It became apparent that lifting body was the key to success because of great versatility. Lifting body study was derived from blunt body theory, developed ten years before, that was characterized by high-rounded noise, useful to dissipate more efficiently heat, even if re-entry trajectories limited (lift to drag ratio far less than 1) and high deceleration weren't suitable for manned flight. M2-F1 was the first lifting body, characterized by triangular shape that gave birth "flying bathtub" or "flying

flatiron" names. The weakness was lateral-directional stability at subsonic speed, in fact pilots experienced dangerous feelings induced by Dutch roll. Adding bodyflap (flap on the back surface of fuselage) and third vertical stabilizer, improvements were remarkable (M2-F3) [5] vol III.

Figure 2.4: NASA lifting bodies. From left X-24A, M2-F3 and HL-10.

Another lifting body developed and tested was the HL-10 (Horizontal Landing-10). Since the beginning, it was clear that this craft was the most successful. Indeed the future Space Shuttle had to look like HL-10 [5] vol.I It was characterized by a flat bottom and rounded top; was an inverted airfoil in cross-section, with a delta planform. As the previous craft was equipped with three vertical fins, useful to improve stability characteristics. At the beginning, flow separation behind outer vertical fins was a severe problem occurring in lateral control. Later, it was modified the leading edge of the fin, so the craft exhibited acceptable transonic and supersonic handling characteristics. As well as NASA, the U.S. Air Force went in the same direction. It was interested in the lifting bodies. At the beginning they studied several shapes: some having variable swept wing configuration (variable geometry), useful to employ a variable-sweep wing in the upper atmosphere airplane, to increase lift to drag ratio and simplify landing approach. "Interference" configuration was additional type of shape for craft. The undersurface was designed to create shock wave (at high speed) to increase lift force. This type of configuration took the name of Waverider. Even though these shapes well aerodynamically performed, it wasn't accounted for heating problems [5]. From previous works, the X-24A took shape. It was conceptually different from the other lifting bodies because it had

positive camber, in cross section, in spite of negative ones. However this version of craft was lacking in stability because rocket exhaust plume impinged on the craft, causing nose-up condition. The improved version of previous craft was X-24B, that, in spite of name was completely different from its predecessor. The aerodynamics relied on double-delta planform, highly swept wing. Bottom surface was made up by a sloping 3°nose ramp for hypersonic trim, and flat in the terminal part. While the top one was characterized by a boat-tail for favourable subsonic lift to drag characteristics. It was powered by XLR 11 rocket engine like previous rocket plane. The tester pilots were extremely satisfied by handling quality of flight at all speed ranges, also without engaging the control dampers. Indeed X-24B earned a rating of 2.5 on the Cooper-Herper pilot rating scale [2] (best value reachable is 1). Although those concepts were manufactured for reaching hypersonic speed, didn't attain that velocity because they were technological demonstrators. However, ground test were carried out at certain speed (until was possible)[5] vol. II. Aforementioned studies, both on lifting bodies and on rocket airplanes (X-1, X-15 and other) laid the foundations for future spaceplanes such as Space Shuttle, since it was established that no needed engine for landing stage. Veicoli costruiti riusabili [1]. During the 50s and 60s hypersonic vehicles were in early stage. Much activity aimed to explore possible configurations and dealing with particular conditions, problems arose. Experimental aircrafts were built to acquire flight data. That activity ended early in the 60s and restarted with other program. The Space Shuttle was the first concept of reusable manned vehicle ever built for operational activities. It represent an ambitious and important milestone in the Space program for different reasons. Versatility was its primary characteristics. Thanks to five vehicles it carried out several missions in orbit, as to deliver space station modules to the International Space Station and it allowed to install corrective optics on the Hubble Space Telescope. Another SS capability was to launch interplanetary probes (Magellano probe, Galileo probe and Ulysses probe) and it was used for performing research in microgravity environment. The system could take off vertically by means of four parts: the bullet-shaped external tank (ET) containing liquid hydrogen and oxygen for SS main engines. Attached to the tank there were two solid rocket booster used to perform necessary lift in the lift-off early stage and the double-delta-winged orbiter. After having reached a certain altitude boosters separated and recovered in the ocean for reuse. Meanwhile, the orbiter and ET continued the ascent phase. When propellant was combusted in the SS engine, another separation took place and thus orbiter reached orbital altitude. Thanks to thermal protection system the orbiter could face atmosphere re-entry. Moreover it could horizontal landing because of its lifting body.
In spite of two catastrophic accident (Challenger,1986 and Columbia, 2003) it was safe enough to attain space every few months, after maintenance. It was the space

[2]It is a pilot rating scale to evaluate handlings capabilities of an airplane.

Figure 2.5: Space Shuttle during lift off.

program more durable in the history, over forty years of operation. In the whole life Space Shuttle was accomplished 120 missions which results in a loss rate of 1.7% (1 in 60), typical value of unmanned space launch vehicles.

At that time rocket propulsion had the potential to reach space, but wasn't suitable for hypersonic flight around the world; it was needed a different approach to the problem. By the 1970s the coming of scramjet engine had produced beneficial effect for hypersonic craft because it had a good specific impulse than rocket engine, even though couldn't operate at low Mach number, so an hybrid air-breathing engine was to be used.

NASP (National Aereo SpacePlane) was an integrated aircraft program that aimed to design and build two research aircraft called X-30, at least one of which was able to attain orbit by flying autonomously in a single stage at speeds up to Mach 25 (18500 miles per hours). A vehicle capable to attain space in a single stage and reuse it, would permit an affordable results, in order to limit costs and making sustainable and accessible space flight.
From the beginning, it was clear that goal of the NASP program was so challenging because of high financial burden and pioneer studies. Thus, to limit the costs it was proposed an "incremental approach", whereby existing technology would be

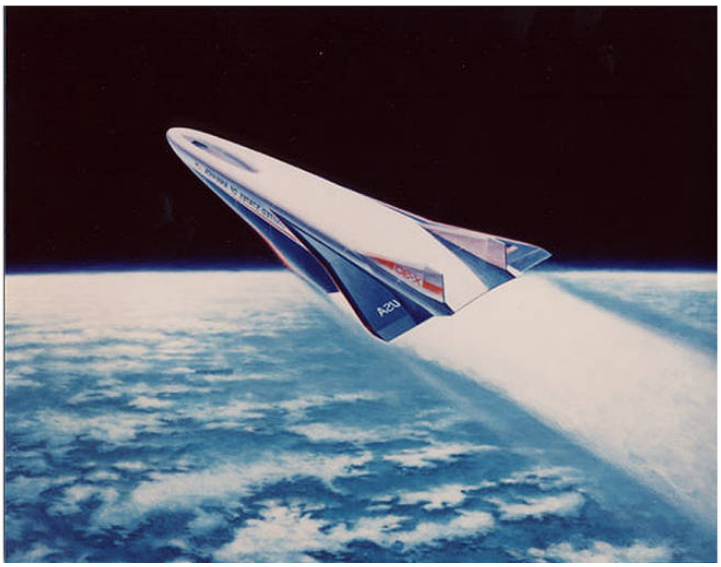

Figure 2.6: Rockwell X-30: NASP spaceplane.

used to achieve certain milestones, in a design and manufacture stages, introducing step-by-step advanced technology. Moreover NASP program was developed by the interaction between different parts including McDonnell Douglas, Rockwell International, General Dynamics, Boeing and Lockheed and Universities in such a way that it employed all resources. The first vehicle provided performance during low speed flight test and the data gathered were useful to take right direction in design. Only the second aircraft would be capable of Single Stage To Orbit (SSTO) flight since adjustments was undertaken. An example of this was the use a mock-up with some rocket boosters to attempt small experiment. Because of no large-scale test above Mach 8, the design and operability was carried out by CFD codes with supercomputers. The X-30 would utilize a multi cycle engine system composed by a low speed subsonic propulsion unit, a mid speed ramjet and then a supersonic combustion ramjet (scramjet). This kind of choice arose in the face of previous study by US Air Force that would combine airbreathing engine with rocket, and NASA with a turboramjet-powered aircraft. The benefit of using combined cycle air-breathing propulsion engine was due to more operational flexibility and an order of magnitude reduction in vehicle gross weight and cost, compared to a rocket-powered vehicle for the same payload weight. Indeed, using a resource directly available in nature, it is more convenient in comparison to take it in a tank. NASP vehicle would use oxygen from the atmosphere (employing air-breathing propulsion). This led to extend flight time because of take-off phase is slower than vertical lift-off (typical of rocket stage propulsion), so generate high thermal stress on airframe. This problem was damped with a cold fuel that could cool the structure through active cooling system. It was developed a particular version of liquid hydrogen, called “slush hydrogen”, a version

with a better density value, more easily to store[3]. New engine architecture and new type of fuel gave origin to potential ozone damage by gas exhaust. Another problem was the sonic boom effects on people and animals, but with a careful trajectory, the latter problem was reduced. There have been several technology advances, especially in materials. Titanium alloys was used as the baseline for the fuselage. Titanium aluminides had great potential for use in leading edges and critical heat areas, indeed withstand up to 900 °C. Another material chose by NASP committee was the carbon-carbon composite with protective coating that showed exceptional potential for use as a light, heat-resistant shell covering. It's very important give priority at materials since they defined the weight of the vehicle, but also affected the coolant flowpath, thus combustor efficiency, and even trajectory. Materials advances are fundamental in hypersonic flight because they affect the design and performance of the engine, the weight of the aircraft and the ability of leading edges that are stagnation points for flow field, to withstand high temperature. Thanks to NASP program substantial advances had been achieved in several fields: inlets, combustor, fuel tanks, CFD codes, materials and liquid hydrogen fuel. Although the program was cancelled in 1994 for huge cost and small improvements on scramjet engine. X-30 has never been manufactured, only test models. However, that will allow a broad basis for future hypersonic vehicle. Moreover, to gain importance towards space, routinization of space launch entail the generation of new opportunities for economics business like satellite and communication activity, science missions, new transport systems and space tourism. In addition, this perspective would produce collateral business that are currently unknown.

The increasing interest to air-breathing propulsion led to develop new engines for hypersonic vehicle. If on one hand low air density meaning low level of oxygen to be burned for combustion so it's difficult to generate necessary thrust, in the other hand, it's valuable in order to carry on board less oxidizer and so the vehicle can be lighter. Hydrogen has been used for fuel to have less environmental impact. It is clear that fully autonomous spaceplane must be able to reach orbit without some support. Therefore, air-breathing propulsion combine with right aerodynamic shape leads to perfect bond in atmospheric transition before spaceplane attain space. The X-43A's engineers designed the aircraft's airframe to be part of the propulsion system: the forebody is a part of the intake airflow, while the aft section functions as an exhaust nozzle.

Scramjet (Supersonic combustion ramjet) is the most suitable air-breathing propulsion for hypersonic applications, studied by engineers from early 70s. In addition, there are other benefits. It's safety, robustness and it offers wide mission flexibility at a low operational cost [12]. The advantage in terms of specific impulse is well highlighted in fig.2.7, in comparison with rocket engine.

[3]It is a combination of liquid hydrogen and solid hydrogen used to increase the density

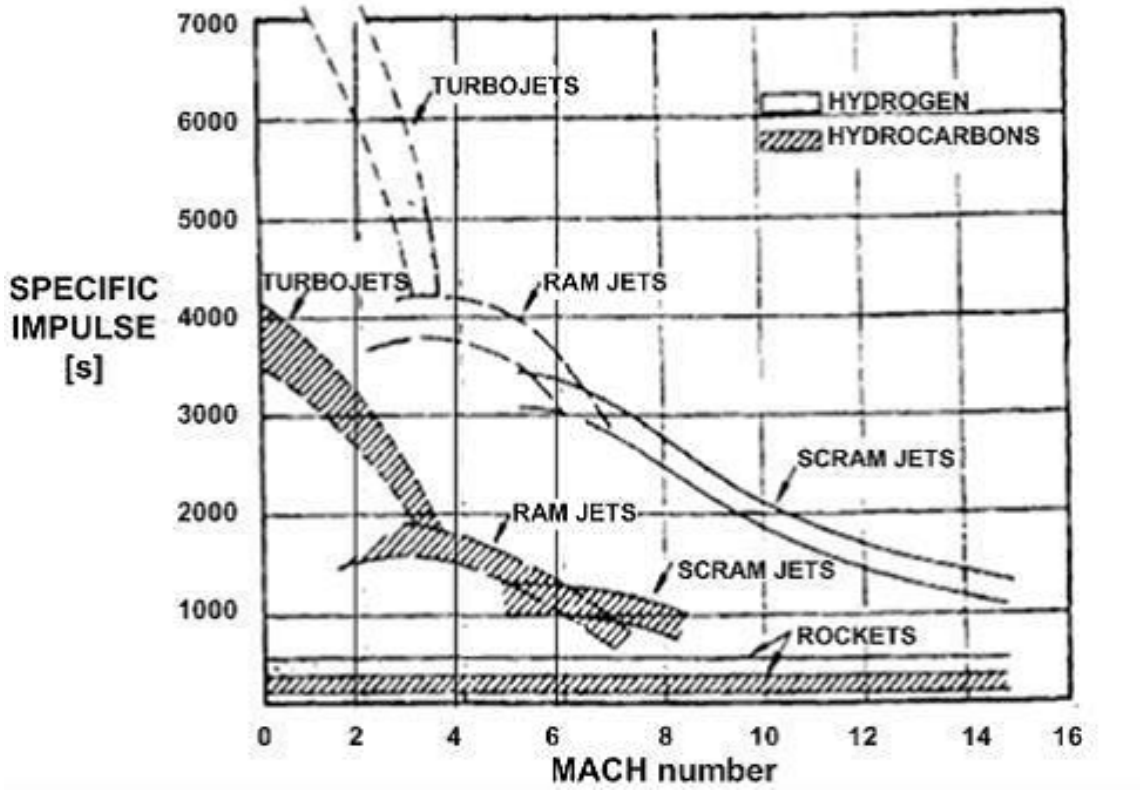

Figure 2.7: Specific Impulse of several kinds of engines as Mach function [3].

Following the cancellation of the NASP in 1994, US lacked hypersonic technology development program. Therefore, cheaper NASA Experimental vehicle X-43 parts of Hyper-X program, inherited NASP technologies. It arisen a hypersonic air-breathing demonstrator called X-43. The goal not only was to validate scramjet propulsion but also test hypersonic aerodynamics and design methods. It was an unmanned lifting body capable of being fully controllable in high-speed flight, even in gliding phase (without propulsion). For the first time a scramjet engine was accommodated on board of the X-43 (Hypersonic Experimental Vehicle). Scramjet engine works well from Mach 4.5 or higher, so the vehicle was coupled with winged rocket, launched by mother aircraft, for attaining the right speed and altitude. During flight test, the vehicle was well instrumented, with over 200 measurements of surface pressure; over 100 thermocouples to measure surface, structure and environmental temperatures; and discrete local strain measurements on the hot wings and tail structure. Internal engine instrumentation was more dense in order to capture internal flow details of the engine. Incredible achievement has been attained by X-43A version. Even thought first flight was a failure, after several changes, in flight 2, X-43A reached Mach 6.83 to 95000 ft. [12]. In the last flight previous speed record has been broken,

the demonstrator reached Mach 9.68 to 110000 ft by 11s of engine operating time.

The direct successor of X-43 is the X-51 waverider. This fact shows increasing interest on hypersonic technology. This project arises by different cooperation between DARPA, NASA and more. The vehicle is a scramjet engine demonstrator that based on different aerodynamic configuration. Indeed, it is able to generate lift by means of shock waves on the ventral surface of the fuselage. Moreover, scramjet was tested with a hydrocarbon fuel: JP-7, unlike its predecessor. The X-51A engine has performed for 210 seconds of 240 seconds for total flight time, after separation form rocket booster (carried by B-52H). After that, the vehicle started with gliding stage for 5 minutes () and splashed down in the Pacific Ocean, approximately 340 NM downrange [10].

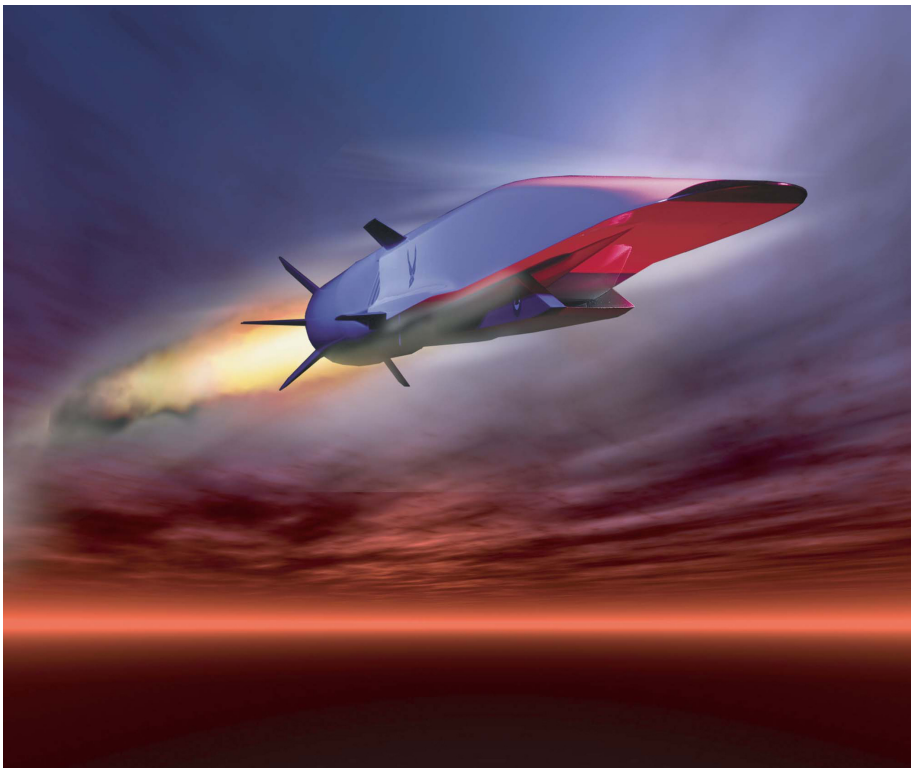

Figure 2.8: X-51 Waverider, hypersonic demonstrator.

The interest in hypersonic technology is spreading like wildfire in other country all over the world. Many research centres are interested to reusable, affordable space access. The first successful flight test of a Scramjet engine was performed by Russia in 1991. It was developed in late 1970s by Central Institute of Aviation Motors (CIAM). It was an axisymmetric hydrogen-fuelled dual-mode scramjet accommodated in front of SA-5 surface-to-air missile. The maximum flight velocity greater

than Mach 6.4 was achieved and Scramjet operation during 77 seconds was demonstrated. These flight test series also provided insight into autonomous hypersonic flight controls. The Defence Research and Development Organization (DRDO) are leading an hypersonic program. It is based on a hypersonic unmanned demonstrator powered by a scramjet engine. Recently scramjet has been tested. After having sustained hypersonic combustion for 20 seconds, it reached 7200 Km/h (2 Km/s). This technology will be able to use for long-range cruise missiles and civil applications such as launching satellites at low cost.

Also in the rest of world was interested to develop a spaceplane. In Europe the response behind a winged, reusable, manned spaceplane arrived soon after Space Shuttle development. By French propose and later helped by European Space Agency (ESA), Hermes should be able to lift six astronauts and 4550 Kg of cargo in Low Earth Orbit (LEO) by means of Ariane 5 launcher. Original load capability was reduced to three astronauts and 3000 Kg of cargo in order to add ejection seats for more safety and acting in response to Challenger fatal accident. But in 1990s, Europe, Russia and United States of American cooperated to build the International Space Station (ISS). The astronauts was carried by Russian Soyuz or American SS and this event marked the end of Hermes program (1993).

Figure 2.9: European spaceplane Hermes.

A few years later, Europe has continued to maintain interest on orbital re-entry vehicle in order to gain in-flight relevant experience for European future launcher and to improve knowledge on re-entry systems. This interest has given rise to Intermediate eXperimental Vehicle (IXV). It is a prototype unmanned reusable spaceplane based

on lifting body shape with two flaps on the back and thrusters for attitude control. The spacecraft attain suborbital speed through Vega launch system and land on its own. The IXV mission performed on February 11^{th} 2015 with success. The direct successor is the Space Reusable Integrated Demonstrator for Europe Return, Space RIDER. It will have the capability to allow experiments in microgravity, such as radiation exposure of materials and deploying small spacecraft. The in-orbit stage of maiden mission will last two-month, than Space RIDER will return to Earth with the payloads stowed in its cargo bay. It's a project strongly promoted by European Space Agency, ESA, and cooperation of Italian Space Agency, ASI, and several European partners such as Italian Aerospace Research Centre, CIRA. It is notable that a strong interest comes from by pharmaceutical industry for testing and developing new molecules. By 2025, the ESA plans to privatise the Space RIDER, with Arianespace like operator.

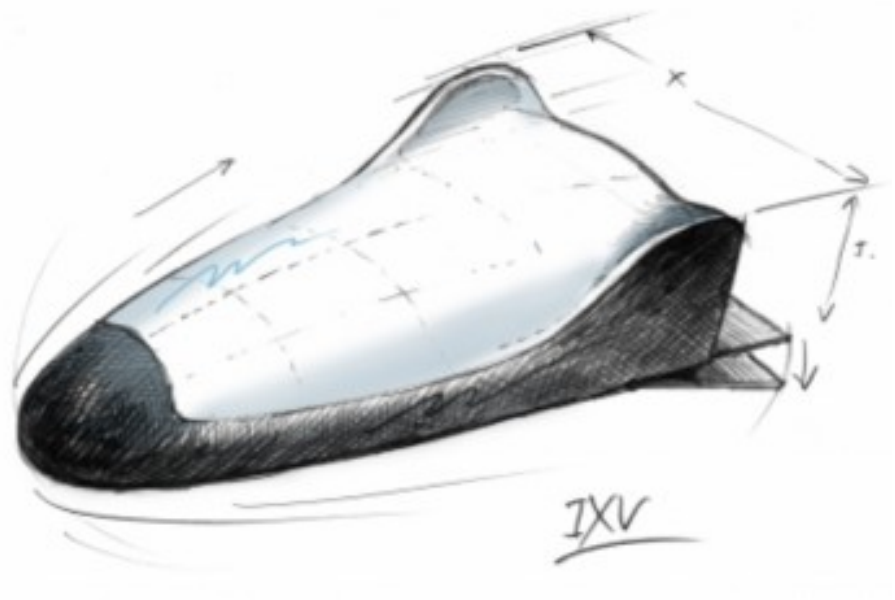

Figure 2.10: Experimental suborbital re-entry vehicle.

Hypersonic technology can find different business interests. Moreover, great importance is given to space exploration, indeed several awards have arisen. X-Prize Foundation is very active in this field. In 2004 it offered 10 millions of dollars prize for the first non-governative organization to launch a reusable crewed spacecraft into space, reaching about 100 km by Earth's surface, twice within two weeks. Ansari X Prize was won by the Tier One project designed by Burt Rutan and financed by Paul Allen, using the experimental Spaceship One. This spaceplane is powered by hybrid rocket engine that it is activate when vehicle has reached an altitude of 15 Km by means of its mother ship (manufactured ad hoc). During flight test

spaceplane was able to break previous altitude record, flying until 112 Km. This project have inspired future trends like space tourism. It is an attractive trade that it is encompassing more and more entrepreneurs. In the wake of Ansari X Prize' s winner, it has manufactured SpaceShipTwo almost ready for future operational flights. Now the ticket price for take part to revolutionary suborbital flight is about 250000$.

Figure 2.11: Suborbital spaceplane SpaceShip Two.

2.0.1 Commercial hypersonic transport

According recently market forecast for air transportation, it is necessary increasing flights all over the world. Therefore, next generation airliners will have to be affordable, sustainable in time and faster than current aircraft. Moreover, you need to find other flight paths in order to optimize air traffic control. In the early 70s, first step in this way was done. Concorde was a supersonic passenger airliner as well as his Russian competitor Tupolev Tu-144. Both aircrafts could be flight in the lower stratosphere (above normal routes) about Mach 2. For expansive operational cost and other problems, it was retired. However recent interest on this field is remarkable. Different companies are developing supersonic aircraft oriented to executive transport such as Boom. As your web site declares, this corporation has signed contracts to guarantee 30 supersonic airliner. Nowadays the concept of hypersonic passenger aircraft is spreading very fast as well. The focus on hypersonic flight is very high because of several technological spin-offs that there are going to be. In the future space exploration such as on Mars, different stage of the mission will be at hypersonic speed. It would be the link between aeronautics and space.

When we are talking about hypersonic flight, several things happen. Flow field is characterized by shock waves very close to the vehicle surfaces that interact with boundary layer. Than materials are very thermically stressed cause kinetic energy of flow is high. Finally, classic propulsion architecture does not provide enough thrust. By considering such efforts, if great progresses have been achieved on the side of the technological insights in most of the areas covered, very poor results were obtained in terms of realization of operational products [6]. This section aims to give an overview on recent researches and future trend about hypersonic passenger aircraft, with a special focus on the European projects underlie H2020 STRATOFLY Project. HyPlane is a six seats hypersonic airplane with the capability of accessing to stratospheric by integrating aeronautics and space technologies. Unlike SpaceShipTwo, it will perform autonomously horizontal take-off and horizontal landing, even though maximum altitude will be 65 Km (SpaceShipTwo above 100 Km) and Mach 4, enough to provide the sensation of weightlessness for some minutes or hypersonic transcontinental airliner. Propulsion system is based on combined-cycle Rocket/Turbine engines. It has chosen a small passenger plane because is relatively easy validate a sustainable operational concept, unlike other commercial designs that tended toward large aircraft. HyPlane is developed by University of Naples Federico II in collaboration with the company Trans-Tech. This shows that European project on hypersonic plane are high.

Figure 2.12: HyPlane.

The Japan Aerospace Exploration Agency, JAXA is working on different topics about hypersonic plane with Sky Fronter project. The main focus of the research

is the development of a hypersonic turbojet engine, fed by liquid hydrogen, that can operate totally from take-off to Mach 5 cruise. Because of air temperature at the intake outer area is very hot ($1000°C$), we are adding a pre-cooler for decrease temperature to about $300°C$. In this way, following combustor can work better. The flat-shaped aircraft holds 100 passengers flying at an altitude of about 25 Km. According to project constrains, airplane is able to transport passengers until 9000 Km away from the point of departure. In the same program, D-SEND project is aiming to reduce "sonic booms" thanks to suitable airframe configuration. Although this study is conducted on supersonic aircraft, in the future it will be worthy for hypersonic airplane.

In 2018 Boeing showed a new hypersonic passenger plane concept that can be military and commercial applications. The plane will be capable of traveling as speed above Mach 5 by a turbofan engine properly modified. Although the airplane is just a concept, it is possible see it flying in 20 or 30 years, when routinization of hypersonic transport will be achieved. This plane will be similar to JAXA's hypersonic airliner.

Several example of hypersonic craft has been showed. it means that a great interest in this kind of technology is deep. In fact, this thesis is supported by Kirkham F., and Hunt J.[6]: they have computed productivity index based on the average number of miles in the same amount of elapsed time, the hypersonic commercial transport should be twice as productive as subsonic transport, in the worst case. It becomes 2.5 times higher, if overland flight is permitted.

Chapter 3

Hypersonic technology EU Co-Funded projects

Since the first studies undertaken on hypersonic transport technology like Hermes project, interest in this kind of field has continued. Multiple analysis have been done by research centres, universities, companies and with support of European governance. The results have brought a wide know-how in hypersonic flight Wide pool of data provide the basis of ongoing H2020 STRATOFLY Project. Incremental approach has undertaken. Going in chronological order, main projects are LAPCAT-I, LAPCAT-II, ATTLAS-I, ATTLAS-II, FAST20XX and HEXAFly. The Long-Term Advanced Propulsion Concepts and Technologies, LAPCAT, was thought to reduce travelling time of long-distance flights. This goal can be archived if Mach cruise number is ranging from 4 to 8. It is clear that main challenge is about affordable high-speed propulsion. So, for this project is worthy to assess different turbine and rocked-based propulsion cycles and concepts. It was regarded ram-compression and active compression in particular. Then, the focus was addressed to heat exchangers, airframe/engine integration optimize, mass-efficient turbines and supersonic combustion experiments and modelling development. Only two of several vehicle analysed were further investigated. The LAPCAT-A2 is a hypersonic aircraft concept knows how to attain Mach 5 in cruise condition by turbine-based combined cycle (TBCC) with pre-cooler. It's based on ramjet engine for supersonic and hypersonic flight, and it has high bypass features for greater efficiency: it's named Scimitar engine. The thrust is powered by four hydrogen-propelled Scimitar. According to Reaction Engines Limited (engine manufacturer) TBCC engine specific impulse is 4170 s, SFC 0.86 lb/(lbf h), good value in comparison with rocket engine.

The second outcome of LAPCAT-I project is based on very faster vehicle than previous: LAPCAT-MR1 can attain a cruise speed of Mach 8. The aim was to perform good aerodynamic characteristics both hypersonic and subsonic. Two kind of propulsion was integrated: an air turbo-rocket for initial stage until it reaches

Figure 3.1: LAPCAT A2 Mach 5 hypersonic transport airplane.

Mach 4. Than a dual mode ramjet propulsion unit activates to thrust until Mach 8 cruise speed. Hydrogen-propelled propulsion unit is puts on back dorsal area preceded by large intake ramp. The aerodynamic performance is based on blended waverider and delta wing concept. The GTOW is fixed at 600 tons. Moreover a kerosene Mach 4 cruiser was analysed based on 250-passenger, Mach 4 civil transport performed by NASA and Lockheed study in 1990. It is a very high swept wing integrated with slender fuselage with four engine settled on ventral fuselage. [

The conclusions summed up that low specific energy of hydrocarbons is not well suitable with high speed and long range flight. Mach 4.5 seems to represent upper limit for Kerosene as fuel while hydrogen makes the aircraft lighter. However intrinsic low density leads to a really long airplane in order to accommodate whole volume of fuel. A range of 20000 Km can be achieved according to realistic routes. Mach 8 vehicle seems to prove a good performance with ATR (Air Turbo Rocket) coupled with DMR (Dual Mode Ramjet). LAPCAT-II involved 16 partners representing six European member states. As the Mach 5 concept had a higher maturity in its conceptual design, it was retained for the next phase of LAPCAT. The same level of maturity could not be achieved for the Mach 8 vehicle. This concept is characterized by high level of propulsion-fuselage integration and this influences overall performance deeply. Indeed they had considered four different concepts:
-an ONERA design based on the PREPHA re-usable launch vehicle; -a more classical vehicle with a ventral engine from ULB/UNIROMA; -an axis-symmetric design from MBDA; -a wave-rider concept from ESA. The first two concepts were merged

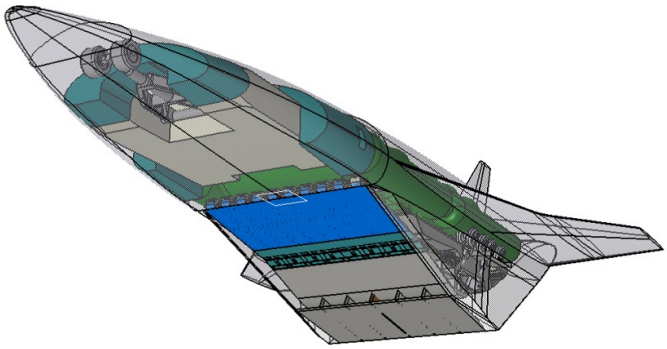

Figure 3.2: Overall layout Onera derived airplane.

to define a new turbo-based vehicle, They were aimed to develop new technology for hypersonic air-breathing propulsion system by means of numerical simulations and test on intake, combustor, injector and nozzle. Originally, the vehicle was to accelerate to M 1.7 by rocket engine, and continuing with dual-mode ramjet. This kind of vehicle could not reach a long distance, a TBCC engine was proposed to replace rocket engine. They were done several kind of studies in pre-dimensioning stage. After they designed air intake geometry and analyse the transition phase between turbo-engine mode and ramjet mode. They showed that it quite difficult to generate necessary thrust from TTBC while closing their intake. Finally they carried out a nose to tail simulation in order to assess the effect of bleeding in fuel-off and fuel-on conditions[11].

The MBDA concept is an unusual sharp vehicle with translating cowl dual mode ramjet (DMR), inspired by NEO axisymmetric nano-launcher. DMR can burn either hydrogen or hydrocarbon in the range M 1.8 to 8. Its operation is distinctive, in fact the vehicle must turn 180 degrees around its main axis, in a way that ramjet engine operates in right way. During first flight stage, thrust generated by hydrogen-fuelled turbojets derived from GE90, after considered different proposals.
Finally, MR2 is based on MR1 concept, that is a waverider configuration with highly integrated dorsal engine. The air passes through a central elliptical intake with a ratio of semi-major to minor axis of 3. This geometry is obtained by a stream-tracing method. Air feeds propulsion unit, that is composed by six ATRs engine that is deployed during operation, below Mach 4. For higher Mach number a dual mode ramjet (DMR) combustion chamber is employed. Both engines generate thrust by liquid hydrogen.

Four iterations on layout are carried out until MR2.4 version. More focus put in cross-section design in order to reduce weight and increase structural stiffness. So strong coupled between airframe and propulsion unit is achieved. The planform area is 2365 m^2 with a span of $41m$. This dimensions led to encompass passenger cabin that has a total volume of 1200 m^3, divided in three areas. So, 312 seats can be

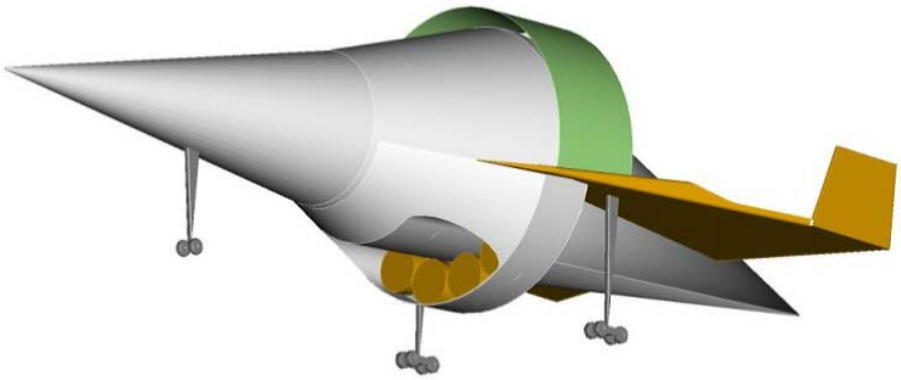

Figure 3.3: Layout of the MBDA Mk4 concept.

accommodate: 300 for paying passengers, 10 for crew attendants and 2 pilots. For the purpose of optimizing internal volume, integrated multi-lobe tank structure has been used. Different kind of antipodal trajectories have been considered. Classic mission performed by MR2.4 is Brussels-Sydney, believed to be feasible according to simulation program ASTOS 7. The flight time would be around $2h55m$. Also mission to Tokyo and Los Angeles have been simulated: $2h13m$ and $2h20m$ respectively. [11]

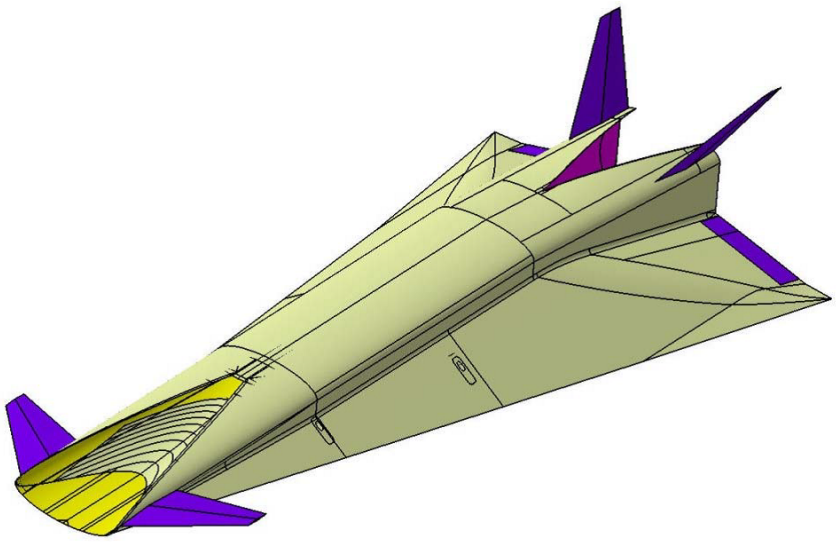

Figure 3.4: MR2.4 concept.

In order to validate and test high speed technologies for future flights, the High-Speed Experimental Fly Vehicles – International High-Speed Experimental Fly Vehicles – International (HEXAFLY-INT) was born. The goals of this project are designing, manufacturing, assembling and flight-testing an unpowered high speed

vehicle. Several kind of experimental investigations are based on: aerodynamic heating, flap and gap-flow separation, transition, shock wave boundary layer interaction, wake and corner flow, internal structure stress determination, internal health monitoring, free stream quantities derivation by Flush Air Data SystemFlush Air Data System (FADS) integration and visual vehicle status. Moreover to validate high temperature protection system, cold structures and sonic boom impact in gliding phase. It must be guaranteed a sub-orbital flight, having an apogee at 90 km, by means of Brazilian VS43 launcher. The experimental vehicle is constituted by two modules: the Experimental Flight Test Vehicle Experimental Flight Test Vehicle (EFTV) and the External Support Module External Support Module (ESM). The second part is used to provide control attitude at the higher altitudes, precisely above 50 km, because EFTV is designed for altitudes ranging from 27 to 33 km. At the upper stage of flight test, aerodynamic forces are negligible, so it is necessary control the vehicle by cord gas reaction control systems thrusters. When ESM no longer needs, it is separated, and so the vehicle continues flight independently [HEXAFLY]. The EFTV is equipped by avionic system, that it made up by inertial measurement unit, GPS, servo-actuators and a flight control computer. Also an in-flight measurement system is useful to acquire pressure and temperature data for post flight analysis.

3.1 STRATOFLY project

3.1.1 Aerodynamics

Aerodynamic affects consistently the range reached by vehicle, so to design a long haul aircraft, it is important optimize flow field around it. Another aspect considered to be important in overall performance is air-breathing propulsion unit, that must be integrated properly, in order to generate thrust. Later fact is non-trivial because in early historical works on scramjet propulsion were so difficult demonstrate that engine produced thrust, and not only drag.
Because of strict constrains, waverider approach is well suitable for hypersonic aircraft in so far as the aerodynamic efficiency is achieved. According to the meaning of Waverider, it can be easily imagine what happens. An attached bow shock wave, or nearly attached, is formed on the lower surface of the aircraft, so high-pressure area on downstream of the shock wave is useful to generate lift force (compression lift). To optimize shock wave shape is necessary that is attached along the outer leading edge of vehicle. This means to seal the high-pressure zone in such a way as to create a uniform flow field (downstream of shock wave) and exclude, or limit, cross-flow in this region. Waveriders have been considered for various types of missions including hypersonic cruise vehicles, single-stage-to-orbit vehicles, air-breathing missiles

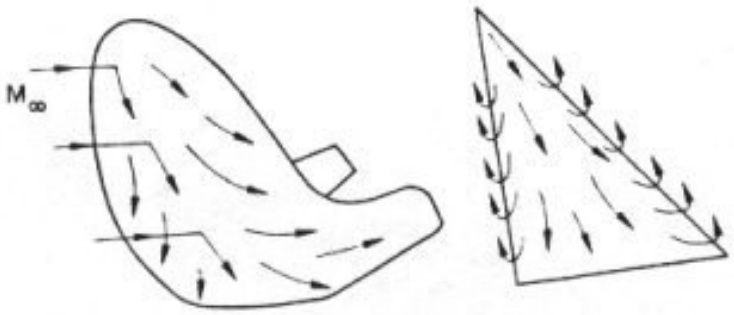

Flow spillage from convex and flat-bottomed vehicles.

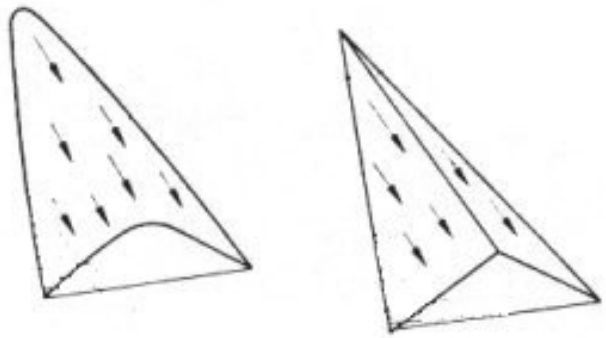

Flow containment by concavity

Figure 3.5: Waverider comparison with other high speed vehicle.

and various space-based applications [2]. Over the years, different waverider geometries have been proposed to improve engine-airframe integration. Basically it can be grouped in two main families [4]: -waverider forebody/inlet integration, the waverider is used only as the forebody of the vehicle to create a pre-compressed zone useful to improve intake performance; - waverider airframe/inlet integration, take advantage from pre-compression surface (bow shock wave) to use as the basis for the whole vehicle, including engine. Even though these two types on integration seems similar, in the second one, propulsion unit is regarded from the beginning and it is integrated completely with airframe. In spite of previous classification, waverider aircraft design is based on inverse methods. It considers for simplicity θ, β, M diagram, valid for supersonic wedge (2D), than for a given oblique shock wave angle (β) and Mach number (of upstream flow field), obtain unique deflection angle that turn out to be the lower surface slope of the aircraft. From this kind of analysis is obtained a Caret shaped waverider. This basic shape doesn't match with volume

efficiency.

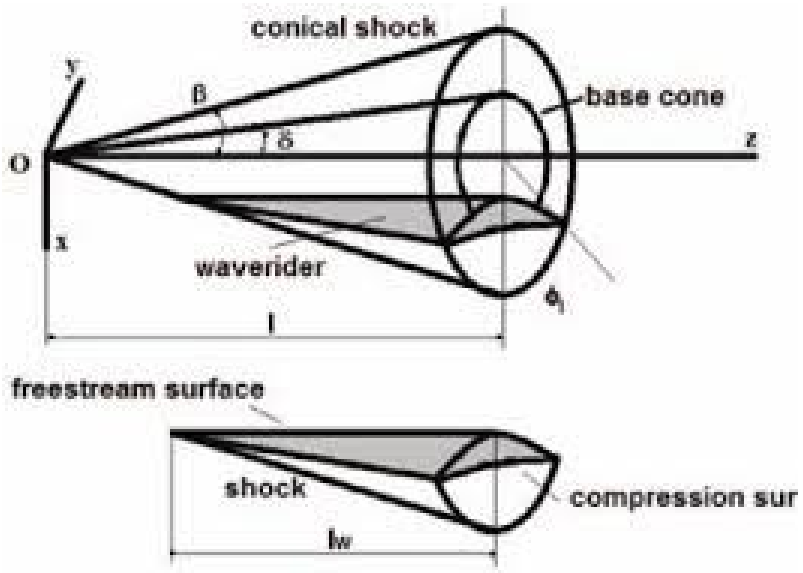

Figure 3.6: Schematic cone-derived waverider.

In 1983 Rasmussen has proposed a better solution in terms of volume efficiency as well as lift to drag ratio. The result is based on shock wave derived from the supersonic flow past a cone. Implicitly it has been considered design approaches along streamline direction but to design wingspan properly, can be used a spanwise design methods. Osculation cone design theory proposed by Sobieczky (1990) is to consider local 3D flow as a conical flow generated by osculating cone in that point. In such a way you can customize shock wave shape and so optimize waverider design to meet the project requirements (volume efficiency, unusual air intake). More versatility can allow to design non-axisymmetric shock wave pattern. In order to avoid pressure gradient in spanwise direction, Mach number and shock wave deflection must be constant in each osculation plane (along streamwise direction). To improve volume efficiency and further compress air flow can be used multistage compression method based on osculating cone. Along streamwise direction the bottom surface of waverider changes in local slope. Basically it is like having multi cone-derived ramps. Another family of this kind of spanwise methods is the osculating axisymmetric design theory. The 3D flow is approximate locally by axisymmetric flow in each osculating plane, no longer of conical shape. As Wang and Qian's study showed, osculating cone design theory and osculating axisymmetric design theory have better characteristics in terms of flow field uniformity, although high lift to drag ratio is higher in conical flow field theory. A further extension from previous theories is the osculating flow field design theory. Customized axisymmetric flow field can be chosen in each osculating plane. It is clear that the harder it is to manage complex

geometry and more computational cost is higher. According a preliminary study [4] based on compare osculating flow field theory with osculating cone theory, they demonstrated that first one method: improved streamwise lift distribution (reduced trim drag), increased vehicle volume, reduced viscous drag through delayed boundary layer transition and improved aft body close-out geometry. Another similar study, which is based on the same comparison, showed an increase of 7% in inviscid lift to drag ratio for waverider derived from osculating flow field theory.

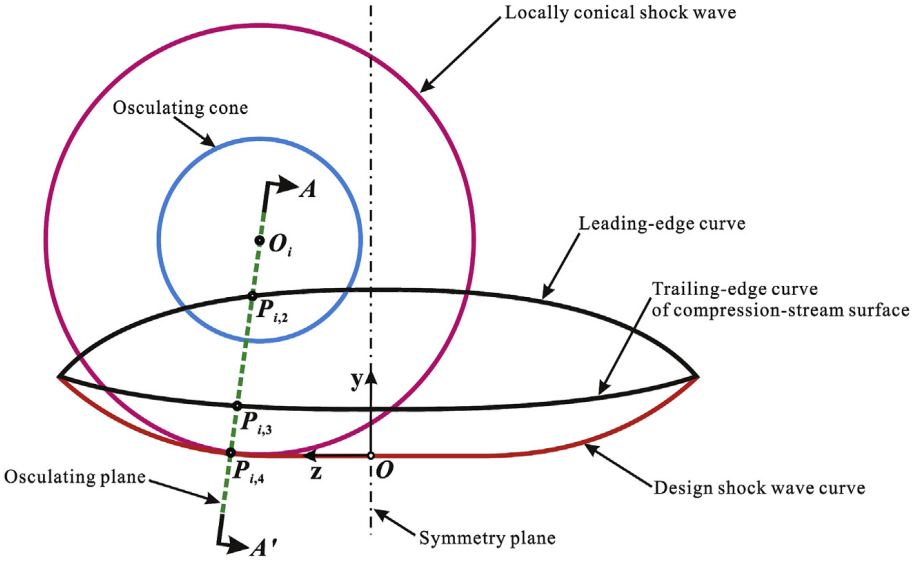

(a) Base plane of waverider

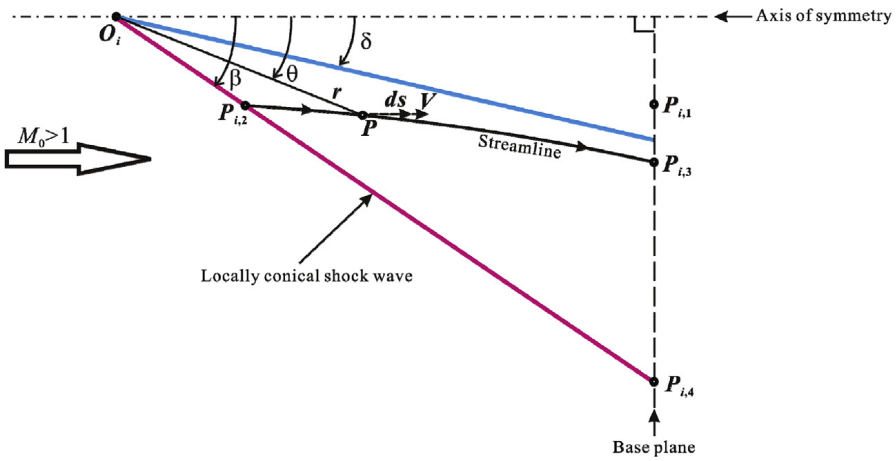

(b) Osculating plane (plane AA′)

Figure 3.7: Schematic illustration of osculating cone theory.

Waverider configuration has demonstrated to perform a worthy aerodynamic performance. In fact, in the early 1970s Kuchemann's studies showed a "lift to drag ratio barrier" for conventional hypersonic vehicles that it was overcome with the advent of first one configuration (waverider). Another barrier has been found. White circle displays in fig.3.8 conventional hypersonic vehicle, limited by L/D max barrier:

$$L/D = 4(M+3)/M$$

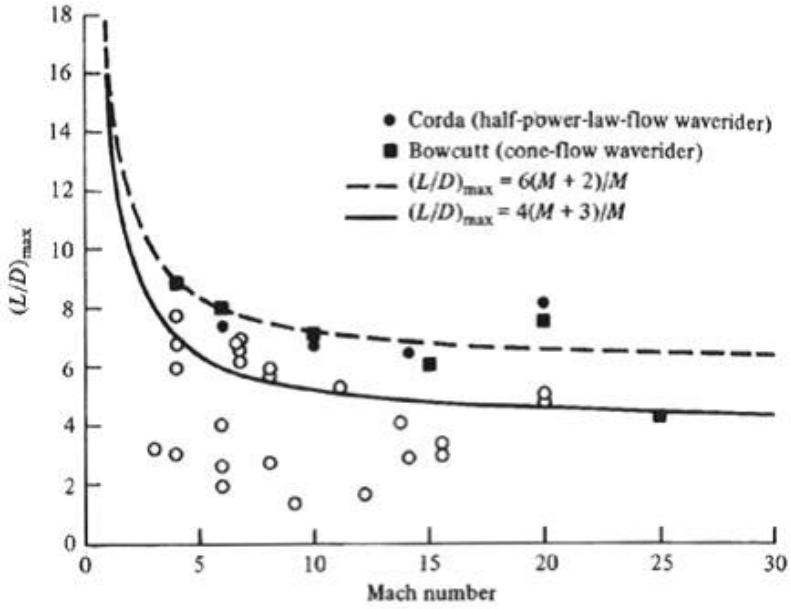

Figure 3.8: Kuchemann L/D barrier.

In subsonic range a delta wing with important sweep angle have a particular behaviour. In fact, sharp leading edge, such as MR2.4 wing and air intake, permits to generate swirling structure because consistent pressure gradients exist. This phenomenon arises mostly at high angle of attack, because difference between windward and leeward increases. As you can see in fig.3.9, there is not only a singular presence of vortex but also a smaller secondary vortex. This happens because high-speed flow near wing surface separates and counter-rotating vortex (secondary vortex) takes place. It leads to a 3D complex flow field, difficult to study with theoretical approach. In the study conducted by Krempus [13], these phenomena can be seen very well by means of CFD simulations.
STRATOFLY MR2.4 aerodynamic design based on an adapted osculating cone method and to optimize internal volume engine unit has accommodated on top. This allows to maximize the available planform for lift generation without additional drag penalties and to optimize the internal volume. This layout guarantees

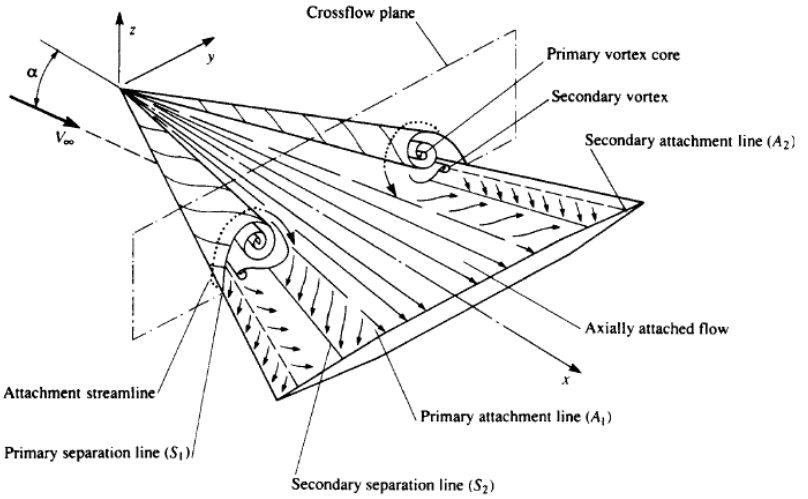

Figure 3.9: Subsonic flow field on delta wing.

furthermore to expand the jet to a large exit nozzle area without the need to perturb the external shape, which would lead to extra pressure drag. The upper surfaces of fuselage and wing almost aligned with velocity vector and so windward side of vehicle produces the greater part of lift. The final shape of plane was achieved by means of four optimization processes to overcome structural integrity, improve volume efficiency and embed sub-systems:

- first configuration (MR2.1, blue in fig.3.10 is characterized by thin cross section so as to optimize wave drag losses. On the other hand this kind of shape is not well suitable for civil transportation because no necessary volume is available. In addition large wetted surface leads to increase skin drag;
- during second configuration (MR2.2, green) the aim was to improve volumetric efficiency;
- in the third one (MR2.3, red), it can be noted integration between airframe and elliptical air intake with beneficial effect of redistribute aerodynamic loads in a better way. However it formed a more complex leading edge;
- the last (MR2.4, black), is definitive one because wetted surface is reduced (wingspan is 41m).

The overall high-speed transport vehicle performance is highly influenced by aerodynamic efficiency (L/D), so after having studied external shape, they take care of intake geometry and integration areas between several parts, in order to limit drag [11]. Several numerical fluid-dynamic analysis were carried out over the past years. The first aerodynamic database was developed by the private company

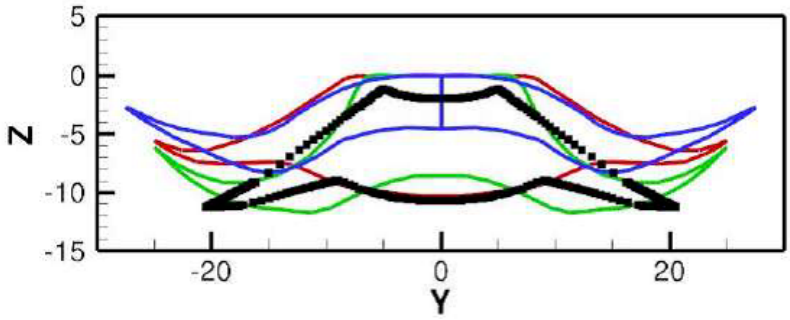

Figure 3.10: Comparison of cross section of various waverider configuration.

Gas Dynamics Ltd, for the LAPCAT project. It was conducted with the help of customised tool, which includes a surface inclination method for inviscid aerodynamic. Different aerodynamic coefficients were evaluated in the all flow regimes, in the following way[14]

$$M = [0.3, 0.5, 0.7, 1.5, 2, 2.5, 3, 3.5, 4, 4.5, 5, 5.5, 6, 6.5, 7, 7.5, 8]$$

Moreover, each coefficient was evaluated in the range -12°to 24° (for each integer number) in the subsonic regime, and $-6°$ to 6° in supersonic and hypersonic range. This discrepancy is due to the vehicle behaviour during flight. It is highly likely that after take-off stage, in subsonic regime, aircraft flies at greater angle of attack in comparison to cruise phase. In addition on that, cross wind conditions were considered, from -4°to 4°. It is clear that Mach number discretization is approximate, especially in subsonic and transonic range where important changes (in comparison to previous regime). However Krempus [13] conducted a further analysis in subsonic range and made a comparison with HEXAFLY vehicle. Krempus's simulations were conducted for take-off Mach number, 0.3, where it was included the runway to assess ground effect. Another two points simulate flightpath at 7 km and 10.6 km altitudes, 0.5 Mach and 0.75 respectively. According with preliminary analysis of the take-of configuration, it was simulated Angle of attack (AoA) of $-2°$ and 0°, for 0.3 Mach. Than an AoA from $-4°$ to 16° for 0.5 Mach and finally 0°and 1°for 0.75 Mach. Several aerodynamic coefficients were calculated by considering contributes of external and internal surfaces as well as engine thrust. Unfortunately, even this aerodynamic characterization is limited although very interesting.

3.1.2 Propulsion

STRATOFLY is a challenging project that aims to take off an unusual aircraft horizontally, fling until hypersonic flight and landing in the other part of the world horizontally. This constrains never such stringent are nowadays difficult. In order

to match this constrains, a particular architecture of engine has been pursued. It's about two kind of motors that share same fuel: liquid hydrogen. It is about Air Turbo Rocket, ATR and Dual Mode Ramjet. The thermodynamic cycle that drives ATR engine is a mix of a turbojet Bryton cycle and Rankine cycle of an expander rocket. Six ATR engines are fed by 2D ATR air intake that spits flow in two ducts, each one each of which pass air through three ATR engines. The number of ATR engines is to produce necessary thrust during take-off stage, taking into account one possible failure. ATR air intake is based on previous 2D air intake of the XB-70, an supersonic experimental bomber of the US Air Force. Because of its origin, ATR air intake performs very well at Mach 3 because six ramps, of which four are adjustable. In addition a system to suction boundary layer has been implemented to prevent severe shock-boundary layer interactions. The single exhaust gas (produced by each motor) goes to a variable throat convergent-divergent nozzle, to increase gas speed, and flows into ATR exhaust gas. At last, flow merges into central main nozzle to complete expansion. The operation of engine based on ramjet architecture (DMR) can work like ramjet or scramjet engine and is made up by few components. Elliptical air intake, with a ratio of major axis to minor axis of 3, feeds elliptical DMR combustion chamber that it is a nearly constant section with particular injectors. Hot air passes through two sequential nozzles: first one has the function to merge elliptical cross section of combustion chamber with circular shape of 3D nozzle. It is characterized by a area ratio of three and length of 13 m. This nozzle is called 2D (nozzle) because no lateral expansion is achieved. The next 3D nozzle is a truncated isentropic expansion nozzle with an area ratio of ten and a length of forty meters. In order to match with external shape of vehicle a rough taper was introduced on its own final section. This part is named "nozzle end piece" in fig.3.11.

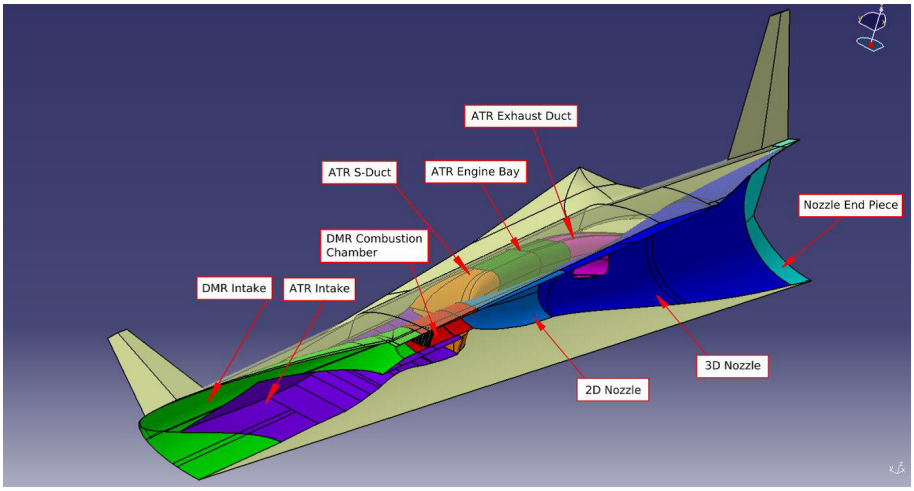

Figure 3.11: MR2 halfmodel with ATR air intake doors retracted and internal flow path.

ATR engines work from take-off phase to Mach 3. During this stage, DMR is shut down although a part of unburned flow passes through the DMR combustion chamber and 2D nozzle, before mixing with hot gases come from ATR unit. From Mach 3 to 4.5 ATR and DMR engines cooperate, so in the DMR combustion chamber are enabled and very hot gas can be expanded into two following nozzles. Beyond Mach 4.5 only DMR engine works. Low speed air intake (for ATR unit) is closed completely by sliding doors. Also the two ATR exhaust ducts, one for each side of ATR exhaust, are closed, because hot gas in 3D nozzle must not be perturbed. If on one hand operation of DMR engine is easy schematically, on the other hand ATR cycle is more complicated. Therefore, a brief description going to be done as follow. ATR is made up to two macro part that work according to Brayton cycle and Rankine cycle. In the first one, two stage counter rotating fan drives two stage counter rotating turbine by combustion of air mixed with hydrogen (gas). Than hot gas expands in nozzle 71 until 812 section. Turbine drives pump that is used for circulating liquid hydrogen to heat exchangers (HEX1 and HEX2) and carries fuel to DMR. Heat exchangers carry out two tasks: they transform liquid hydrogen in gas hydrogen, that can be used in turbine, and cool down hot nozzle. An easy scheme is depicted in fig.3.12.

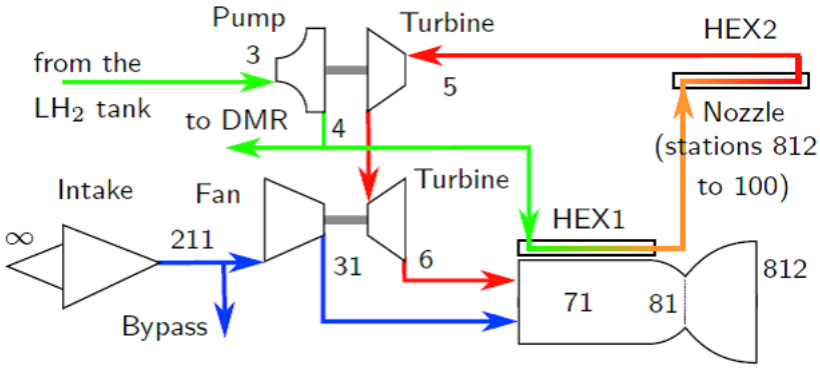

Figure 3.12: ATR cycle schematic.

Different analysis and simulations carried out in recent years, both aerodynamic and propulsive, on MR2 vehicle. Vehicle system is characterized by wide range of operation never reached before, in fact, during flight several flow regimes are attained, i.e. subsonic, supersonic and hypersonic. Therefore it's really unattainable a complete simulation with current resources. Nose-to-tail numerical simulation of the full-scale MR2 vehicle were conducted by ESTEC by means in-house code, coupled by 1D combustion tool. The TAU code is a second order finite-volume flow solver for Euler and Navier Stokes Equations in the integral form. AUSMDV flux splitting scheme is coupled with MUSCL gradient reconstruction to achieve second

order spatial accuracy. According to previous representative reference configurations such as the HyShot II Scramjet, they have studied the supersonic combustion phenomena with a validated approach. In order to simulate a scramjet combustor into DMR duct, detailed chemical kinetics were implemented: the flow is considered a reacting mixture of thermally perfect gases. Million is the order of magnitude of mesh nodes. At the beginning, 9 millions of points are used to become 14 millions after several gradient-based refinement. Also CIRA carried out aerothermal analysis on MR2.4 vehicle by a dedicated code based on compressible Navier Stokes. It is a density-based finite volume approach with cell-centred method, flux difference splitting second order ENO-like upwind scheme for the convective terms [7]. In addition, commercial code FLUENT 13 was used for unstructured grids. This type of comparative works is well suitable in the complex hypersonic field in order to verify adhesion among two type of CFD codes. These simulations are aimed to discover and characterize hypersonic flow field around aircraft: Mach 6 and 8 are chosen for AoA of -2°, 0°, +2°. The results obtained by CIRA and ESTEC are well comparable. For nominal cruise speed (Mach 8) the leading edge shock is well aligned with the wing, in a such way that waverider configuration matches. Inside the elliptical air intake, shock generated by first ramp is well settled inside, just under intake's lip, so air spillage does not happen. Just near downstream of the shock impingement (inside the air intake), a recirculation area arises due to high pressure. The second shock, reflected by the first one, impacts on the bottom wall of combustor chamber. In that position injectors are accommodate because low speed downstream of the shock is a good factor to stabilize combustion process. Another behaviour can be

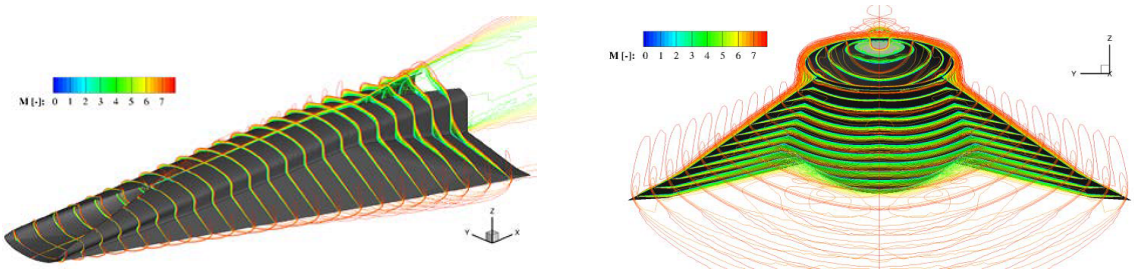

Figure 3.13: External flow field Mach 8.

seen for Mach 6. First shock generated inside air intake does not impinge the internal surface of intake because lower speed leads to higher wave angle than Mach 8 condition. This permits a non-zero mass flow spillage outwards, which reduces intake efficiency by 7% of captured theoretical air mass. Although it is a non-negligible leak, this value is comparatively low, because off-design conditions were regarded. This also influences size and strength of the recirculation area inside cowl. Oblique leading edge shock settles downward external surface of waverider has a higher wave angle than Mach 8 condition, so spillage occurs close to wing tip. About concerning

effect of the angle of attach can be seen an almost linear behaviour. High lift goes hand in hand with high drag in a different way. In cruise speed condition, flight level, i.e. T=D, is only reached with negative angle of attack, ranging from -2° to 0°. The aerodynamic efficiency was computed in a manner that quantify the real benefits of waverider configuration. Only external drag (external surfaces) is considered. As expected, maximum L/D was attained for cruise Mach (8) and 0°AoA. Severe decrease can be seen for negative AoA because vehicle is tilted down and so oblique shock wave is created on top: downward lift degrades efficiency. Mach 6 efficiency shows a slightly higher value due to Reynolds effect because of lower viscous drag. The value takes a value ranging from 6 to 7. CIRA carried out another worthy study in order to evaluate and compare turbulence and laminar behaviour. Three turbulence models were compared: compressible Spalart-Allmaras Spalart-Allmaras (SA), original version of SA and $k-\epsilon$ model. Slight difference in terms of lift (4.7% difference) was found between laminar and turbulent models. Conversely drag force is much different , both for pressure and viscous drag. According CIRA, the best turbulence model is compressible Spalart-Allmaras because internal drag (net thrust) was almost balanced by external drag. During cruise flight, the balance should be achieved completely [7]. In order to verify aerodynamic coefficients of the MR2.4, DLR Cologne carried out several test. The tested model was manufactured in titanium because it offers greater durability in comparison to aluminium and is lighter than steel. It is 1:120 scale representation, so length is 720 mm and maximum span width is about 342 mm. As you can see in fig 3.14, an aerodynamic support was mounted from behind. They tested only supersonic and hypersonic flight condition, with the following Mach value: 3.5, 4.0, 5.3, 6.0, 7.0 and 8.7. Results of the load cells give a good matching with numerical data, although measured normal force coefficient is higher than predicted by CFD.

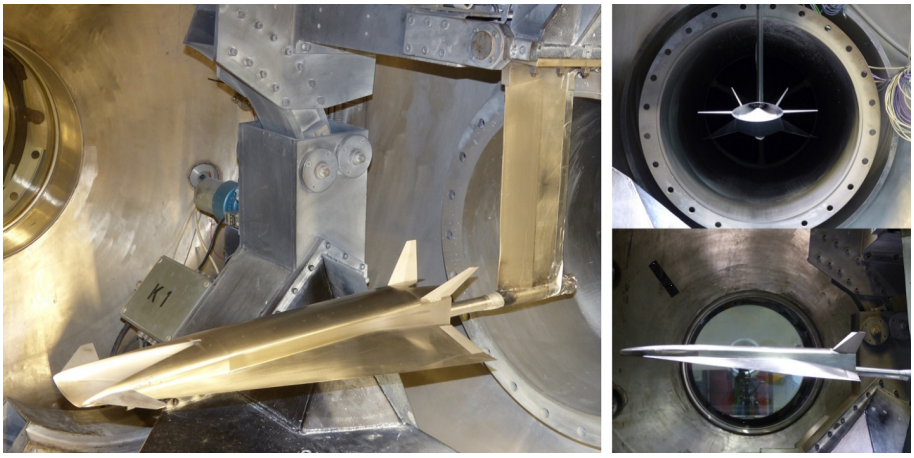

Figure 3.14: LAPCAT II aeromodel used for experimental tests.

A further study more challenging and relevant carried out by DLR and ONERA

in HEG and F4, respectively, to conduct free jet combustion experiments of integrated scramjet propulsion systems. It was a test never seen before. A scale model is based mainly on MR2.4 with an integrate airbreathing propulsion unit, without wing. Since free-flying configuration was teste, Kevlar threads initially suspended mock-up that was swept away by the arrival of the flow. Following the conclusion of the test time, two support legs terminate the model movement. Thrust computed by two kind of technologies: visual tracking and accelerometers mounted inside the mock-up, in conjunction with pressure measurement on the internal model surfaces. Campaign of measurements led to compute velocity and acceleration by integration of displacement, so that combustion process creates a necessary thrust to overcome drag. Since complexity of experiment, a hybrid approach was adopted: numerical and experimental. In order to calculate axial net force (along body X axis), thrust computed by HEG experiment, in fuel-on condition, was subtract from drag force by CFD result (fuel-off condition). A net force is computed for an AoA of 0°and -2°. In the first case -93 N are not necessary for propulsion although taking into account the uncertainty of the measurement, a positive balance is obtained. In the second one (-2°), 73 N is an encouraging value. In addition, CFD data based on considering boundary layer completely turbulent and hence values represents conservative estimate. A comparison with CFD model for thrust calculous showed an increase of 15% of drag force [11]. Better results for experimental approach, which however they need to be improved.

Figure 3.15: STRATOFLY MR3 vehicle.

In order to implement incremental approach in design process, MR2.4 vehicle has been modified but has not changed deeply. This improved version aims to be much closer to operational one. In fact, important differences are related on the internal layout. Volume cabin is more voluminous than previous: from 1200 m^3 to 1400 m^3.

In addition, compact cabin is proposed instead of “H-shaped cabin”, since the easy rule “compact is better than dispersive”. During emergency phase or boarding procedures, new shape pays off. Inevitably, the internal settlement of sub-systems are changed. Many sub-systems has been developed and optimized in a way that weight estimation becomes always better. In particular the sub-systems highly developed are the propulsive and Thermal and Energy Management (TEMS). The Thermal Protection System (TPS), the Environment Control Life Support System (ECLSS) and the propellant subsystem are at a good level of design thanks especially to their interfaces with the TEMS [15]. Conversely, Flight Control System (FCS), avionic and electrical sub-systems has been only designed at high level. They are improving continuously. Regarding external shape of vehicle, two evident modifies has been introduced. The absence of V-shape hole upon surface of engine (among two fins), in the afterbody. Also, body-flaps are considering currently. In the next chapters CFD analysis are carried out.

Chapter 4

Numerical method

Numerical method is very useful in different kind of physics problems because is repeatable, accurate and cheaper than experimental one. In addition, for particular cases it is the only way to obtain results, especially when no test section of wind tunnel can accommodate a huge mock-up or the inability to test airplane at hypersonic speed for a sufficient time. CFD is supported by gradually increasing in computational power although several limitations must be taken into account:

- CFD model can be slightly different compared to CAD model;
- based on kind of physic model used, can be different with real solution;
- accuracy of numerical code;
- convergence error.

CFD approach is based on fundamental governing equations of fluid dynamics: The continuity, momentum and energy equations. They constitute a set of scalar equations for continuity and energy, and a vector equation for momentum, can be split in three Cartesian coordinate system. This three mathematical equations derive from as many as physical principles:

- mass is conserved;
- Newton's second law;
- energy is conserved.

The set of adiabatic and inviscid equations, known as Euler equations, can be represented in different forms, both in integral and differential one. Also, they can be used in conservative or non-conservative form. The final result does not chance but the kind of representation significantly affects numerical methods.

$$\frac{\partial \rho}{\partial t} + \nabla \cdot (\rho \boldsymbol{V}) = 0$$

$$\frac{\partial (\rho u)}{\partial t} + \nabla \cdot (\rho u \boldsymbol{V}) = -\frac{\partial p}{\partial x}$$

$$\frac{\partial (\rho v)}{\partial t} + \nabla \cdot (\rho v \boldsymbol{V}) = -\frac{\partial p}{\partial y}$$

$$\frac{\partial (\rho w)}{\partial t} + \nabla \cdot (\rho w \boldsymbol{V}) = -\frac{\partial p}{\partial z}$$

$$\frac{\partial}{\partial t}\left[\rho\left(e + \frac{V^2}{2}\right)\right] + \nabla \cdot \left[\rho\left(e + \frac{V^2}{2}\right)\boldsymbol{V}\right] = -\frac{\partial (up)}{\partial x} - \frac{\partial (vp)}{\partial y} - \frac{\partial (wp)}{\partial z}$$

Range of application is wide although several hypothesis need to be regarded. Most important is continuum assumption, that is, fluid particle must be small enough to be considered continuum in relation to reference length (that depends on kind of problem), but big enough to assess statistically significant thermodynamic variables. This propriety can be evaluate through the Knudsen number. It is a dimensionless number that relates a reference length of problem with free mean molecular path. If the value is much smaller than 1, continuum hypothesis is valid. Another assumption is that magnetic field and electric field are neglected. Especially when high-speed flows are considered, chemical reactions can't be neglected, due to ionization of molecules.

This set of equations are not enough to compute results because we have five equations in terms of six unknown flow-field variables p, ρ, e, u, v, w. Hence, it is essential to include at least one more equation. In aerodynamics, it is generally effective to use ideal gas law to the exclusion of particular cases. Basically, it assumes that intermolecular forces are negligible. The equation of state is:

$$p = \rho R^* T$$

where p is the static pressure, ρ is the density, R^* is the specific gas constant (gas constant divided molar mass of the gas) and T is the static temperature. Again, it presents another unknown static temperature. For a calorically perfect gas can be used a univocal relation between internal energy (e) and static temperature through the specific heat at constant volume, c_v:

$$e = c_v T$$

An important part of these equations consists in characterize them with regard to the kind of geometry. In other words, boundary conditions are very important in the problem and profoundly affect results. Depending on the type of flow, several choice can be done. For inviscid flow, no constrain forces the air particles near the wall to have zero velocity, as in the viscous one. Therefore, for a rigid body, flow velocity vector on the wall must respect tangency condition.

$$\boldsymbol{V} \cdot \vec{n} = 0$$

Regarding boundary conditions associated with the temperature, several ones can be applied in terms of what you know. T of fluid can be match T_{wall} or through Fourier's law is possible to make explicit instantaneous heat flux with (static) temperature gradient at the wall. Besides this, adiabatic wall can be chosen if there is no heat flux. It is clear that when you consider Fourier law, another equation to solve is added.

For compressible flows, we are in presence of coupled system of nonlinear partial differential equations that are very difficult to solve analytically and so numerical method are suitable to compute solution with calculator. In order to calculate a solution with a machine, partial differential equations are discretized by means of the finite volume method[1]. Also a limited domain is subdivided into smaller elements that form the mesh. In other words, these equations is converted in an algebraic equation for each element of mesh. So, we renounce to know continuous solution for having punctual one. In this thesis was used Fluent, a commercial software by Ansys. It is a versatile code that is characterized by two kind of flow solvers: Density-based and Pressure-based. Historically speaking, Density-based solver is suitable for high-speed compressible flows, so it was used. In this method velocity field is obtained from the momentum equations. Density is computed by continuity equation and pressure by equation of state. Equations are reformulated in other terms because they are much more suitable for numerical calculation. In compact form we subdivided column vectors as follows.

$$\frac{\partial}{\partial t}\int_V \boldsymbol{W} dV + \oint \boldsymbol{F} dA = \int_V \boldsymbol{H} dV$$

Where vectors $\boldsymbol{W}$ and $\boldsymbol{F}$ are defined as:

$$\boldsymbol{W} = \begin{Bmatrix} \rho \\ \rho u \\ \rho v \\ \rho w \\ \rho E \end{Bmatrix}, \boldsymbol{F} = \begin{Bmatrix} \rho \boldsymbol{V} \\ \rho u \boldsymbol{V} + p\hat{i} \\ \rho v \boldsymbol{V} + p\hat{j} \\ \rho w \boldsymbol{V} + p\hat{k} \\ \rho E \boldsymbol{V} + p \boldsymbol{V} \end{Bmatrix}, \boldsymbol{H} = \begin{Bmatrix} 0 \\ 0 \\ 0 \\ 0 \\ E + p/\rho \end{Bmatrix}$$

[1]Fluent uses this type of approach

Here, ρ, $\boldsymbol{V}$, E and p are the density, velocity vector, total energy per unit mass and pressure.

Convective scheme plays an important role in the Euler Equations because is a nonlinear term, that in high-speed flows turns out to be predominant one. Since it is useful compute variable values on the interface (between two contiguous cells), a numerical scheme needs to be used. Two classic scheme approach are Flux Difference Splitting and Flux Vector Splitting. From the last family derives the Advection Upstream Splitting Method (AUSM), that provides a better solution in discontinuities in comparison to other scheme and is free of oscillations at stationary and moving shock. AUSM scheme first computes a cell interface Mach number based on the characteristic speeds from neighbouring cells. The interface Mach number is than used to determine the upwind extrapolation for the convective flux [16]. The other term of equation is represented by time derivative term, that in the steady-state formulation is neglected. However, in this code it is not. In the steady case, it is assumed that time marching proceeds until a steady-state is reached and so must be taken into account [16]. Temporal discretization of the coupled equations can be attain by two formulations: implicit or explicit. This choice affects duration of the simulation.

Chapter 5

CFD analysis

In this chapter, the method employed to compute global aerodynamic forces and moments will be clarified. After initial conditions are defined, several parts of vehicle was simulated by CFD approach. Than, flow field analysis relate to single models will be addressed. The simplified approach pursued in this work is justified by different reasons. First, STRATOFLY MR3 vehicle is not in the well-established stage of design. Further improvements need to be made, especially in flight mechanics. Therefore, it is not convenient to reach an high level of precision in relation to time. Second, wide range of conditions were simulated, especially in subsonic and transonic regime, where sudden changes in aerodynamic forces and moments occur. Finally, massive geometry is computational expansive, particularly when prism layers are generated to capture boundary layer. The simplified approach is based on computing aerodynamic forces and moments on three different parts of vehicle, through inviscid fluid dynamics equations with coupled energy equation, namely Euler equations. Viscosity terms and conductives ones are neglected, so physic model does not correspond with real case. At first, semi-wing and flaperon (flap and aileron), placed near trailing edge of wing, are coupled in the same model, mod1. Because of lacking in flight mechanics of aircraft, canard wings were reconsidered, as in LAPCAT-II vehicle configuration. So, only one aerodynamic surface was analysed in another model, *mod2*. Two specular flaps (respect to the symmetry plane of vehicle) are placed among fins and rudders, on the top surface of the fuselage. They are called bodyflap to distinguish them by other flap. These last two elements could be used both in longitudinal control and in lateral one. Third model is made up by single bodyflap with a fin and rudder, placed on part of top fuselage surface, *mod3*. This simplification was undertaken in a way that leading edge does not influence flow field, trying to reproduce unperturbed upstream conditions.
These models are simulated for different configuration of geometry. For *mod1* the inclination of flaperon is chosen to be 0°(baseline *mod1*), +20° and -20°, according to reference system in fig.5.1. For each configurations it is chosen a angle of attach ranging from -6°to +6°with step of 2°. While instead mod2 is tested for 0°(baseline

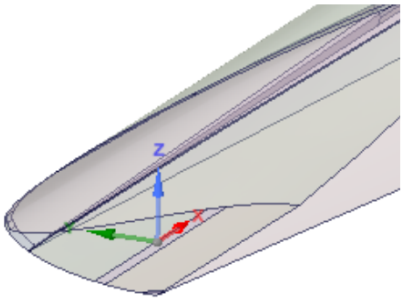

Figure 5.1: Aerodynamic reference system.

mod2), +10°, +20°, +30°. Since *mod3* includes both vertical empennage (fin and rudder) and bodyflap, single behaviour is studied. To evaluate bodyflap effect only rudder is placed in undeflected position (0°) while bodyflap is oriented in -10°, -20° and -30°. Instead, when rudder effect is evaluated, inclination of the bodyflap is at 0°. For the last two models angle of attack is assumed to be 0 because it has been deemed to be irrelevant on aerodynamic coefficients.
In order to compute global aerodynamic coefficients of the vehicle, data coming from external simulations of vehicle are added up with three contributes deriving from aforementioned models. The whole vehicle is made up to all parts (flaperon, bodyflap, rudder and fin) in undeflected position and to compute skin friction drag an engineering law is used. These additional terms are computed in relation to baseline model. Therefore for each model and configuration is obtained a delta coefficient between i-th configuration, such as β+20° for *mod1* and *mod1* baseline.

Thanks to Langener's work [8], that he simulated reference flight path for MR2.4 vehicle, the same of its successor: MR3, it is possible to extrapolate upstream flow field conditions on fixed speed. In order to capture significant variations, simulations are performed for certain points of trajectory, especially in transonic phase. Mach numbers selected are:

$$0.3,0.5,0.7,0.8,0.95,1.05,1.20,1.50,1.70,2.00,3.00,4.00,5.00,6.00,7.00,8.00$$

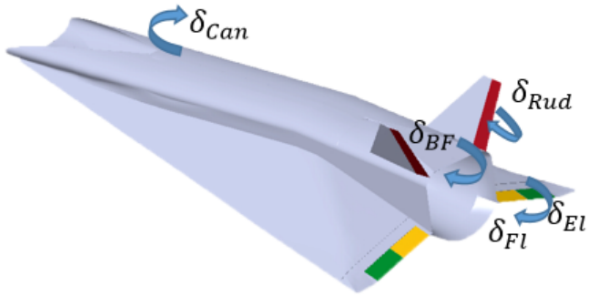

Figure 5.2: Signs convention for control surfaces.

By using Mach-altitude diagram [8], it can trace to pressure, density and temperature. In the following tab.5.1 all conditions are show.

5.0.1 CFD setting

Before simulations are launched, initial setting needs to be performed. Following summary is done:

- Density-Based solver;
- steady state formulation;
- energy equation activated;
- inviscid (Euler equation);
- implicit formulation;
- AUSM (convective flux);
- Green-Gauss Cell Based (to calculate the gradients);
- second order Upwind.

M	T [K]	p [Pa]	U [m/s]
0.3	291.00	101695.71	102.55
0.5	291.00	101695.71	170.92
0.7	284.47	89362.57	236.59
0.8	273.89	73229.57	265.32
0.95	215.96	19353.62	279.76
1.05	215.96	18372.51	309.21
1.2	215.96	16824.78	353.39
1.5	215.96	13957.15	441.73
1.7	215.96	12466.35	500.63
2	215.96	10625.13	588.98
3	216.96	6415.22	885.51
4	218.82	3549.13	1185.74
5	220.17	2876.79	1486.74
6	226.03	1715.16	1807.68
7	230.81	1179.22	2131.14
8	236.17	913.00	2463.71

Table 5.1: Far field conditions.

In order to understand and evaluate how solution is relevant in terms of convergence, a criterion should be selected. It is set on significant parameters in relation to considered model. Difference between i-th iterate and previous one is set on *1e-5* for lift coefficient on significant surfaces. For *mod1* (wing, flap and aileron), lift coefficient is computed by flap and aileron. For *mod2* (canard) by itself. Then, for *mod3* by bodyflap and rudder respectively.

It is fundamental to check continuum hypothesis because Euler equations could be inappropriate, especially at high altitude where density is very low. Knudsen number is a dimensionless number that relates two quantities: free mean molecular path with reference length. If the number is much less than 1, fluid can be considered continuum. We need to get in the disadvantageous situation, namely, 30 km altitude reached at Mach 8. According to [9], at 100000 ft, (about 30 km) mean free path is $4.9110^{-}6m$. For our problem, reference length can be vehicle length, 94 m.

$$Kn = \frac{\lambda}{L} = \frac{4.91 \cdot 10^{-6}}{94} = 5.22 \cdot 10^{-8} m \ll 1$$

It is verified this important hypothesis that permit to validate mathematical model. Another interesting dimensionless number is Reynolds number. It relates inertial forces with viscous ones and it is utilized to quantify type of flow; if viscosity is predominant or flow accelerations are important. Before calculating aforementioned number, viscosity can be calculate by means of Sutherland's law. It is a simplified

model that describes this quantity as function of temperature through the following equation:

$$\mu = \frac{C \cdot T^{3/2}}{\chi + T}$$

Where C and χ are constants. Their value is $1.46 \cdot 10^{-6}(Pa \cdot s)\sqrt{K}$ and 110 K. Therefore, Reynold number can be computed for all trajectory points as:

$$Re = \frac{\rho U L}{\mu}$$

As a result, we obtain an high Reynolds number, always greater than 10^8. In conclusion flow field around vehicle is fully turbulent, from noise to tail. This fact can be used in the future simulations.

5.0.2 External domain

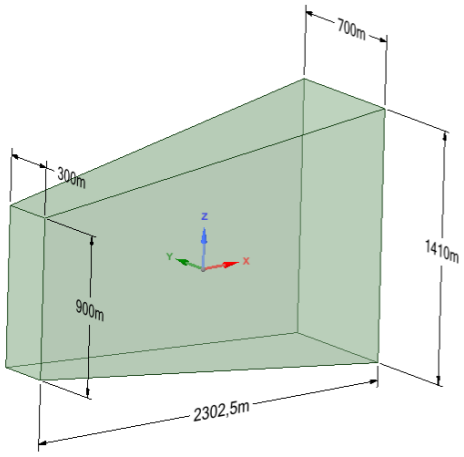

Figure 5.3: External domain with quotes.

Since external aerodynamic simulations were performed, an external domain must be used. In subsonic and transonic range, domain need to be wide enough to avoid disturbance of the flow field in all direction. In supersonic or hypersonic

regimes, domain could be much smaller than sub-transonic domain because shock waves (o discontinuities for inviscid treatment) do not permit to propagate signal in the upstream direction, so model enclosed into external domain does not perturb the upstream flow field. Rather than using two different domain, it was preferred to use a sub-transonic range in whole flow regime. This solution is clearly more versatile than to diversify external mesh.
External domain is a prism with trapezoidal base. The dimensions are depicted in fig.5.3. Z axis of reference system is located at a distance of 1092.5 m from left surface (300 m X 900 m) and 1210 m from right one (700 m X 1410 m). Y distance from reference system and trapezoidal area is -1.85 m. In Z direction, reference system is equally spaced. The reference frame coincides with front point of right semi-wing.
Since half models were simulated because flow field is specular in XZ plane, trapezoidal-form surface that is parallel to XZ plane, is treated as "Symmetry plane" in Fluent. Rectangular surface on the right, of fig.5.3, is considered as "Pressure outlet". Two parameters are specified: static pressure and total temperature that match with upstream conditions. The other four surface are treated as "Far field pressure". One cinematic and two thermodynamic quantities are set; Mach number, static pressure and static temperature respectively.
After defining external domain, following models are subtracted by external domain. The resulting geometry will be used for CFD simulations.

5.1 Baseline vehicle

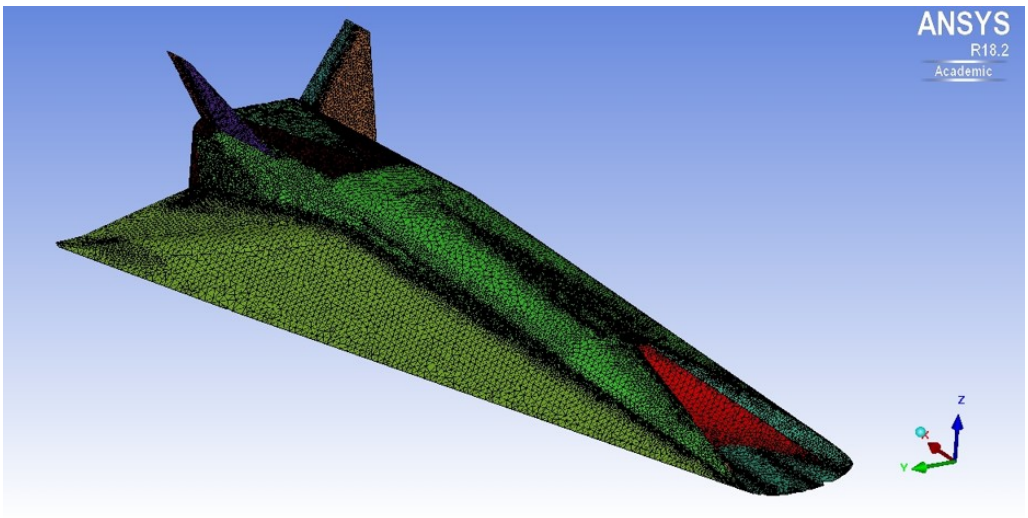

Figure 5.4: Mesh model of the baseline vehicle. Front view. 2 Million of cells.

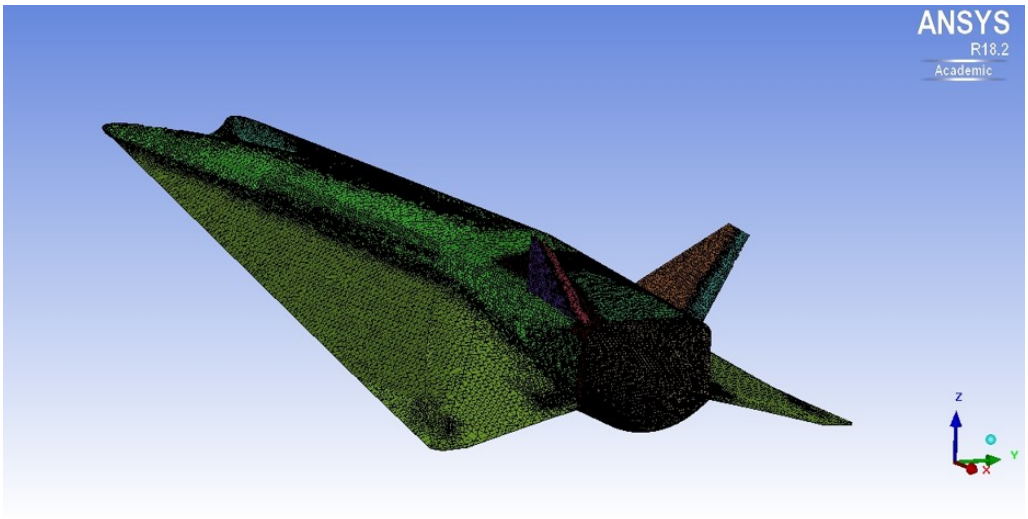

Figure 5.5: Mesh model of the baseline vehicle. Rear view. 2 Million of cells.

In order to calculate aerodynamic coefficients, simplified model is based on CFD simulations that are carried out on base vehicle model. Half of airplane is considered, with flap, aileron, fin and rudder. In this model internal aerodynamic is included as well, however for the sake of simplicity, ATR duct is closed: only DMR duct is open.
To calculate aerodynamic coefficients from CFD simulations two transformations formulae are considered: it is useful to calculate them in wind axis rather than in body axis, as below:

$$C_L = C_z cos(\alpha) - C_x sin(\alpha)$$

$$C_D = C_z sin(\alpha) + C_x cos(\alpha)$$

Moment coefficients are calculate by reference system placed on symmetry plane, and tangent with front region of intake.
Unlike wing, flap and aileron model, and, bodyflap and rudder, canard is not present on baseline vehicle. Therefore that contribute is added entirely to the coefficients of baseline vehicle (by external and internal aerodynamic). For the other two model, delta coefficient are regarded only, because those control surfaces are already included in the vehicle coefficients. So:

$$C_{L_{tot}} = C_{L_{vehicle}} + C_{L_{canard}} + \Delta C_{L_{flaperon}} + \Delta C_{L_{rudder}} + \Delta C_{L_{bodyflap}}$$

$$C_{D_{tot}} = C_{D_{vehicle}} + C_{D_{canard}} + \Delta C_{D_{flaperon}} + \Delta C_{D_{rudder}} + \Delta C_{D_{bodyflap}} + C_{D_{viscous}}$$

$$C_{My_{tot}} = C_{My_{vehicle}} + C_{My_{canard}} + \Delta C_{My_{flaperon}} + \Delta C_{My_{rudder}} + \Delta C_{My_{bodyflap}}$$

Although simulations are based on inviscid equation, in C_D formula viscous contribution is present. It is due to correction formula assuming to flat plate model. For future studies about stability, it's important to calculate moment coefficients on center of mass of vehicle. To accomplish this, an easy formula can be used:

$$C_{My_{CM}} = C_{My} + C_z \frac{x_{cg}}{l_{veh}}$$

By earlier studies about fuel consumption and distribution of the mass, it has been seen a difference of 2.97 m: in pre take-off stage, the center of mass is approx. at 49.98 m along X-axis. Then, during landing stage, it reaches 52.95 m.
Hence, in order to calculate coefficients for a specific vehicle attitude, it is necessary to add right ones. It is clear that the contributions of undeflected surfaces are equal to zero.

5.2 Wing, flap and aileron

Wing is shaped by two surfaces, upper and lower, that is centrally integrated with intake, engines and nozzle. In order to better perform in supersonic and hypersonic regimes, delta planform is used with a similar asymmetric deltoid cross section. In base attitude, angle of attack is other than zero, therefore at 0° AoA can generate lift. In order to delay formation of shock wave, maximum thickness is located downward, in analogy to supercritical airfoil. Wingtip is curved upward in a way that reduces ΔC_P, in order to improve wingtip behaviour. Flaps and ailerons are placed on inclined trailing edge (on YZ plane) to comply with waverider configuration. This location is a natural layout for this kind of wing. The purpose of these surfaces is to change longitudinal attitude by pitch moment, but they affect lateral control as well. With the aim to improve manoeuvrability they can rotate autonomously: as rotate upwards, moment is positive and vice versa. Wide control scenario can be so studied.
Since top surface of the wing is less wide than bottom one, because of fuselage shape, a connection occurs between internal edges of wings and symmetry plane, along spanwise direction. These surfaces can be recognized in *mod1* mesh by rough cells, since is not important for the purpose of analysis. Mesh model aims to give a good resolution where there are significant variation of thermodynamic and cinematic quantities. In particular way, special interest was placed on deflected surfaces (flaperon), that are the only deflected. Another aspect takes into account is the solution time. All these surfaces are configured as "Wall".
Wing has a swept angle of about 81°. Flap have a simple geometry; rectangular shape is featured by length and width of 5.16 m and 3.1 m, respectively. Trailing edge apex angle is about 10.1°.
Surface mesh is generated by local refinement on different surfaces of body. Element

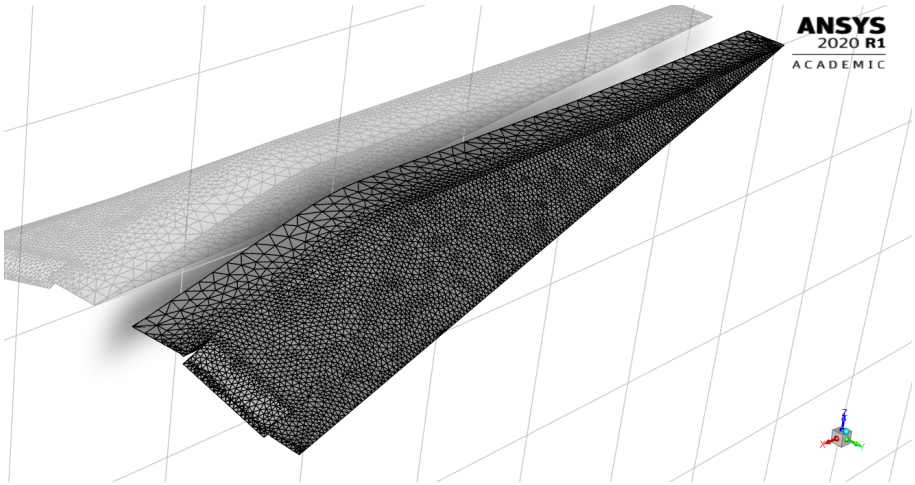

Figure 5.6: Surface mesh of *mod1* +20 °.

size for wing surface is 0.55 m and growth rate 1.23. For flaperon surface 0.5 m and 1.20 respectively. In order to capture variations of the involved quantities, cells near flaperon edges are refinement with these parameters: 0.40 m and 1.10.

Flaperon 0°

At subsonic speed flow field under wing is compressed. In the back zone, where a part of the surface is less inclined (in comparison with the front one), flow is more aligned and tends to be less perturbed by 3D effects of the wing. The upper surface is characterized by convex surface, which coincides with maximum thickness location; it causes a suction area downward. It is where consistent part of lift is created. Due to high lateral inclination (on YZ plane), spanwise component of the flow is more considerable, so convex surface produces another effect: it straightens the flow. At lower speed (M 0.3), a large wingtip vortex is generated from the start of leading edge, so a great upper wing zone is involved. As Mach number increases, this effect is always less significant: swirling region is confined near wingtip. This is consistent with classic trend of lift-induced drag. Trailing edge is curved slightly upwards and produce a slight compression on top wing surface.
At Mach 0.8 flow field becomes transonic, due to presence of shock wave, right after convex surface. The shock is more intensive near wingtip because of a higher supersonic speed. A limited supersonic region after convex surface is created because maximum Mach is just over sonic condition, 1.07. At M 0.95, shock wave mentioned before is to a more advanced position, preceded by an expansion, blue region in fig.5.13. Maximum Mach number reached is about 1.8, pretty higher than previous one. This fact is due to significant difference of upstream temperature (from 273.9 K to 215.9 K) for reason of altitude change: at equal speed, Mach number is

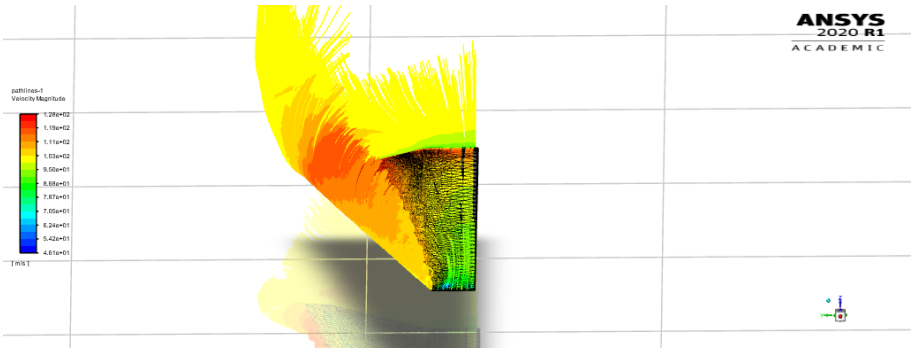

Figure 5.7: Leading edge vortex for Mach 0.3 at $\alpha = +6$ °

higher for lower temperature of the fluid.

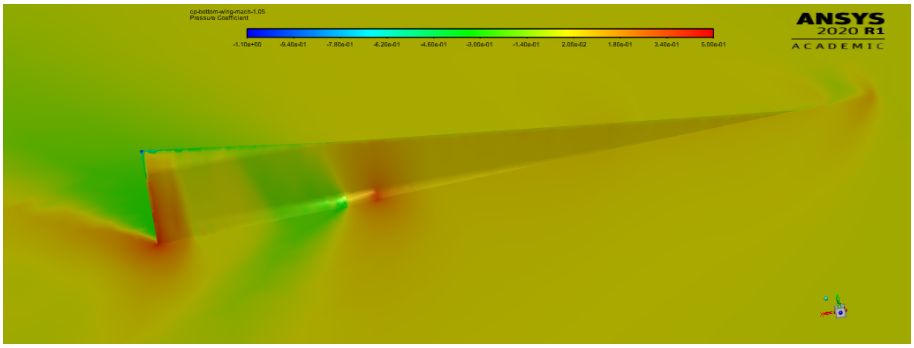

Figure 5.8: Bottom surface of wing. Mach 1.05.

By the presence of the junction (wing-symmetry plane), at about two third of the lower surface (of wing), an expansion takes place, than a shock wave arose. It is for the change of inclination. If one hand ventral discontinuity generates a compression region downstream of it (upward force), in the other hand dorsal shock produces similar effect but downforce is produced. Net effect can be seen in fig.5.9, where C_L is higher than previous (Mach number), so high pressure on lower surface overcomes one of upper surface. C_D rises to a greater degree since upper surface is more tilted on XZ plane. Net contribute leads to lose efficiency in transonic range.

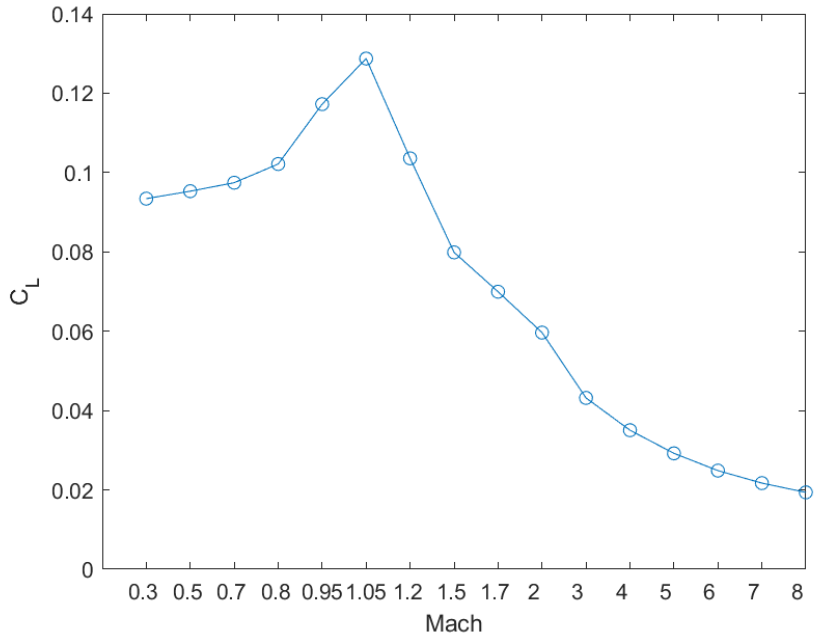

Figure 5.9: C_L-Mach plot for baseline layout.

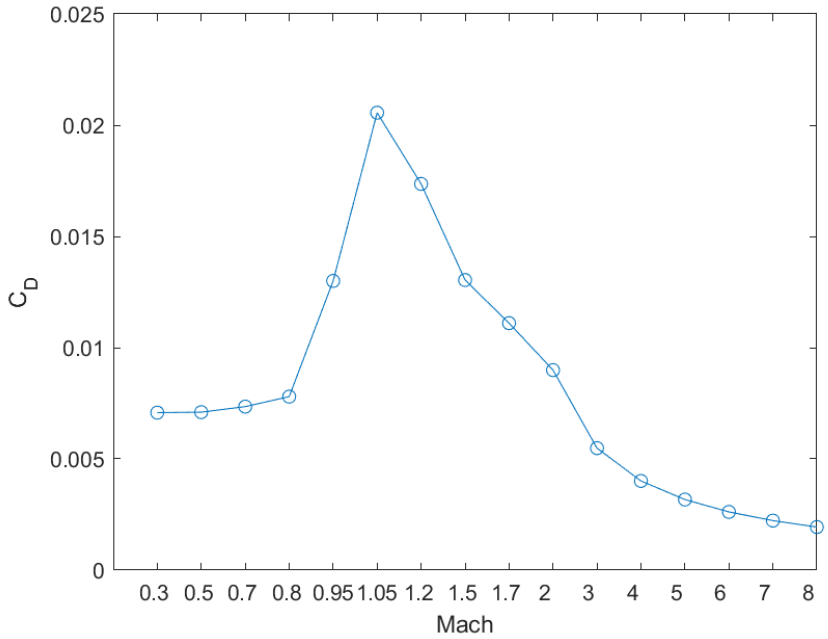

Figure 5.10: C_D-Mach plot for baseline layout.

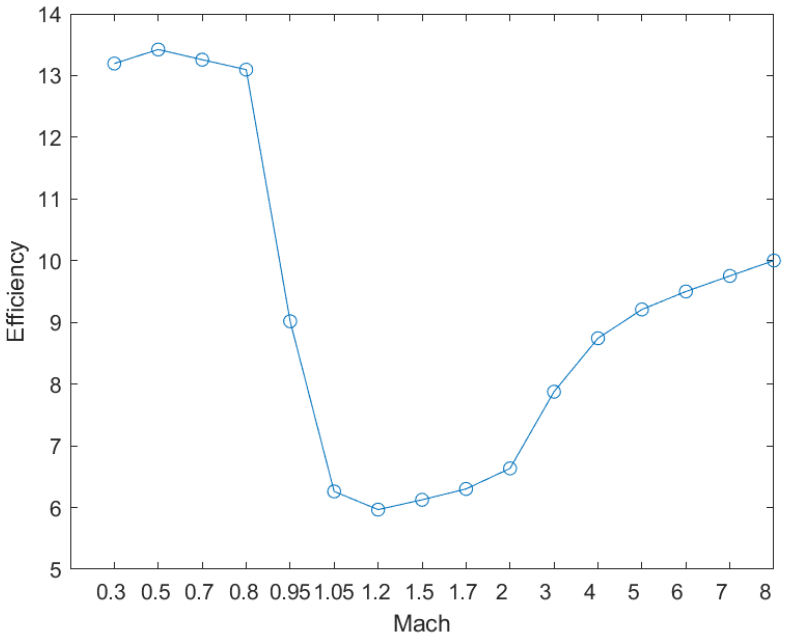

Figure 5.11: Efficiency-Mach plot for baseline layout.

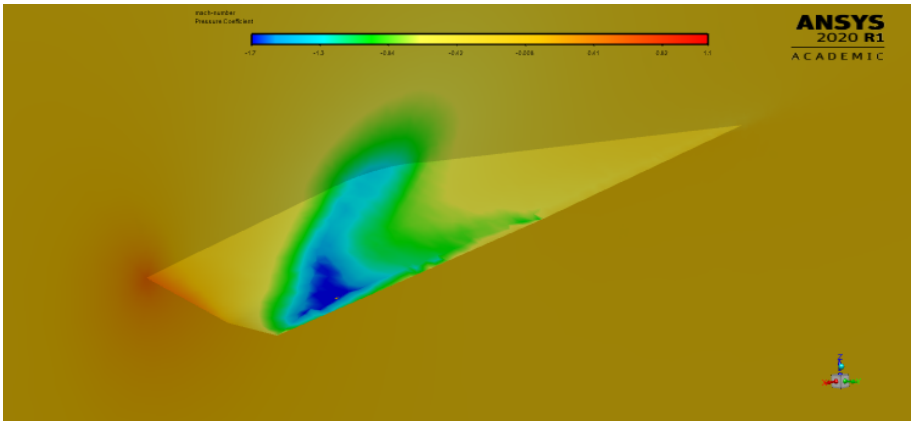

Figure 5.12: C_P field on *mod1* 0°, Mach 0.5.

This reasoning is true for M 1.05, but some differences appear. Front region of wing is characterized by discontinuity at the bottom surface and expansion at the top, on leading edge, which affects all flow field downstream. Region between convex surface and trailing edge is now fully supersonic; this suction region increase both C_L (maximum value) and C_D (maximum value). Since flow is faster, shock wave takes shape on trailing edge. On bottom surface near Trailing edge (TE) brings up another discontinuity, because high pressure downstream is created by shock on TE

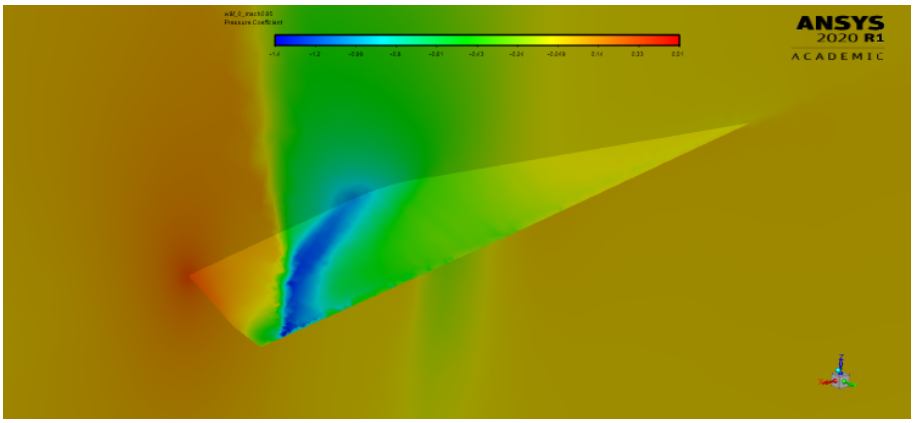

Figure 5.13: C_P field on *mod1* 0°, Mach 0.95.

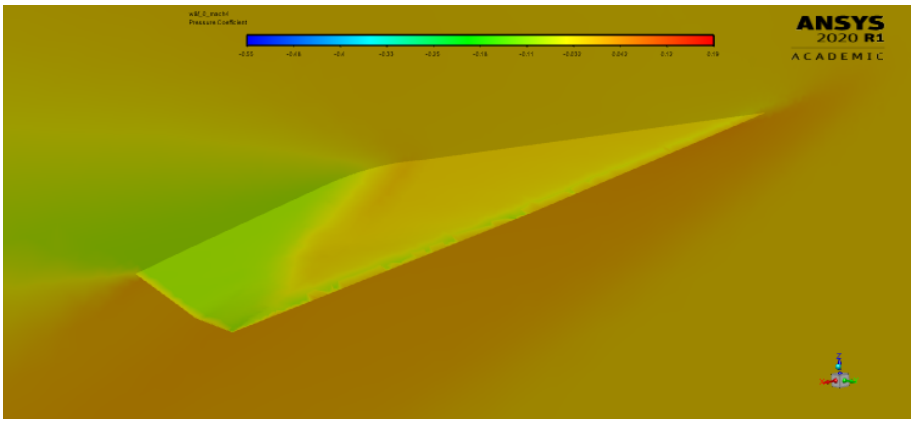

Figure 5.14: C_P field on *mod1* 0°, Mach 4.

(on upper surface): it is a beneficial effect for lift.
As speed increases, flow field near surface is more aligned because of greater inertia, and discontinuities are less tilted. At hypersonic and high supersonic speed, efficiency tends to increase, due to first shock wave that is even more near bottom surface; it "seals" ventral flow better and better. In addition, wingtip spillage is dumped.

Flaperon +20°

As it can expect, flow around wing is similar than baseline configuration, but significant difference are underlined. Region affects by changes is clearly near flaperon. Dorsal flow on surface aforementioned is now accelerated. Conversely, ventral flow is slowed down.

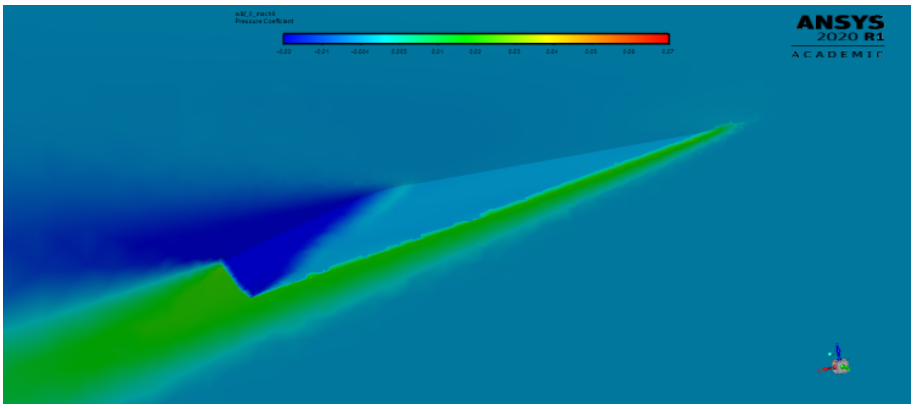

Figure 5.15: C_P field on *mod1* 0°, Mach 8.

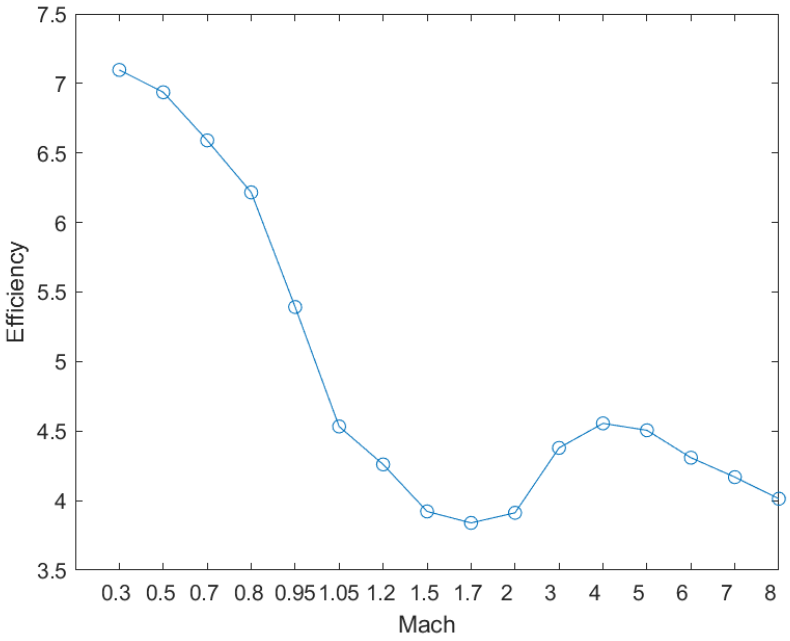

Figure 5.16: Efficiency-Mach plot for +20° layout.

Critical Mach number is reached at lower speed than baseline *mod1*: 0.7. On top convex edge of flaperon an expansion takes place, followed by discontinuity, at about one third of its length. This occurs because supersonic speed after expansion has to match with subsonic flow downstream. Maximum Mach reached at this speed is about 1.25. Right after shock, flow can't deal with adverse pressure gradient, so it separates, region depicted in darker blue, 5.18. Even if in inviscid equation separation shouldn't happen, artificial viscosity does it. Although this behaviour

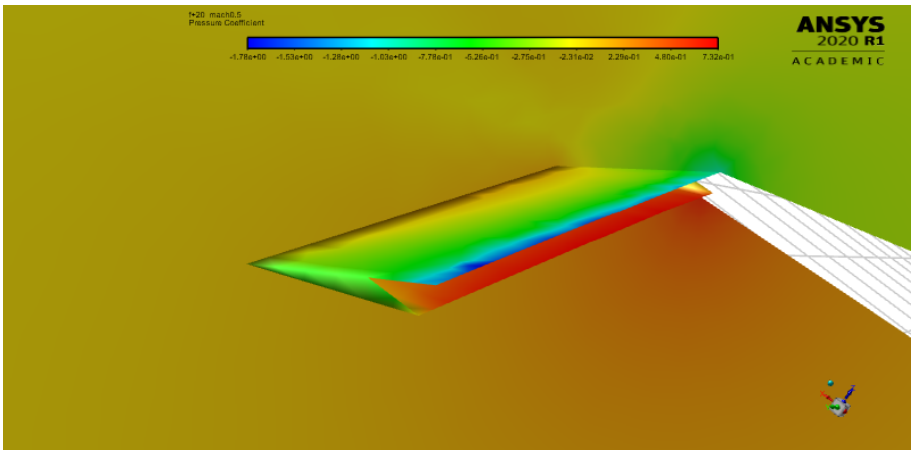

Figure 5.17: C_P on tilted flaperon of +20°at Mach 0.5.

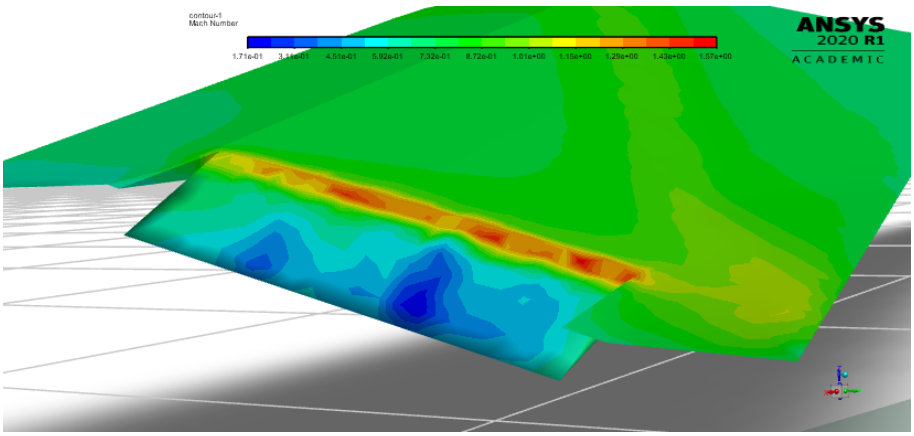

Figure 5.18: Mach number on tilted flaperon of +20°at Mach 0.7.

leads to improve C_L, wide separate region affects C_D, increasing it. Efficiency decays significantly: from 13, of previous layout, to 6, for M 0.8. As speed increases, discontinuity on flaperon goes backwards until it stabilizes on trailing edge. On the bottom surface of wing a normal shock arises near flaperon at M 1.20. As speed increases, it goes to external edge. In short, discontinuity on top surface occurs at lower speed than baseline layout, the opposite on bottom surface. From M 5 to M 8, efficiency decreases, changing the trend seen before completely. This because at very high speed, drag force on deflected flaperon is so high.
A particular difference is on flaperon edge of the upper surface. In fact, after expansion region at hypersonic speed, there is a low speed area (could suggest an high-pressure zone), fig.5.19, although in that location pressure field is consistent with suction zone: is a low-pressure zone.

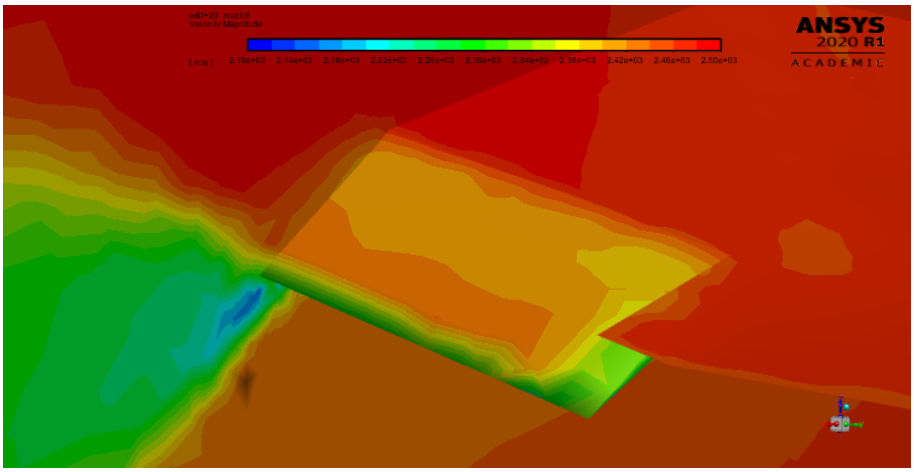

Figure 5.19: Velocity magnitude on +20°layout at Mach 8.

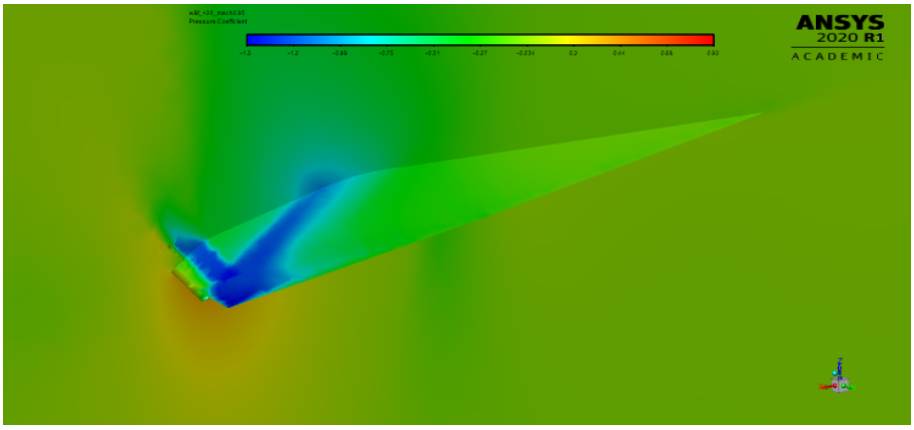

Figure 5.20: C_P field on *mod1* +20°, Mach 0.95.

Flaperon -20°

For this configuration, one might think that specular behaviour occurs, in comparison to *mod1* +20°. This does not happen because wing section isn't symmetric. When flow passes around convex surface (dorsal region) a suction region occurs, but than flow slows down by the present of flaperon. In accordance with efficiency plot 5.22 suction region after "hump" is limited by flaperon. At the same way with *mod1* +20°, critical Mach number is reached at M 0.7. It creates a normal shock on bottom side of flaperon, after a little expansion. Shock moves forward until it stabilizes on TE for Mach number at least 1.05. From M 0.8 to M 0.95, little separation on the bottom surface occurs. For M 0.95, flow around convex surface (wing) becomes supersonic through supersonic expansion. Than a shock occurs downstream because of high-pressure on flaperon. This last shock moves forward until concave edge (among

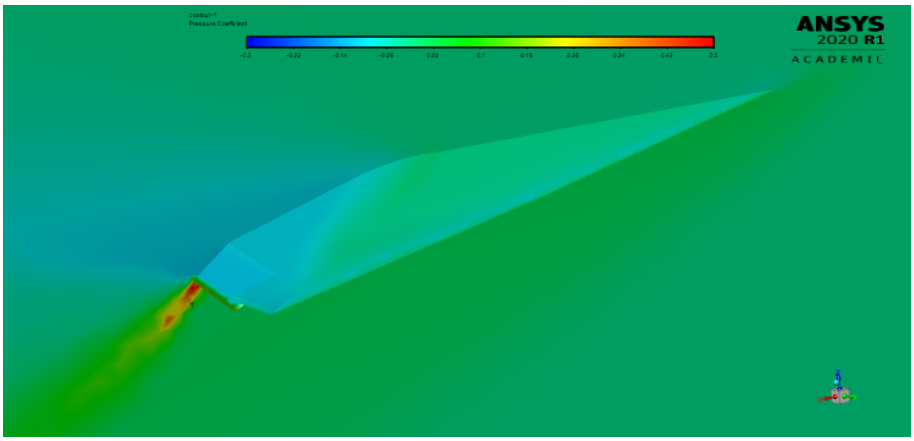

Figure 5.21: C_P field on *mod1* +20°, Mach 4.

top surface of wing and flaperon).In short, first discontinuity is located on bottom surface of the flaperon (M 0.7), than it takes shape after convex surface on top wing (M 0.95). In a similar way, other discontinuities take shape as in previous layout. When vehicle approaches to hypersonic speed, efficiency increases like in baseline mod1. This is due to shock wave that shapes under vehicle and it avoids pressure leak (from low to high), as happens in baseline configuration.

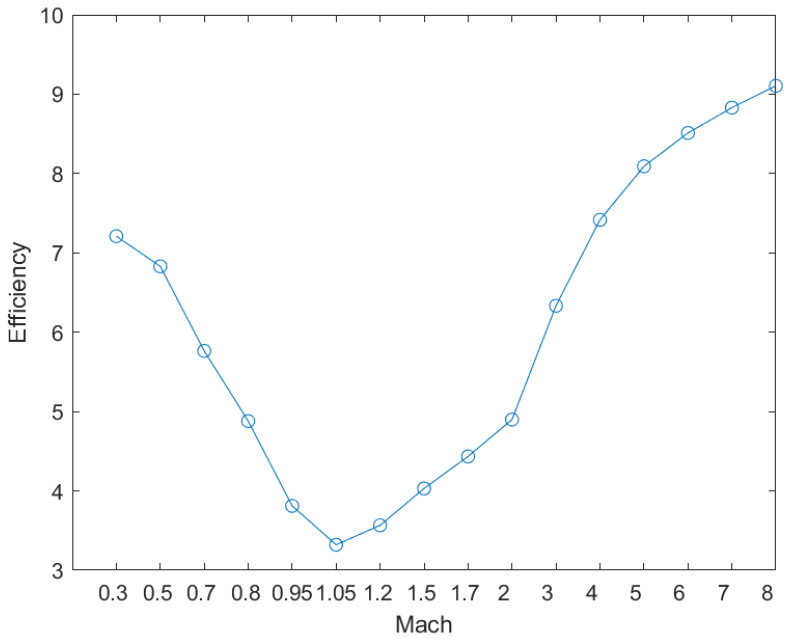

Figure 5.22: Efficiency-Mach plot for -20° layout.

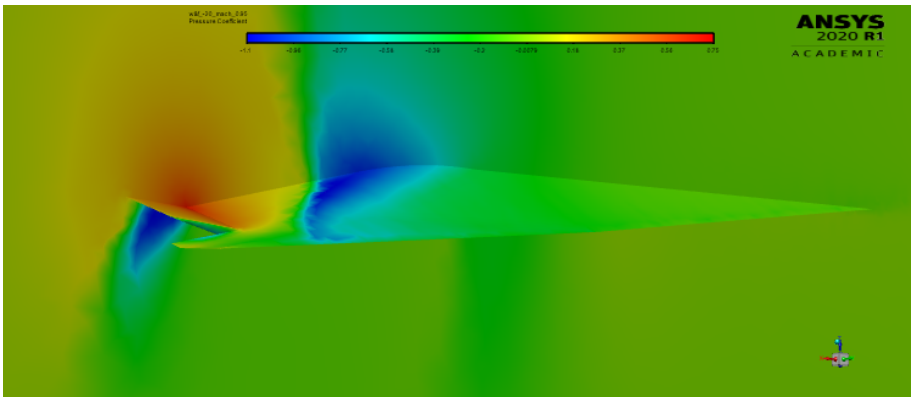

Figure 5.23: C_P field on *mod1* -20°, Mach 0.95.

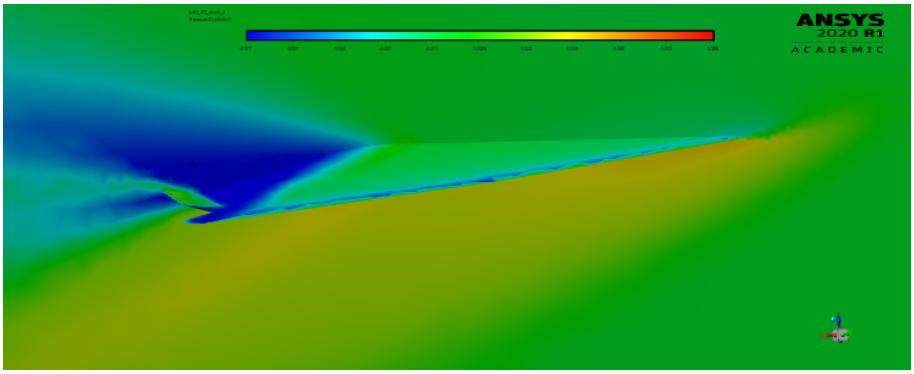

Figure 5.24: C_P field on *mod1* -20°, Mach 4.

AoA effect By figure 5.25 a bi-linear trend can be noted in subsonic range. As AoA increases, large suction on dorsal surface of wing takes place, near wingtip. It is caused by wingtip vortex that acts as vortex lift. Also area after convex surface (top surface of wing) tends to accelerates the flow. These two effects reach maximum value for M 0.95. When speed rises, this effect is even more attenuated by greater inertia of fluid particles and shock wave. For supersonic and hypersonic speed, C_L tends to be linear. In almost all AoA range, C_L is positive, except from M 2 to M 8 for $-4°$ and $-6°$. This occurs because oblique shock wave on leading edge of wing changes flow field on dorsal surface, as well as on ventral one by an expansion beam, that leads to speed up flow. At lower speed this mechanism is overcome by suction generated by convex surface.

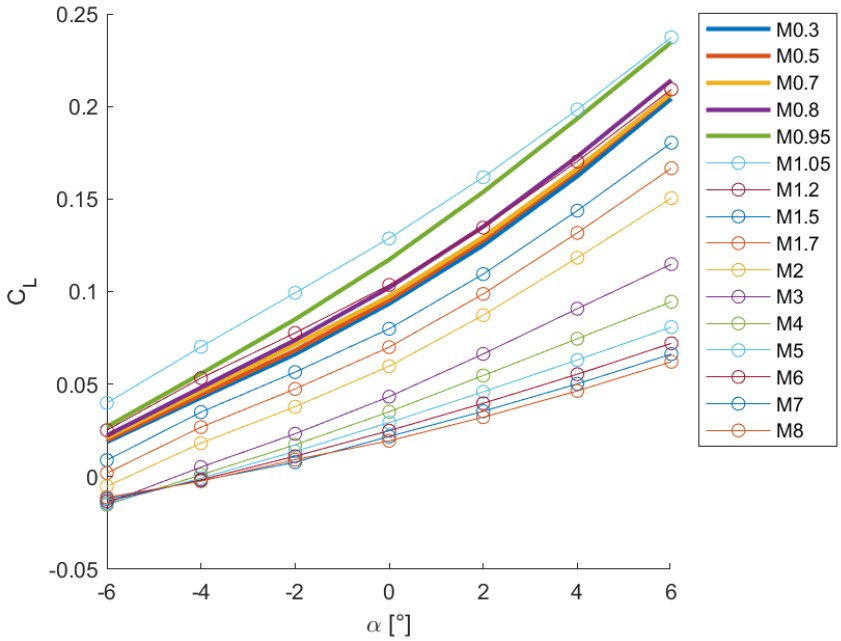

Figure 5.25: C_L-α for all speed range. Baseline layout.

Unfortunately, drag force rises very quickly at high AoA, in particular on subsonic range. In fact, main difference are located on wake region; at subsonic speed less kinetic energy leads to wide low pressure area, unlike what happens at greater speed. Wingtip vortex is another factor that affects C_D trend, through the same mechanism seen before. Low pressure on dorsal wing produce high drag because of high tilt of surface near TE. 5.27 is quite significant in terms of longitudinal stability. It can be noted that as AoA increases, C_{Mz} becomes even more negative. This means to achieve a necessary requirement for longitudinal static stability in all speed range, but it is not sufficient for baseline layout. Greater margin is attained from subsonic to low supersonic range because of same effect that creates bi-linear trend on C_L plot. By considering flaperon deflected of $-20°$, a better but limited stability in pitching can be achieved. In this configuration, deflected surface generates a downward force, which balances the nose down moment by wing. By looking the fig.5.29, it is not enough to reach longitudinal stability, especially in transonic regime. For this reason, canard and bodyflap have been introduced; they will be analysed after. Even worst is the behaviour for a tilt of $+20°$, fig.5.28. One substantial problem is due to the absence of aerodynamic trim for all speed range and AoA, except for restricted range

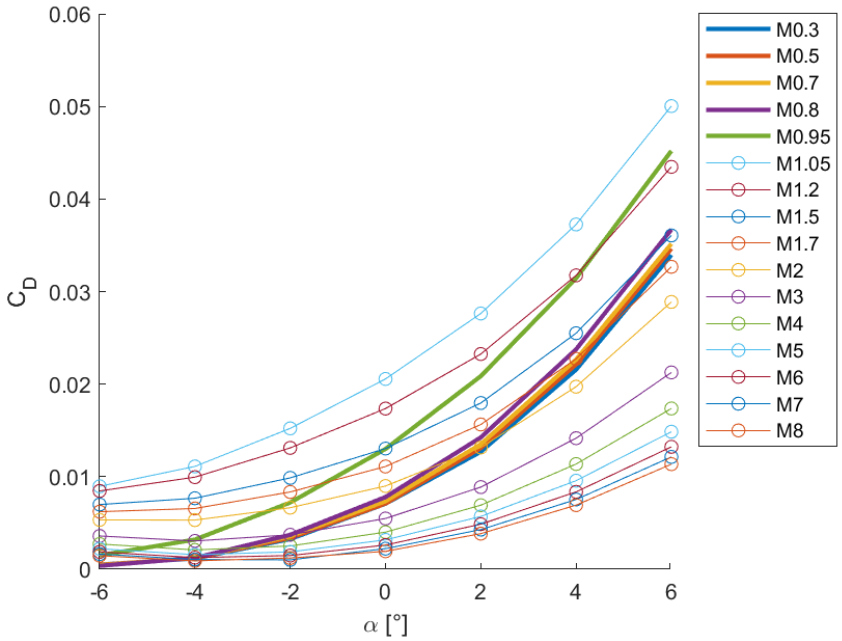

Figure 5.26: $C_D - \alpha$ for all speed range. Baseline layout.

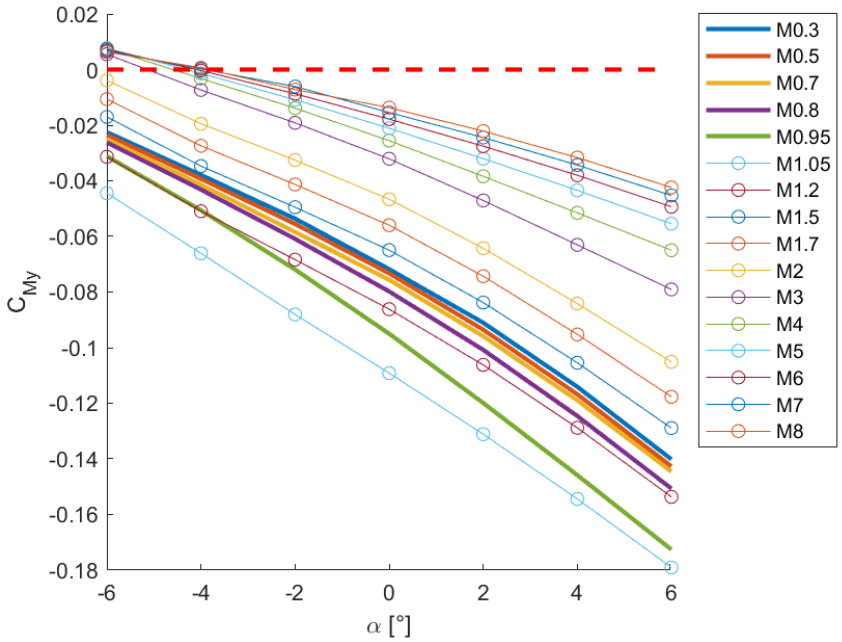

Figure 5.27: $C_{My} - \alpha$ for all speed range. Baseline layout.

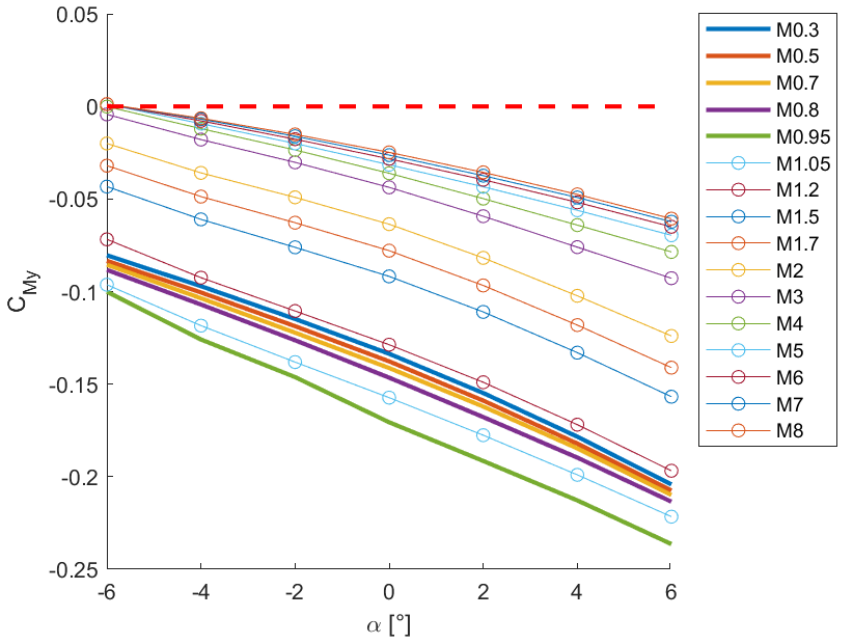

Figure 5.28: $C_{My} - \alpha$ for all speed range. +20° layout.

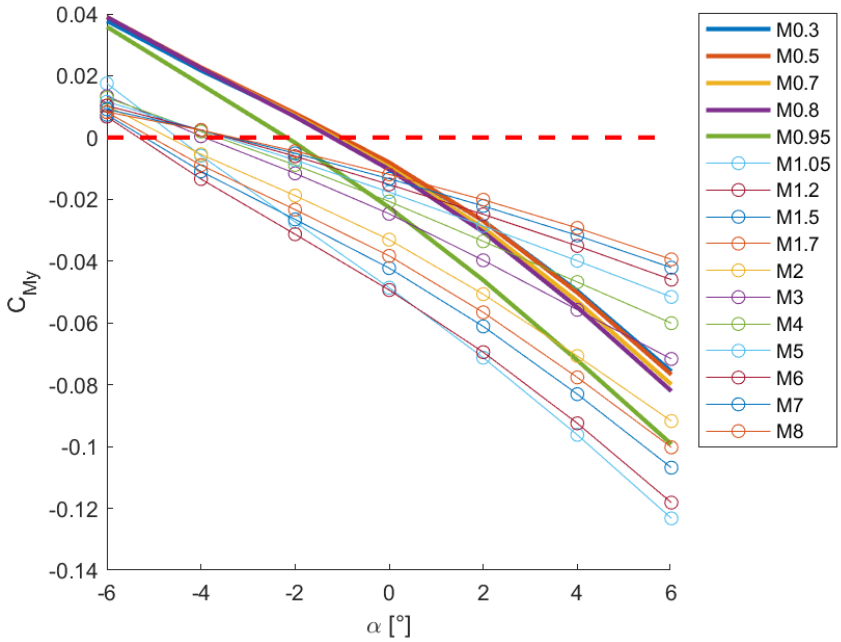

Figure 5.29: $C_{My} - \alpha$ for all speed range. -20° layout.

and only for $-6°$.

Δ Coefficients

On figg.5.30, 5.31, 5.32 are depicted delta coefficients: ΔC_L, ΔC_D and ΔC_{My}, for all tested deflections of flaperon and the most significant AoA ($-6°$, $0°$ e $+6°$). For this model, Δ coefficients are computed for two configuration: $\beta - 20°$ and $\beta + 20°$, compared to baseline configuration ($\beta 0°$), and for all AoA.

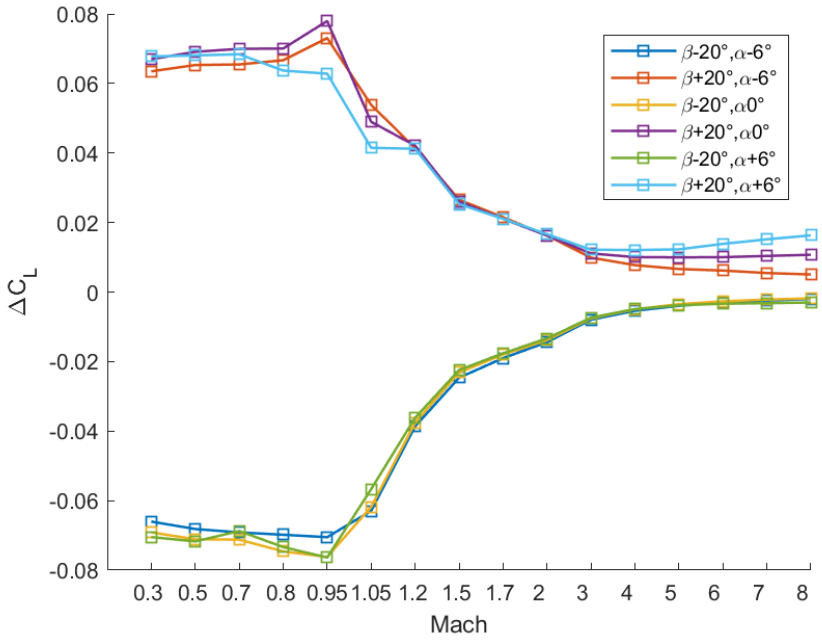

Figure 5.30: Δ lift coefficients for *mod1*.

Two effects can be noted by these plots: effect on deflection of flaperon and on AoA. Due to asymmetric cross section of wing, first effect agrees to this fact; yellow and purple lines on ΔC_L plot are asymmetric compared to X axis. Than, deflection of flaperon is more significant at low speed than high one, for all β deflections. In fact at low speed any deflection affects downstream and upstream flow field, so wing too; at high speed this does not happen. Now AoA effect on ΔC_L produces three different behaviours: in subsonic range and for negative α, it is lower in absolute value than other (red and blue lines, fig.5.30). It is because vortex lift doesn't act at that AoA. In transonic region ΔC_L decays more quickly for $\alpha = +6°$ than other, for all β (light blue and green lines), although this effect is more visible for $\beta + 20°$. In fact, in this configuration, shock wave occurs on dorsal surface (after expansion fan) and

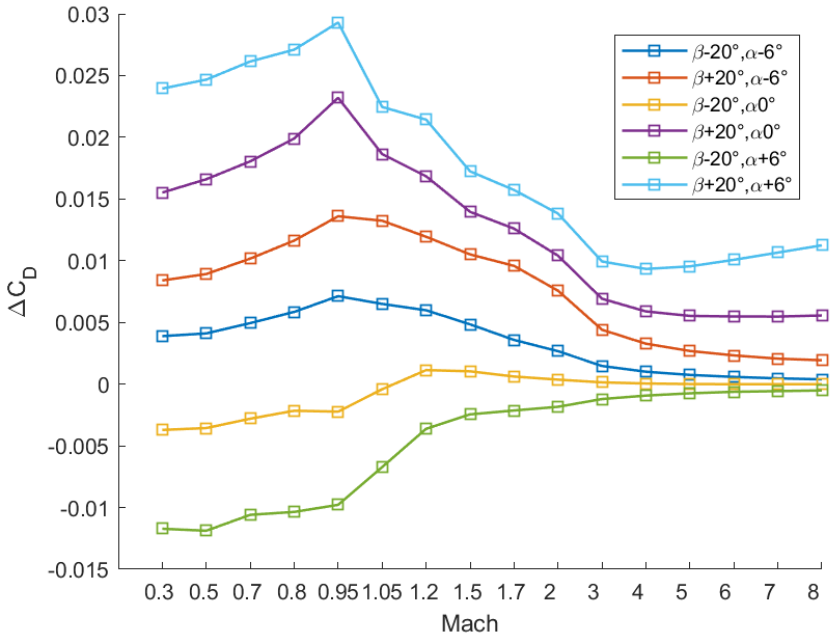

Figure 5.31: Δ drag coefficients for *mod1*.

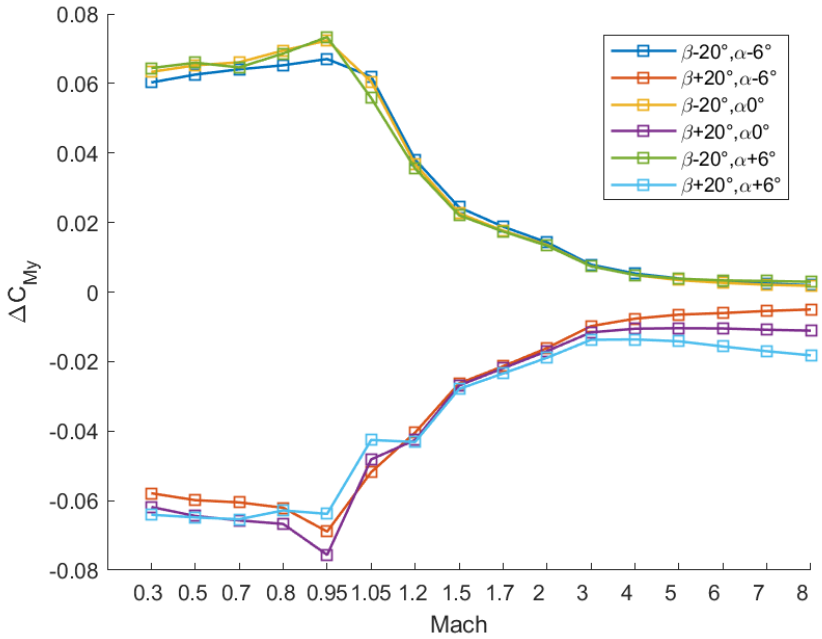

Figure 5.32: Δ pitch moment coefficients for *mod1*.

so it reduces lift force on flaperon. For the other configuration ($\beta - 20°$) happens the same phenomenology but on ventral surface while for baseline configuration doesn't happen. Third effect can be seen in hypersonic range: $\beta + 20°$ configuration mostly affects aerodynamic than $\beta - 20°$. At positive deflection of flaperon, bottom surface of wing perturbs slightly airflow, therefore deflected surface is much more effective than negative rotations.
ΔC_D plot has a particular behaviour in subsonic range for negative deflections. For 0° and +6° AoA, yellow and green lines, give a negative contribution. Although it can be counterintuitive, negative rotations mitigate high-pressure region on ventral surface of wing and increase low-pressure region around dorsal surface (near flaperon). So this mechanism acts on C_D of wing , not on flaperon. In conclusion C_D is lower in this configuration than baseline. Same AoA effect at hypersonic speed can be seen for C_D as well. Since pressure drag is much smaller than lift force, fig.5.32 is specular than C_L. Furthermore Δ values are equal to C_L because Δ coefficients show net effect.

5.3 Canard

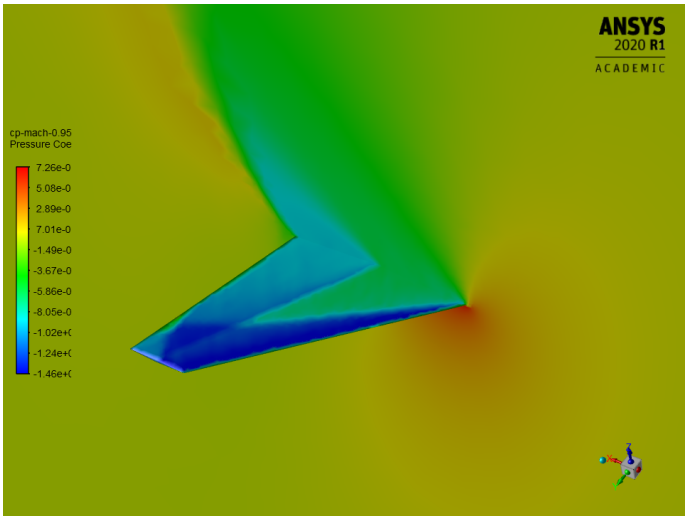

Figure 5.33: C_P field pressure on canard top surface 10°, Mach 0.95.

Also for this model, the connection surfaces are used, with the same principle previously explained. This aerodynamic surface has a swept angle of 45°. It is a diamond airflow with taper ratio of 0.32 and wingspan of 8.7 m. This kind of airfoil shape is usually used for supersonic and hypersonic range because at those speed sharp leading edge keeps shock wave near body, avoiding the occurrence of bow shock. However you can see in efficiency plot5.40 that in subsonic range efficiency

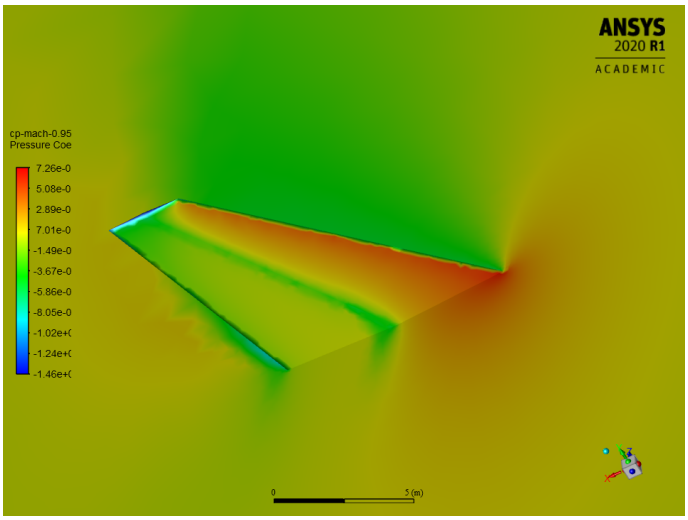

Figure 5.34: C_P field pressure on canard bottom surface 10°, Mach 0.95.

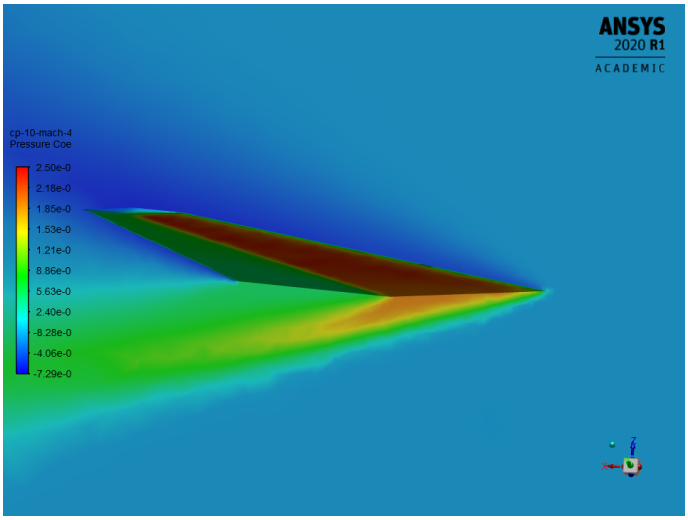

Figure 5.35: C_P field pressure on canard bottom surface 10°, Mach 4.

is greater than supersonic one. This is due to inviscid model that doesn't consider boundary layer and so possible separation, especially on convex edges of canard. This fact is even more present as AoA is higher.
Flow field around canard is not really complex. At subsonic speed and $\alpha = 0°$ flow is similar because of geometry. Therefore in whole speed range, C_L is about zero as well as C_D: on dorsal side airflow has spanwise component, due to swept wing. At M 0.95 a shock wave arise near leading edge, both on top and bottom surface: this leads to increase drag because difference of pressure occurs between divergent cross-section and convergent one (divergent cross-section means region of surface

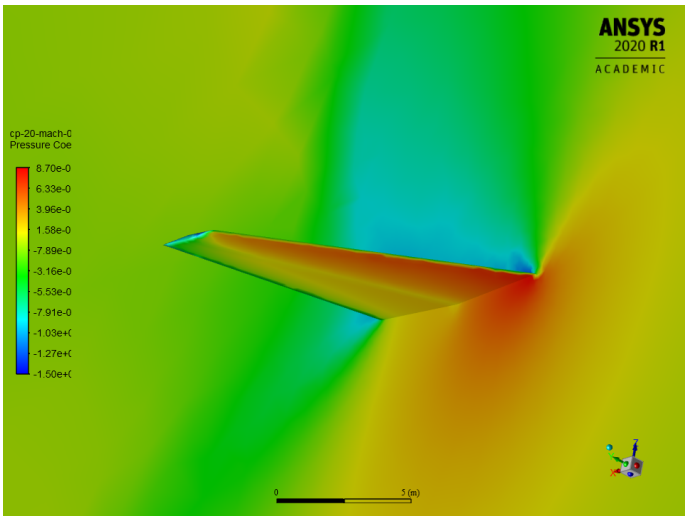

Figure 5.36: C_P field pressure on canard bottom surface 20°, Mach 0.95.

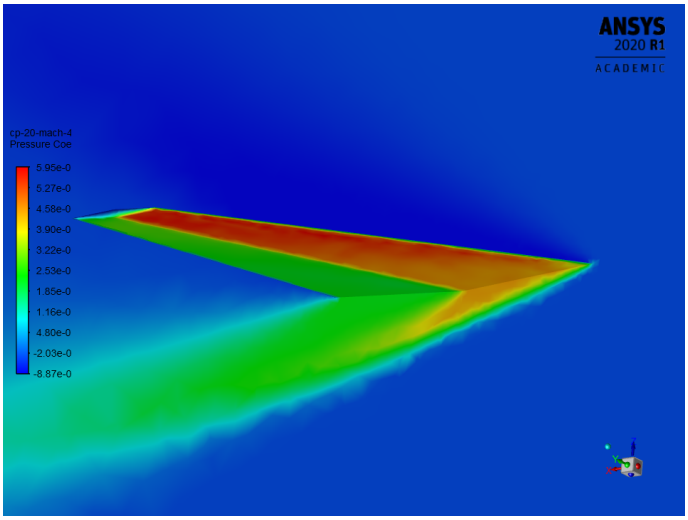

Figure 5.37: C_P field pressure on canard bottom surface 20°, Mach 4.

between Leading edge (LE) and maximum thickness). At supersonic speed a shock wave takes place on LE, than on sharp edge a supersonic expansion that precedes another shock wave on TE.
As AoA increases, flow becomes strongly 3D and asymmetric because of difference of pressure between dorsal and ventral side; this fact is magnified by considerable swept angle. At M 0.95 a shock wave occurs on ventral surface and extends for limited wingspan. This is due to lower maximum thickness and chord length on wingtip, in fact in this region flow isn't able to slow enough and also is more tilted than internal one (external perpendicular component of velocity vector is lower than

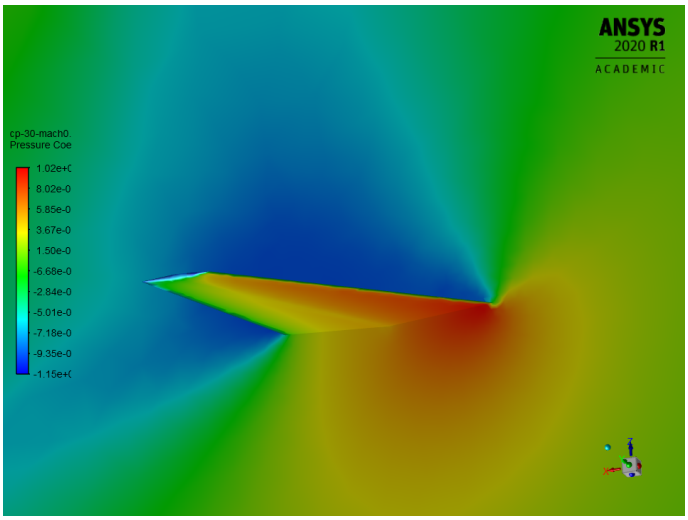

Figure 5.38: C_P field pressure on canard bottom surface 30°, Mach 0.95.

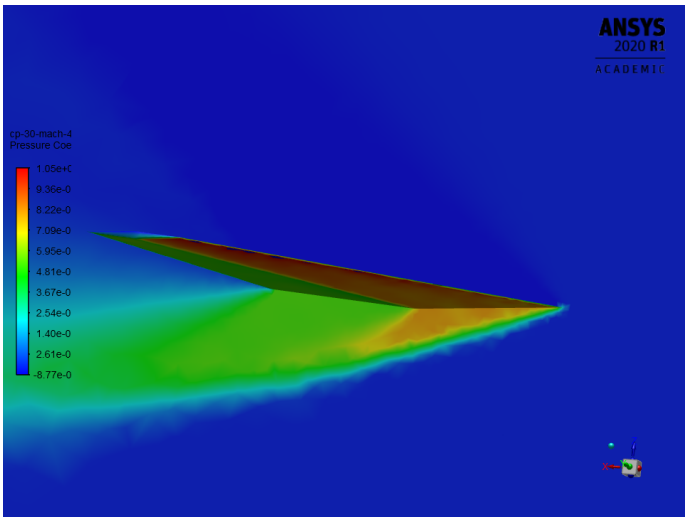

Figure 5.39: C_P field pressure on canard bottom surface 30°, Mach 4.

internal), so, after sharp edge it accelerates until an another shock wave occurs on trailing edge. On bottom surface two expansion beam can be seen along sharp edge and TE.
When unperturbed flow becomes quicker than speed sound on dorsal surface two expansions occur: near TE and over sharp edge, than a shock wave on TE slows down flow speed. On ventral surface a strong shock wave on LE is followed by a small expansion on convex edge and than on TE a weaker shock wave leads to downstream condition.

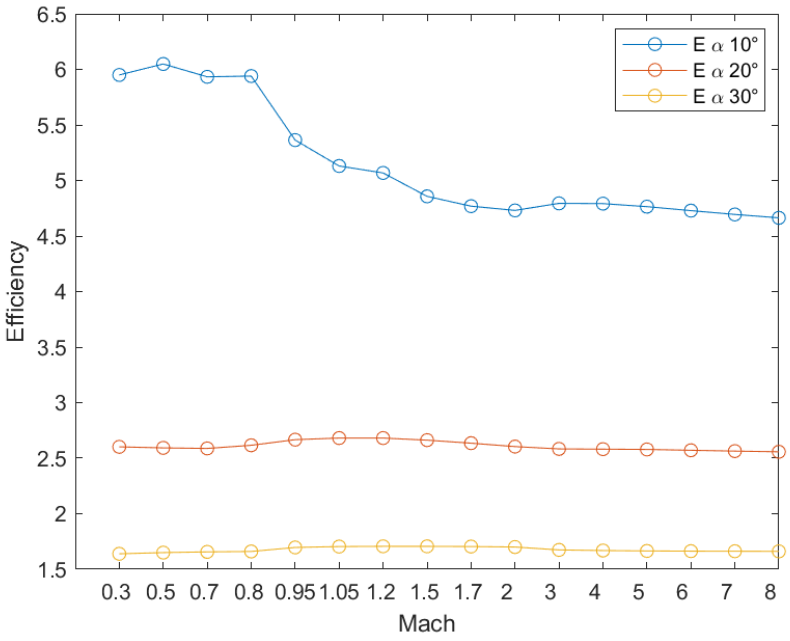

Figure 5.40: Canard efficiency for three deflected configurations.

5.4 Bodyflap and rudder

In order to limit number of mesh elements, in this geometric model partial fuselage on STRATOFLY MR3 is considered. Last 28.46 m, along X direction, of fuselage is considered. Wide in Y direction measures 6 m. Since for meshing geometry must be "watertight", three surfaces are used to close it. It was paid more attention at these surfaces, so as to limit disturbances towards upper flow field, although in the real case, below this segment of fuselage, nozzle takes place. On the forebody, bodyflap, fin and rudder are located as in fig.5.41. Rectangular trapezoid planform of the first has the following size: 24.78 m^2. Unlike cross section of flap, that of bodyflap has a small thickness to the TE because little volume is available into fuselage. The purpose of this surface is to improve longitudinal stability and to reach trimmability condition in all speed field.
Because of intrinsic roll instability due to negative dihedral angle of wing, fin and rudder are tilted of 38.1° in YZ plane to improve it. Than with this layout rudder can be employed as elevator as well. In comparison with conventional configuration this one reduce wetted surface, so even drag. They have trapezoidal planform, 47.07 m^2 and 21.15 m^2 respectively. Free terminal part of the fin is concave and it extends for 1.55 m (along axis).
On first part of fuselage surface, at constant inclination, flow pressure doesn't change

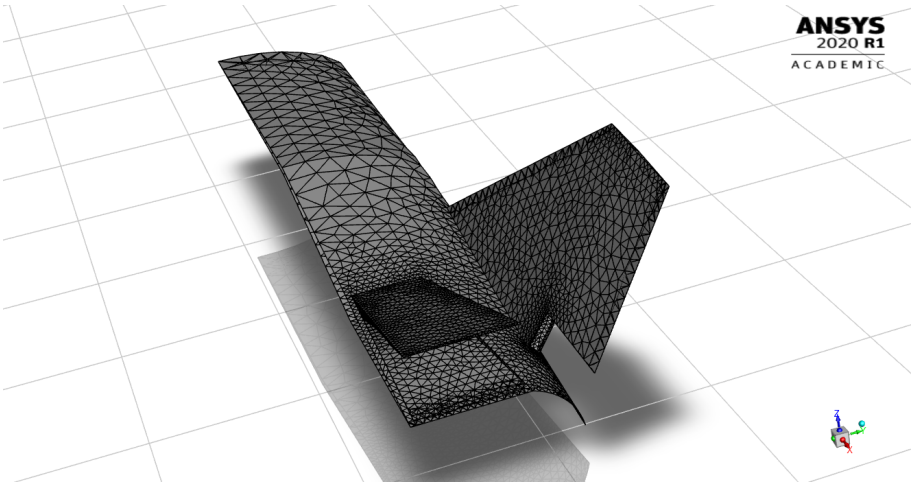

Figure 5.41: Mesh model for *mod3*. Bodyflap is tilted of -20°, rudder 0°.

significantly since surface is almost completely aligned with flow direction. Only towards the tip pressure slightly increases locally, because surface is wide near convex edge. Than an expansion takes place over edge that connects two contiguous fuselage surfaces. Due to different bend radius, the acceleration of the airflow is not uniform; is marginally higher near symmetry plane than outwards. Continuing to bodyflap, signal of downward pressure (high) affects flow locally. Therefore C_P is negative for large portion of surface, it becomes greater than zero for the last 1.7 meters approximately from TE: net pressure contribute on bodyflap is negative.
Due to curvature effect of edge and geometry of fin, delta pressure is generated between inner surface and outer. On the first surface, a low-pressure region occurs and vice versa for outer one. It results in non-zero force produced. Along spanwise of fin, airflow is quiet similar to that of swept wing. In fact, looking from the side, airflow around inner surface is deflected to the root for leading edge, but than goes to tip for gradient pressure among dorsal and ventral surface. On outer surface this behaviour acts in opposite way. First mechanism can be explained by considering two parallel fluid streamlines, perpendicular to LE. The innermost, near the root, passes before than external one, so acceleration on LE takes place in advance than other. Due to different pressure of two streamlines, external one goes to internal one. On rudder surface, airflow tends to slow down because of triangular cross-section, until C_P becomes greater than zero. However, for a large part of surface is less than zero, to the exclusion of approx. one meter from TE. Airflow on rudder is not symmetric because of asymmetry of flow originates from fin: C_P on inner side is greater than outer, in absolute value. For this reason C_{Mz} is positive.
As Mach increases, supersonic expansion and shock waves occur. For M 0.8 flow becomes transonic but flow field does not really change. When M reaches 0.95, flow field is extremely different than previous: vanishing shock and expansion are

created on the underside of “LE fuselage" and upside, respectively, than an intense expansion is created over edge of fuselage; it is followed by a slight shock. Shock is due to inwash effect that is visible after edge of fuselage. Considering also specular part of mod3, in relation to plane of symmetry, flow field creates a sort of convergent section by vertical surfaces presence; deceleration of flow is unavoidable. Because of difference between supersonic flow around fuselage and subsonic one by downstream condition, another shock arises near TE. It is more intense than previous and impinges on rudder surface.

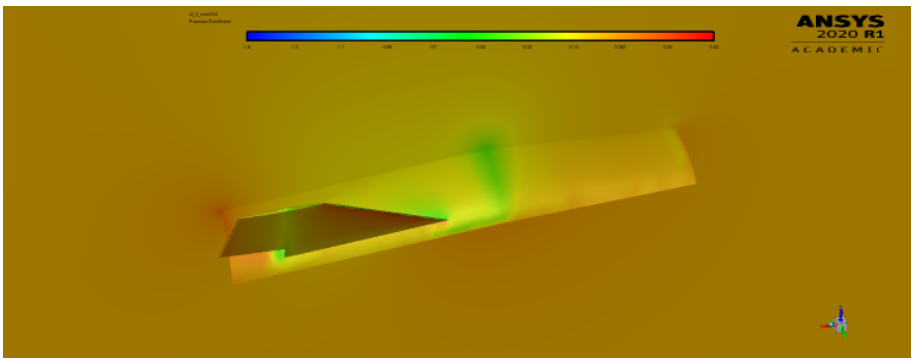

Figure 5.42: C_P field pressure on *mod3* bodyflap 0°, Mach 0.5.

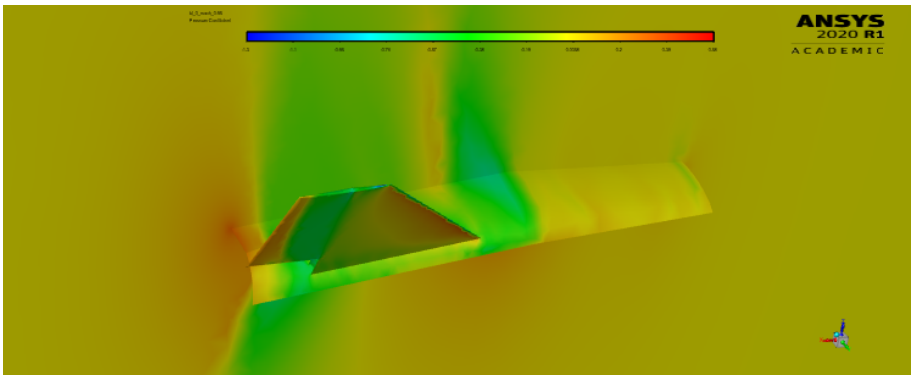

Figure 5.43: C_P field pressure on *mod3* bodyflap 0°, Mach 0.95.

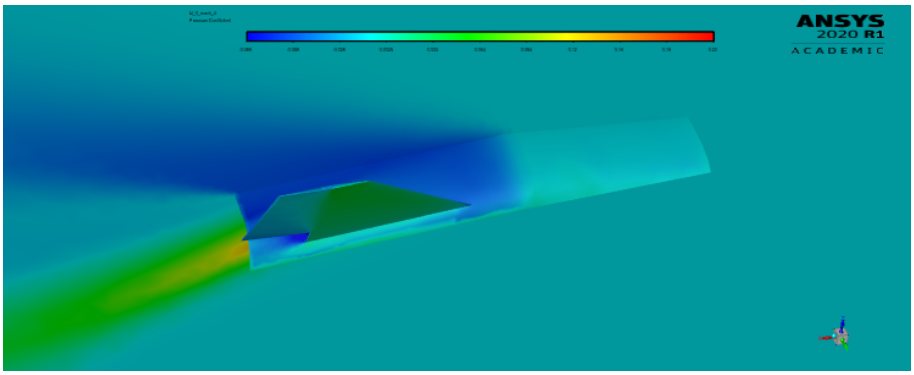

Figure 5.44: C_P field pressure on *mod3* bodyflap 0°, Mach 4.

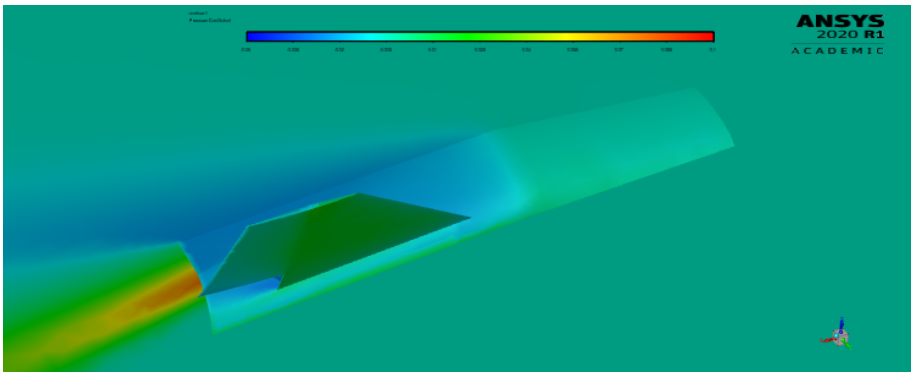

Figure 5.45: C_P field pressure on *mod3* bodyflap 0°, Mach 8.

On inner surface of the fin, airflow becomes supersonic because of an expansion near LE, than flow slows down, although C_P is always less than zero. It happens the opposite situation on external side: subsonic flow is slight accelerated. Thus on rudder surfaces occur two supersonic expansion over edges of discontinuity (between fin and rudder), followed by two shock wave: on outer surface (of rudder), shock wave is shifted to TE than internal one. As it can see in fig.5.57, C_{Mz} is positive because airflow is not symmetrical. This mechanism leads to change the behaviour of rudder for this configuration and speed only. This behaviour of flow field is similar for M 1.05 but now shock waves are on TE of rudder. In addition, a reflected shock takes place on internal surface of fin after expansion, than another reflected shock creates a particular region highlighted in fig.5.50.
From M 3 to cruise speed, first expansion on fuselage (over the convex edge) is tilted to the point that unperturbed airflow affects flow around external region of fin and rudder, 5.53: this produce a diminishing of ΔC_P, so also absolute value in C_{Mz}. At these speed flow field is even more aligned for high inertia forces and so, particular shock waves pattern seen in transonic and low supersonic regime is absent.

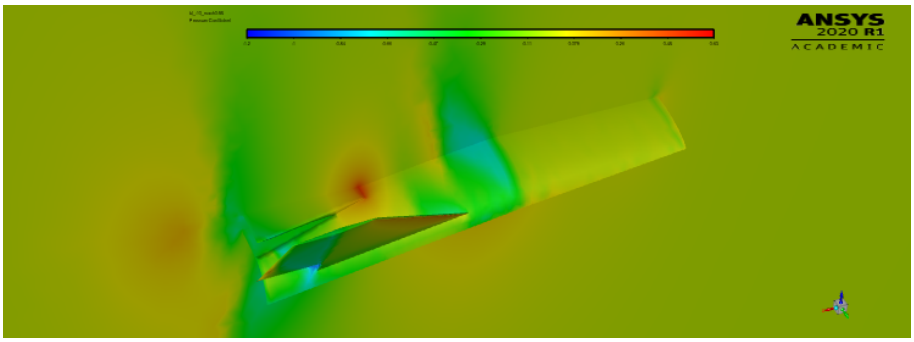

Figure 5.46: C_P field pressure on *mod3* bodyflap -10°, Mach 0.95.

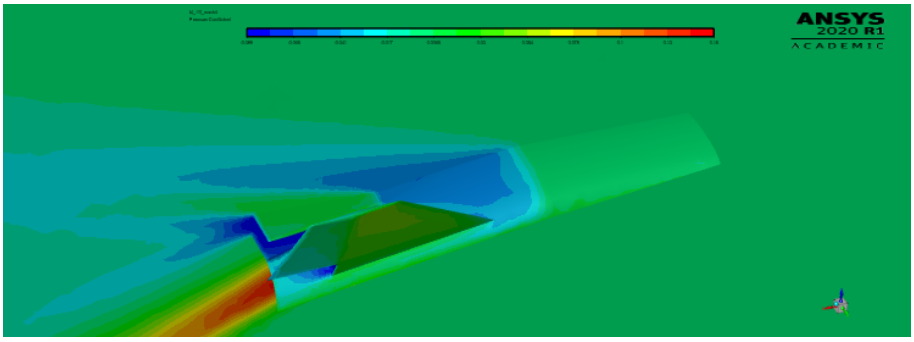

Figure 5.47: C_P field pressure on *mod3* bodyflap -10°, Mach 4.

When bodyflap is tilted by -10°, the behaviour changes completely. C_L is now less than zero, and so surface can be used to alter vehicle attitude by means of positive pitching moment generated. Therefore initial acceleration of the airflow (over edge of fuselage) is slowed by bodyflap deflection. Moreover bodyflap affects evolution of flow field around fuselage. High-pressure region, generated by the presence of bodyflap, affects inwash component of airflow, which it traduces in the absence of particular shock waves pattern aforementioned. This is perceived on LE of fin as well; now flow is more aligned with that surface and this effect is even more noticeable as β_{Bf} rises.
At M 0.95 and $\beta_{Bf} - 10°$, a stronger shock wave takes place on fuselage after first expansion (convex edge), for most of spanwise length and before fin LE. As deflection increases, discontinuity moves to upstream because of higher pressure over bodyflap. Then internal expansion, that derives from the connection between fin and rudder, affects external area near TE of bodyflap, fig.5.54 in blue. For this reason discontinuity on bodyflap, near TE, is absent in this case.
When speed reaches M 1.05 ($\beta_{Bf} - 10°$) shock wave in front of bodyflap is closer to this last. Therefore it is stronger in comparison with baseline *mod3*, and impinges on internal surface of the fin. This behaviour affects significantly the aerodynamic

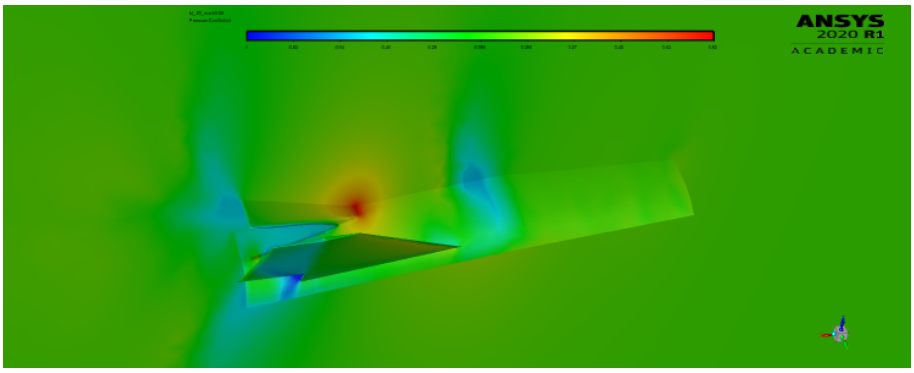

Figure 5.48: C_P field pressure on *mod3* bodyflap -20°, Mach 0.95.

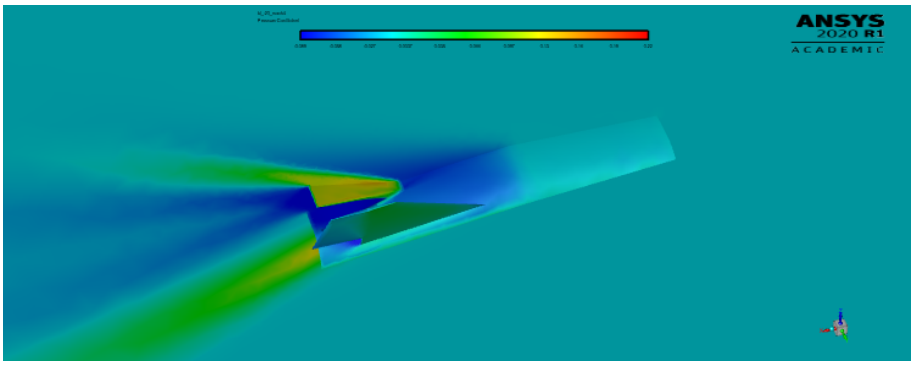

Figure 5.49: C_P field pressure on *mod3* bodyflap -20°, Mach 4.

characteristics: C_{My} rises for all configurations, fig.5.55. Now on the TE of bodyflap, there is an expansion instead of shock wave.
As speed increases, shock wave that impinges on fin is even more curved. Now it interacts with expansion generated by connection between fin and rudder, consequently the effect produced by this expansion is mitigated, fig.5.56. Mach number for which this occurs, it depends to bodyflap rotation. By Mach 3 onwards, this shock doesn't interact with rudder surface.

Rudder effect As you can see in fig.5.57, aerodynamic coefficients aren't symmetric because flow field is already asymmetric in baseline configuration: negative rotations of rudder are more effective than positive one. This happens because when flow is speed up by deflected surface of fuselage, greater suction region is produced on inner surface of rudder. Conversely, when you consider positive rotation, the accelerating effect of fuselage acts negatively: high-pressure region is mitigated.
It is notable an effect induced by positive rotations of rudder on bodyflap, for M 0.95. Due to position of rudder, a shock is produced on fin and along the entire fuselage

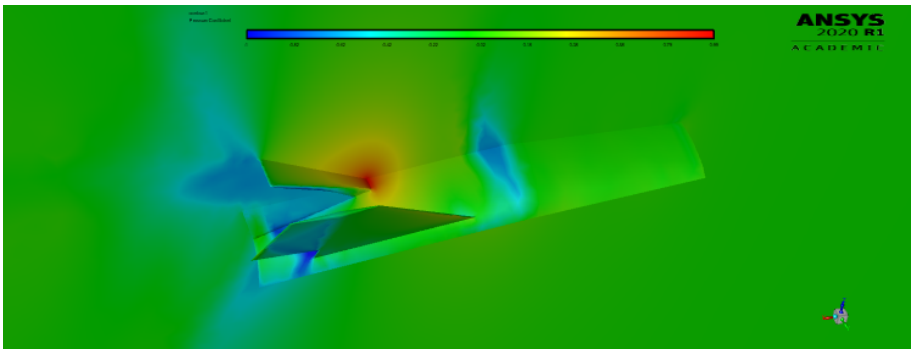

Figure 5.50: C_P field pressure on *mod3* bodyflap -30°, Mach 0.95.

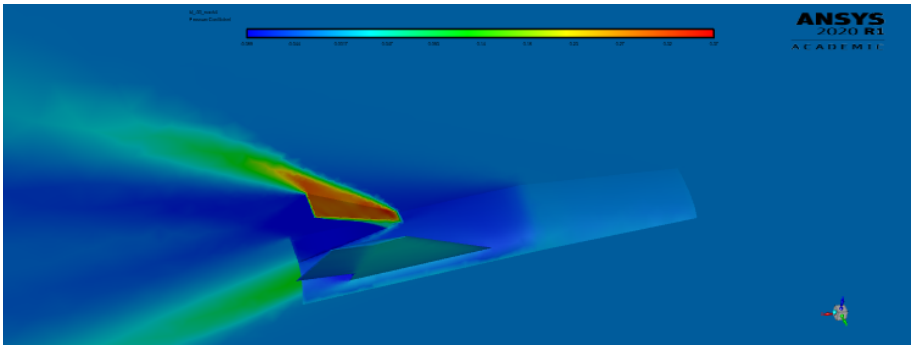

Figure 5.51: C_P field pressure on *mod3* bodyflap -30°, Mach 4.

(in Y direction): downstream of the shock a high-pressure region takes place, and so bodyflap can benefit from this, fig.5.58. Between M 2 and M 3 expansion waves, on convex surface of fuselage, are tilted very much, so unperturbed freestream interacts with the tip of rudder and fin as well. For positive rotation angle (rudder), higher pressure on internal surface (Mach freestream is lower) increases yawing moment. In the other hand, for negative angle, higher pressure reduces suction region (on internal surface). Consequently, in terms of C_{Mz}, the discrepancy between M2 and M3 in the first case is thinned, while is remarkable in the second one, fig.5.57.

Δ C_P comments As we expected ΔC_L is less than zero because all negative deflections generate negative lift force. In subsonic range Δ C_L rises in absolute value as rotation angle increases because of low-pressure region under bodyflap. The more bodyflap is tilted, the greater suction region. Maximum value all Δ coefficients is ranging from M 0.95 and M 1.2 (transonic range). This is due to shock wave that occurs at the front of bodyflap for all deflected surfaces while in baseline configuration doesn't happen.
Solid lines represent same solutions by panel method previously performed: solutions

Figure 5.52: Reflected shock induced by inner surface of fin. Mach 1.05 on the left, Mach 1.2 on the right.

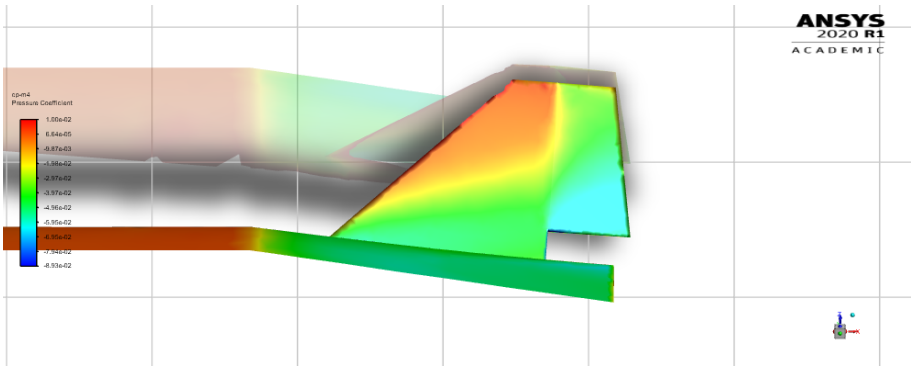

Figure 5.53: Effect of supersonic expansion on fin and rudder. Pressure field at Mach 4.

range goes to M 1.5 to M 8, for all bodyflap deflection, and for deflections of +10° and -10° for rudder. These curves fit relatively in hypersonic range, especially for low deflection angles, while don't fit well in supersonic. This is due to intrinsic nature about this model: it is a simple and fast method based on potential flow, so viscosity is neglected. At hypersonic speed inertial forces are greater than viscous ones; this shows good fit in that range of velocity. Δ coefficients for rudder confirm trend seen for absolute coefficients, namely, asymmetry with respect to the $X = 0$ axis for ΔC_L. It can be especially seen in hypersonic range because of interaction of freestream with tip area. Trends on speed range are met: in subsonic range all coefficients rise as Mach number increases; in transonic range peaks are reached; at higher speed tend to reach asymptotic condition for loss of dependence for freestream Mach on oblique shock relations. Also in this case a solution by means of panel method is given, but for -10°and +10° deflection only. As for bodyflap case, CFD and panel methods fit approximately at higher speed because density ratio tends to constant value $(\gamma + 1)/(\gamma - 1)$.

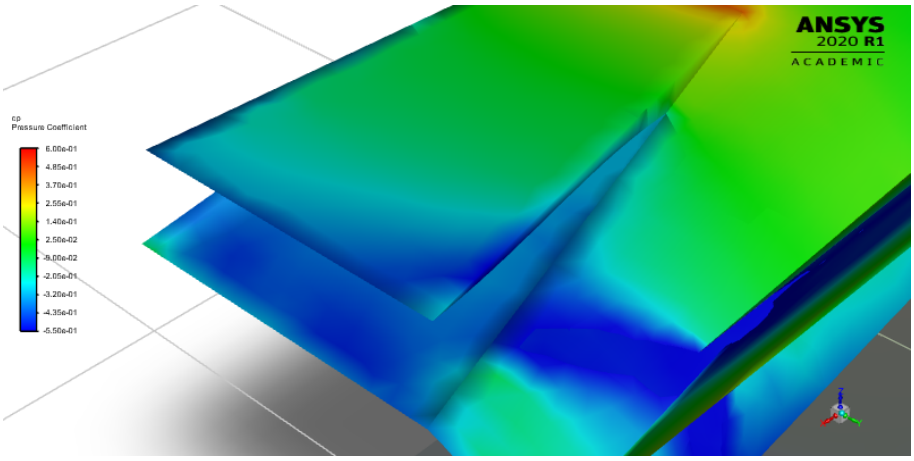

Figure 5.54: Supersonic expansion affects bodyflap surface. Pressure field at Mach 0.95, bodyflap -10°.

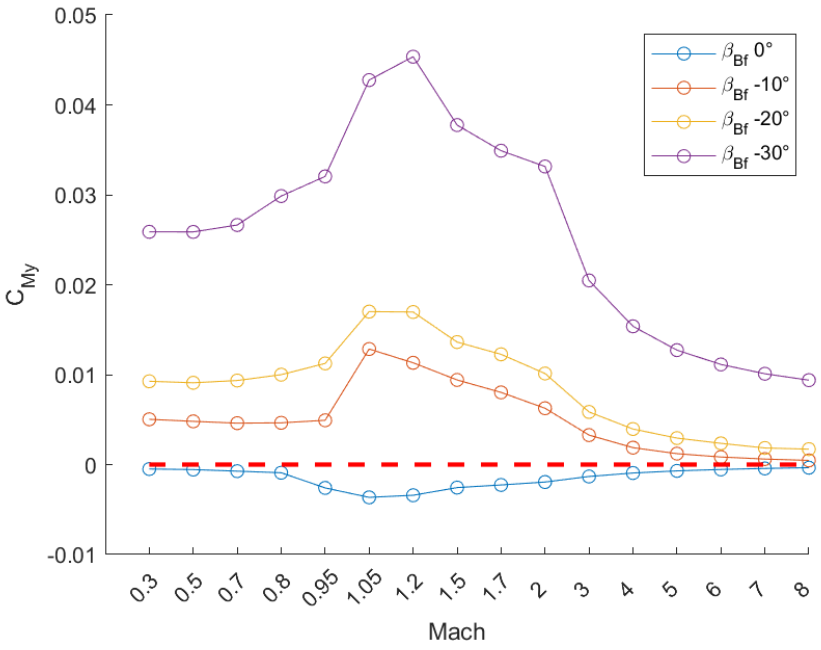

Figure 5.55: C_{My}-Mach for all bodyflap configurations.

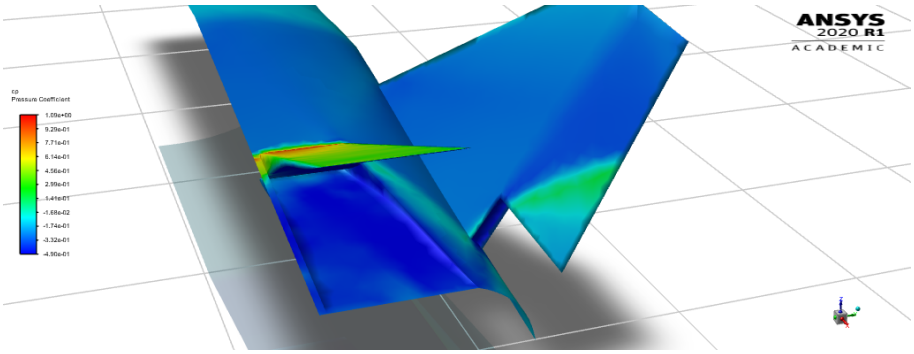

Figure 5.56: Curved shock wave impinges on rudder displayed by pressure field. Bodyflap -30°, Mach 2.

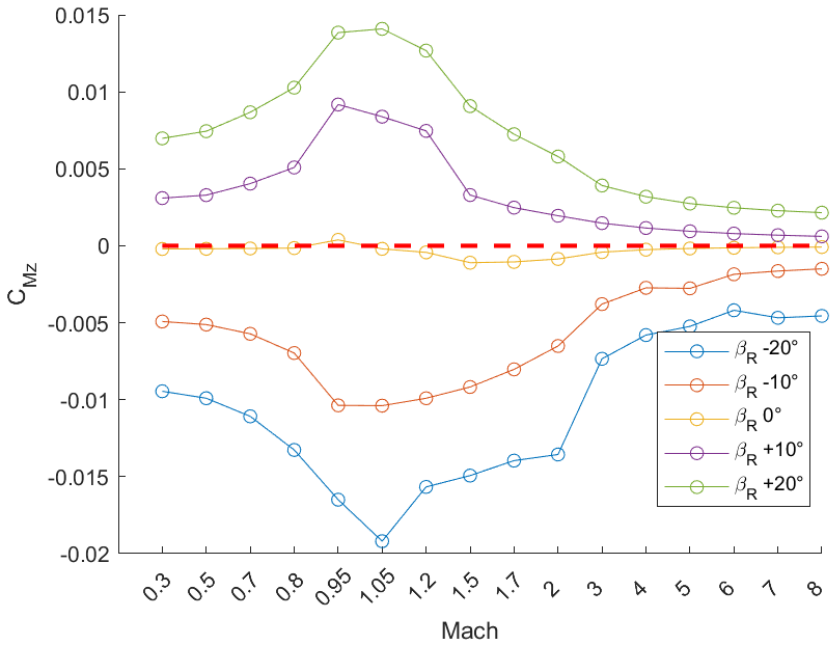

Figure 5.57: C_{Mz}-Mach for all rudder deflection.

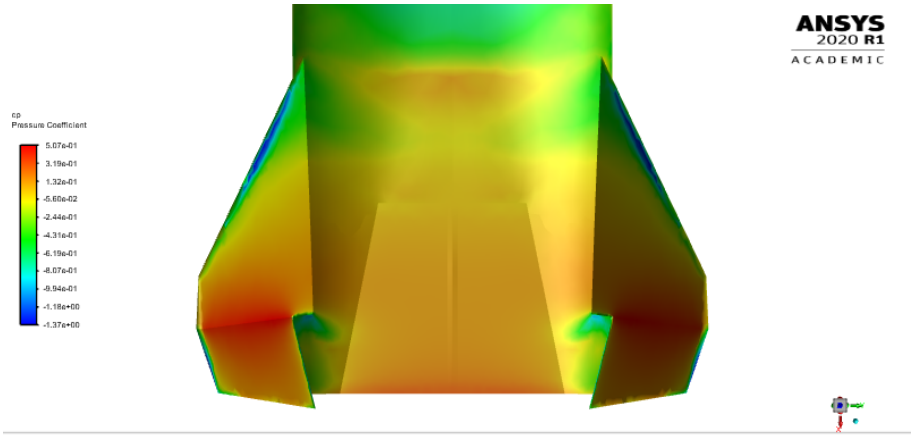

Figure 5.58: Shock wave generated on fin displayed by pressure field. Rudder +20°, Mach 0.95.

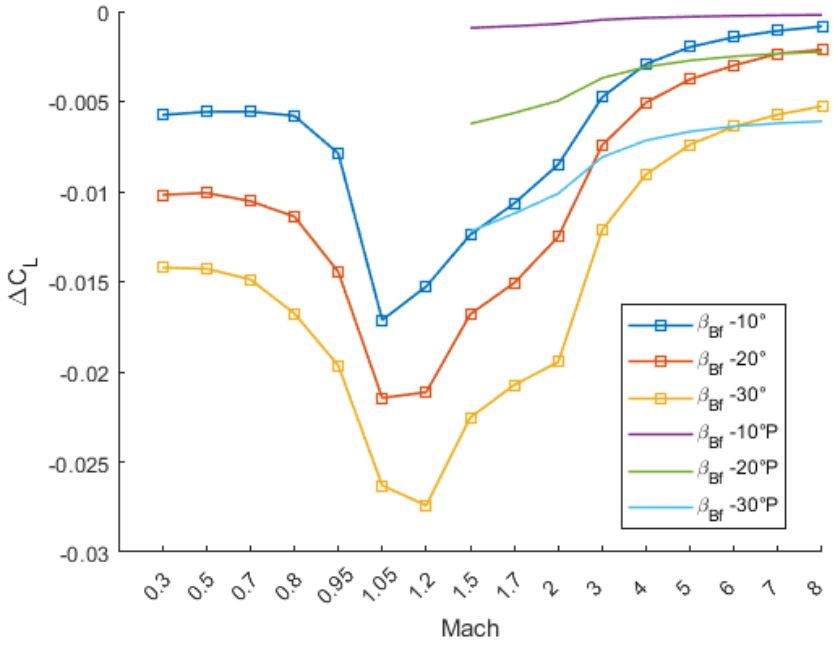

Figure 5.59: Δ lift coefficients for bodyflap.

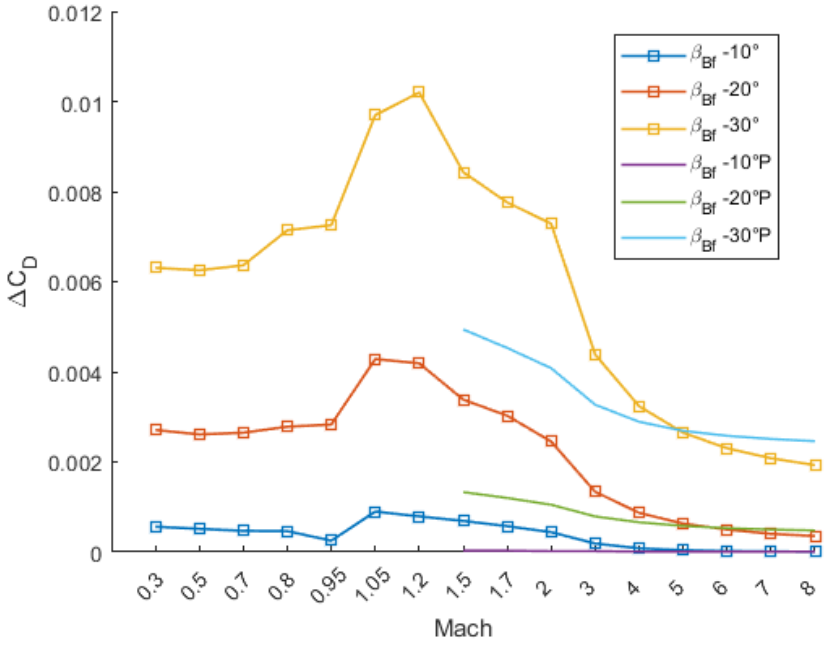

Figure 5.60: Δ drag coefficients for bodyflap.

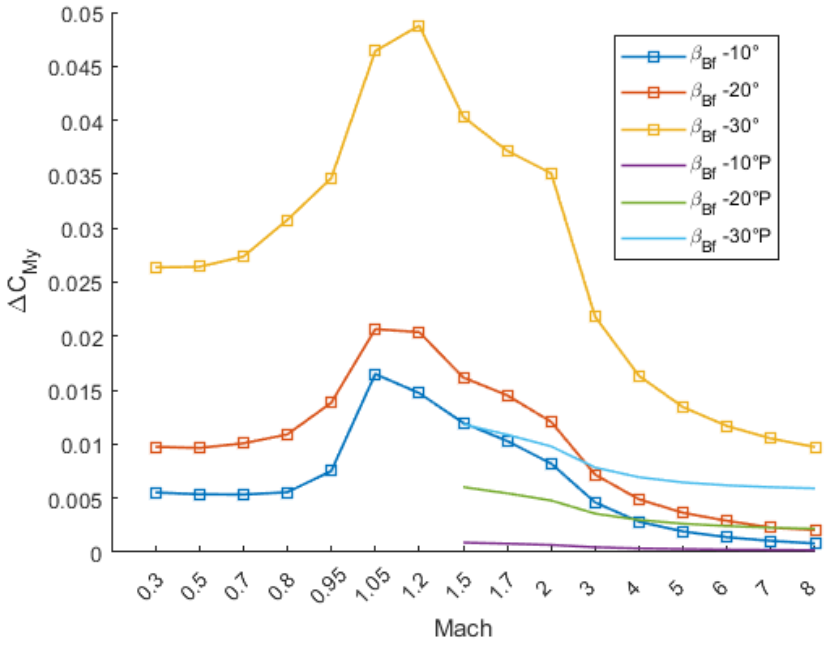

Figure 5.61: Δ pitch moment coefficients for bodyflap.

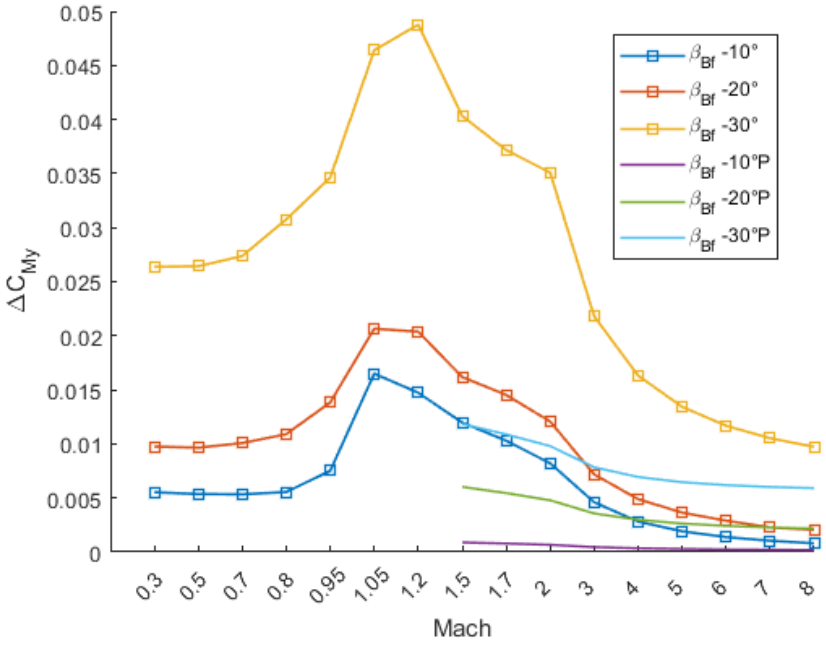

Figure 5.62: Δ lift coefficients for rudder.

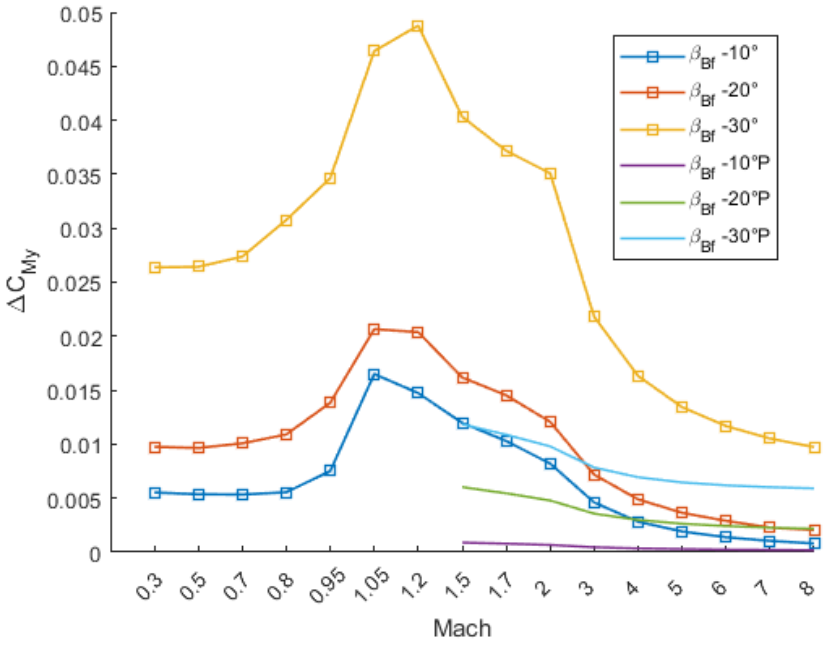

Figure 5.63: Δ drag coefficients for rudder.

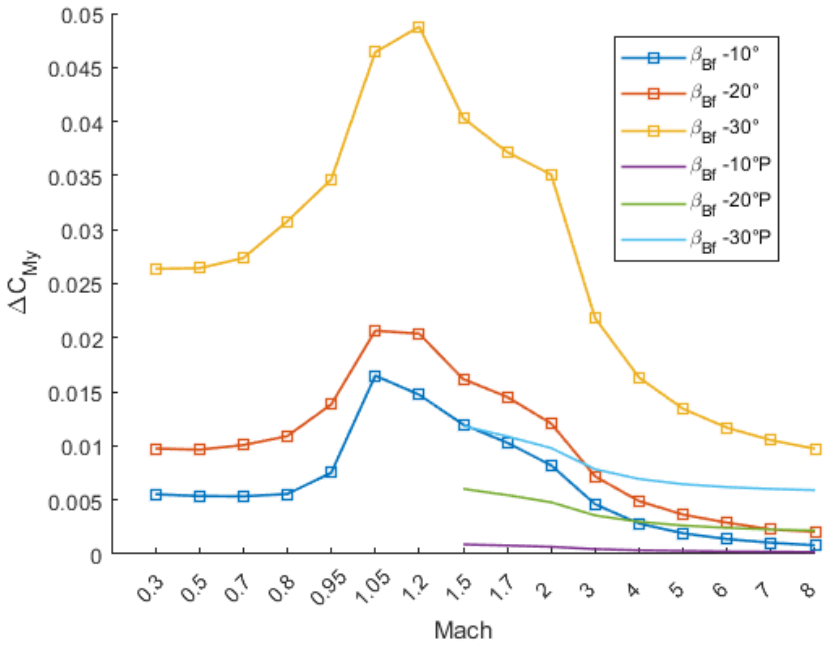

Figure 5.64: Δ yaw moment coefficients for rudder.

Chapter 6

Conclusion

In order to assess aerodynamic characteristics of main control surfaces of MR3 airplane, a large amount of CFD simulations (528) were performed. The intent was to utilize a better tool than panel method (previously employed), for aerodynamic characterization of control surfaces, in a wider range of speed. By means of these data, stability evaluations and subsequent more accurate trajectory simulation will be performed.
The obtained outcomes are quite comforting, because coefficients have similar trends in all speed range. Furthermore, through detailed flow field analysis conducted in previous chapter, data make physical sense. However, physical model utilized is based on several intrinsic assumptions that can significantly change results. Having neglected viscosity terms in momentum and energy equations has its implications. In the real case, separation regions can occur when we regard more inclined surfaces, especially in subsonic range, because ones with sharp edges aren't appropriate for that range of speed. Besides, at high-speed, shock waves can induce separation.
These facts lead to significantly affect both lift and drag forces, by reducing efficiency. Secondly, since vehicle is very long, in the real case a thick boundary layer takes place: it affects flow field such as shock waves position. Than, substantial part of total drag for a streamlined body (as MR3) is due to skin friction, that is a viscous contribute. So drag force is always underestimate.
However, some problematics are partially compensate by the fact that only delta coefficients are taken into account; relative value should be more accurate than absolute one because inaccuracy are compensated. Another aspect deviating from physical model chosen is the high-speed effect: aerodynamic heating has a non-negligible consequence, especially at stagnation points. Furthermore, at hypersonic speed, chemical reactions may occur where flow is warmer: there phenomena affect flow field.
"Compartmental approach" doesn't take into account mutual interaction between control surfaces, fuselage (partially for mod3) and engine. Particularly, when you

consider bodyflap and rudder, hot air, that comes out from nozzle, affects downstream flow. Instead for canard wing, interference effect isn't considered because simplified model was used. Although aerodynamic coefficients have been computed by means of easy method, which has clear aforementioned limitations, in early stage of design process it may give good information about control surfaces effect. Moreover, this method is characterized by relative fast obtaining speed of data, and so, it is suitable for parametric analysis.
In order to know the behaviour of control surfaces for different configurations, further analysis must be undertaken. At the same time, it would be needed to carry out some simulation through more accurate physical model, such as RANS with compressible Spalart-Allmaras turbulence model, as suggested CIRA [7]. Hence, a comparison between these data could be useful to quantify the difference, and to find corrective factors to improve simplified model outcomes.
Looking at aerodynamic coefficients, the greatest changes, compared to Mach number, are located in transonic regime where shock wave change completely characteristics of flow field. More detailed trend can be achieved by choosing a different sequence of speed. Moreover, since several control surfaces, when deflected, can anticipate the formation of shock wave (at lower Mach number), this behaviour should be analysed accurately in high subsonic regime, in order to be congruent with subsonic flight path; it is necessary to delay shock wave formation close to inhabited areas.

Bibliography

[1] Bentley, M. A. *Spaceplanes*. Springer, 2009;

[2] Cockrell C. E., Huebner L.D:, *Aerodynamic Characteristics of Two Waverider-Derived Hypersonic Cruise Configurations*, 1996;

[3] Chiesa S., Russo G., Fioriti M., Corpino S, *Status and Perspectives of Hypersonic Systems and Technologies with Emphasis on the Role of Sub-Orbital Flight*, 2015;

[4] Feng D., *An overview of waverider design concept in airframe/inlet integration methodology for air-breathing hypersonic vehicles*, 2018 ;

[5] Hallion R., Schweikart L., *The Hypersonic Revolution Case Studies in the History of Hypersonic Technology*, 1998;

[6] Kirkham F. S., Hunt J. L. *Hypersonic transport technology*, Elsevier, 1976;

[7] Langener T., Steelant J., Roncioni P, Natale P. and Marini M. *Preliminary Performance Analysis of the LAPCAT-MR2 by means of Nose-to-Tail Computations*. 18th AIAA/3AF International Space Planes and Hypersonic Systems and Technologies Conference, 2012;

[8] Langener T., *Trajectory Simulation and Optimization of the LAPCAT-MR2 Hypersonic Cruiser Concept*, 2014;

[9] Liu S. K., *Numerical Simulation of Hypersonic Aerodynamics and the Computational Needs for the Design of an Aerospace Plane*, 1992;

[10] Rondeau C. M., *X-51A Scramjet Demonstrator Program: Waverider Ground and Flight Test*, 2013;

[11] Steelant, J., *Achievements Obtained for Sustained Hypersonic Flight within the LAPCAT-II project*, 2015;

[12] Voland R. T. et. at.,*X-43A Hypersonic vehicle technology development*, 2006;

[13] Krempus D., *Evaluation of the Aero-propulsive Performance of a Hypersonic Aircraft during the Acceleration Phase*, 2017;

[14] Bader P., *Preliminary design of a Thermal and Energy Management Subsystem for hypersonic vehicle concepts*, 2019;

[15] Bajeli B., *STRATOFLY Project: analysis of the Concept of Operations of a Hypersonic Civil Passenger Transport Aircraft*, 2019;

[16] ANSYS Fluent User's Guide